RAMAN SPECTRA OF SOLIDS

A thesis presented for the degree of
Doctor of Philosophy in Physics
in the University of Canterbury,
Christchurch, New Zealand.

by

J.H. Christie

1973

ABSTRACT

The results of work in two different aspects of Raman spectroscopy are presented.

Part I describes a systematic and comprehensive calculation of selection rule tables for three- and four-photon Raman interactions. As a preliminary step, explicit quantum-mechanical expressions for the scattering tensors are obtained, enabling the symmetry of the tensors to be analysed. It is found that these tensors do not possess the symmetry previously ascribed to them in the literature. Selection rule tables are calculated using standard group theoretical techniques. The results show that it may be possible to measure, by means of high-order Raman spectroscopy, energy levels which cannot be measured directly by conventional spectroscopic techniques.

In Part II, an experimental investigation of the Co^{2+} ion in $CdCl_2$, $MnCl_2$, $CoCl_2$ and $CdBr_2$ using conventional Raman spectroscopy is described. In these crystals, the Co^{2+} ion experiences a trigonal crystal field which gives rise to a low-lying manifold of six doubly-degenerate energy levels with a total splitting of about 1000 cm^{-1}. Spectra have been recorded at room, liquid air and liquid helium temperatures for varying concentrations of Co^{2+} ions in the host crystals, enabling all energy levels to be measured in each of the four cases. Close fits with crystal field theoretical calculations are achieved. The results are compared with those previously obtained by infrared absorption experiments, and the superiority of Raman spectroscopy as a technique for measuring low energy transitions is shown. A preliminary investigation of antiferromagnetic $CoCl_2$ is presented.

ACKNOWLEDGEMENTS

This thesis would not have been completed but for the assistance, discussions, advice and encouragement from many people, including virtually the entire staff of the Physics Department of the University of Canterbury, and many of my fellow postgraduate research students.

In particular I would like to thank Dr D.J. Lockwood for his considerable assistance and for the original suggestions for this work, Ivan Johnstone for performing computer calculations and for assistance with experiments, the late Hamish Kerr for his help with experiments, R.W. Tyree for his patience and skilful maintenance of the equipment, Dr G.D. Jones for many helpful discussions and much useful advice, and Dr R. Syme and Professor B.G. Wybourne for their continued interest and encouragement.

I wish also to thank the New Zealand University Grants Committee for a Post Graduate Scholarship.

Assistance with computing costs was provided by the U.S. Air Force Office of Scientific Research under AFOSR Grant No. 1275-67.

John Christie

5 December 1973

CONTENTS

PART II

RAMAN LIGHT SCATTERING IN COBALTOUS COMPOUNDS

LIST OF FIGURES

LIST OF TABLES

P A R T I

SELECTION RULES FOR THREE- AND FOUR-PHOTON RAMAN INTERACTIONS

CHAPTER 1

INTRODUCTION

When a system of nuclei and electrons is subjected to an external electric field, a field-dependent dipole moment is produced. This induced moment, $\underline{\mu}$, may be expanded as a power series in the applied field, $\underline{E}$:

$$\underline{\mu}(\underline{E}) = \underline{\underline{\alpha}}.\underline{E} + \underline{\underline{\beta}}.\underline{E}^2 + \underline{\underline{\gamma}}.\underline{E}^3 + \cdots \qquad (1.1)$$

The linear term adequately describes the induced moment for moderate field strengths, but when intense fields are used, the β and γ terms may become significant. At optical frequencies, high-powered lasers have been used to produce nonlinear effects such as second- and third-harmonic generation, and frequency mixing. The polarizability expression (1.1) also describes inelastic, or Raman, scattering processes, in which the state of the irradiated system after the interaction differs from the initial state. Attainable field strengths, such as are required to produce two-photon stimulated Raman scattering, are sufficiently intense to produce observable higher-order Raman scattering.

Selection rules for the Raman process described by β were calculated by Cyvin et al.[1] following the first observation of three-photon Raman scattering[2]. Three-photon electronic Raman scattering has been observed in K and Rb vapours[3,4] under near resonance conditions. In 1965, Dumartin et al.[5] observed the ν_7 line of benzene in an inverse Raman experiment carried out near the threshold for stimulated Raman emission;

these authors attributed the relaxation of selection rules to the high value of the laser field. This view was subsequently confirmed by Ievleva and Karagodova[6], who calculated the transformation properties of the γ tensor for the group D_{6h}, which describes the symmetry of the benzene molecule, and showed that the ν_7 line, forbidden by the α selection rules, is allowed by those for γ. In addition, Ozgo[7] has calculated transformation properties of γ for the 32 crystallographic point groups.

In Chapter 2 of this work, diagrammatic perturbation theory[8,9] is used to investigate the explicit form of the Raman tensors corresponding to the β and γ terms in the polarizability expansion. In the earlier work[1,6,7], with the exception of that of Li[10], the selection rule calculations were made under the assumption that the β and γ Raman tensors are totally symmetric with respect to interchange of the component indices, although the tensors do not by definition possess this symmetry. It is found, on examination of the symmetry properties of β and γ, that in cases favourable for observation of the higher-order effects which they describe, the nonsymmetric components are not negligible. Accordingly, in Chapter 3, the selection rules for the nonsymmetric β and γ Raman tensors, as well as for the symmetric γ tensor, are calculated for the important molecular point groups, including the crystallographic point groups. In Chapter 4, the results and their application are discussed, and optimum experimental conditions for the observation of three- and four-photon Raman effects are postulated.

CHAPTER 2

THEORY

2.1 SCATTERING PROCESSES

The total radiated intensity per unit time of an oscillating electric dipole moment is given by[11]

$$I = (4\omega_0^4/3c^3)|\underline{\mu}|^2 \qquad (2.1)$$

where ω_0 is the frequency of the emitted light, c the speed of light and $\underline{\mu}$ the dipole moment. For Raman and Rayleigh scattering, the appropriate moment is given by equation (1.1), which may be written in cartesian form as

$$\mu_\rho = \sum_\sigma \alpha_{\rho\sigma} E_\sigma + \sum_{\sigma,\tau} \beta_{\rho\sigma\tau} E_\sigma E_\tau + \sum_{\sigma,\tau,\nu} \gamma_{\rho\sigma\tau\nu} E_\sigma E_\tau E_\nu + \cdots \qquad (2.2)$$

where $\rho, \sigma, \tau, \nu = x, y$ or z. The linear term in the expansion (2.2) gives rise to the well-known two-photon Raman effect, in which the emitted light has frequency $\omega_0 = \omega_1 + \omega_{if}$, where ω_1 is the frequency of the incident light, and $\hbar\omega_{if} = \hbar(\omega_i - \omega_f)$ is the energy difference $(E_i - E_f)$ between states i and f of the irradiated system. If i = f, the light is scattered with no change in frequency, and the α term corresponds to ordinary Rayleigh scattering. In a similar manner, the β and γ tensors describe a variety of elastic (i = f) and inelastic (i $\neq$ f) scattering phenomena such as frequency doubling, optical rectification and three-photon Raman scattering (β); frequency trebling, second-order Rayleigh scattering, and four-photon Raman scattering (γ).

Noting equation (2.1), it will be observed that the intensity of the scattered light has a fourth-power dependency on frequency for all these scattering phenomena.

2.2 DIAGRAMMATIC PERTURBATION THEORY

The quantum mechanical expression for the first-order polarizability may be readily found using second-order time dependent perturbation theory[12†]:

$$\alpha_{\rho\sigma}^{if} = \hbar^{-1} \sum_j \left(\frac{\langle f | M_\rho | j \rangle \langle j | M_\sigma | i \rangle}{\omega_{ji} - \omega_1} + \frac{\langle f | M_\sigma | j \rangle \langle j | M_\rho | i \rangle}{\omega_{ji} + \omega_0} \right), \qquad (2.3)$$

provided that ω_0 or ω_1 does not coincide with a resonance frequency of the system. In such cases, equation (2.3) is modified by substituting $\omega_j - i(\Gamma_j/2)$ for ω_j, where $\Gamma_j = 1/\tau_j$, and τ_j is the mean lifetime of state j. $\underline{M}$ is the operator representing the electric dipole moment of the system, and the summation is over all states of the system. Note that $\alpha_{\rho\sigma}^{if}$ is non-symmetric with respect to interchange of ρ and σ.

Derivation of expressions for the higher order tensors becomes increasingly more difficult, in part because perturbation calculations generate transient terms and unwanted information about scattering processes other than that which is the subject of the calculation[8]. These complications can be avoided by making use of "diagrammatic perturbation theory"[8,9]. The theory establishes rules for the construction of diagrams which enable expressions for scattering tensors to be written down directly, whilst

† $\langle i|\underline{M}|j\rangle$ in this reference is equivalent to $\langle j|\underline{M}|i\rangle$ in this work.

simultaneously giving an insight into the physical nature of the interactions.

It is instructive to consider the diagrams relating to the more familiar α tensor before applying the technique to the hyper-Raman effect. The diagrams corresponding to the terms under the summation in equation (2.3) are given (in the same order) in Figure 2.1.

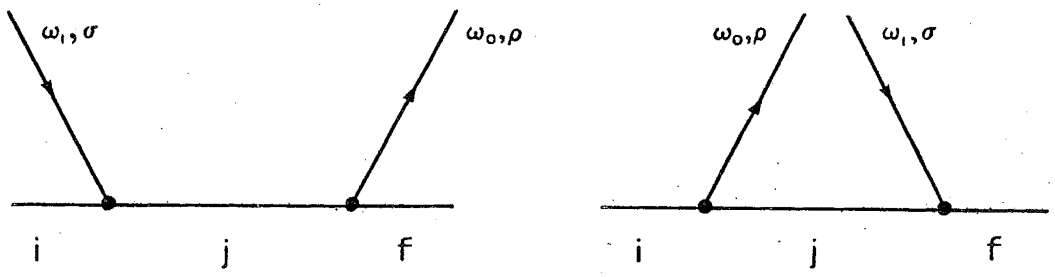

Fig. 2.1 Perturbation diagrams describing the terms contributing to the α Raman tensor.

When interpreted according to the rules given in references 8 and 9, the result may be written down directly, and it is exactly the equation (2.3).

2.3 THREE-PHOTON INTERACTIONS

As has been mentioned previously, the polarizability expansion (1.1) relates to a wide variety of elastic and inelastic, linear and nonlinear scattering phenomena. In this section, and in the rest of this chapter, we shall be concerned with inelastic processes only; i.e. those in which the initial and final states of the system differ.

The β term in (2.2) corresponds to several nonlinear effects, including three-photon Raman scattering and induced emission and absorption. The quantum mechanical expression for the β tensor is

$$\beta_{\rho\sigma\tau}{}^{if} = \frac{1}{\hbar^2}\sum_{j,k}\left(\frac{\langle f|M_\rho|k\rangle\langle k|M_\tau|j\rangle\langle j|M_\sigma|i\rangle}{(\omega_{ji}-\omega_1)(\omega_{kf}-\omega_0)} + \frac{\langle f|M_\rho|k\rangle\langle k|M_\sigma|j\rangle\langle j|M_\tau|i\rangle}{(\omega_{ji}\mp\omega_2)(\omega_{kf}-\omega_0)}\right.$$
$$+ \frac{\langle f|M_\tau|k\rangle\langle k|M_\rho|j\rangle\langle j|M_\sigma|i\rangle}{(\omega_{ji}-\omega_1)(\omega_{kf}\pm\omega_2)} + \frac{\langle f|M_\tau|k\rangle\langle k|M_\sigma|j\rangle\langle j|M_\rho|i\rangle}{(\omega_{ji}+\omega_0)(\omega_{kf}\pm\omega_2)} \qquad (2.4)$$
$$\left. + \frac{\langle f|M_\sigma|k\rangle\langle k|M_\rho|j\rangle\langle j|M_\tau|i\rangle}{(\omega_{ji}\mp\omega_2)(\omega_{kf}+\omega_1)} + \frac{\langle f|M_\sigma|k\rangle\langle k|M_\tau|j\rangle\langle j|M_\rho|i\rangle}{(\omega_{ji}+\omega_0)(\omega_{kf}+\omega_1)}\right).$$

This equation was obtained using diagrammatic perturbation theory; it agrees with expressions for β given by Li[10], and Akhmanov and Klyshko[13]. The diagram given in Figure 2.2 gives the term

$$\frac{\langle f|M_\rho|k\rangle\langle k|M_\tau|j\rangle\langle j|M_\sigma|i\rangle}{(\omega_{ji}-\omega_1)(\omega_{ki}-\omega_1\mp\omega_2)}$$

which reduces simply and directly to the first term in (2.4).

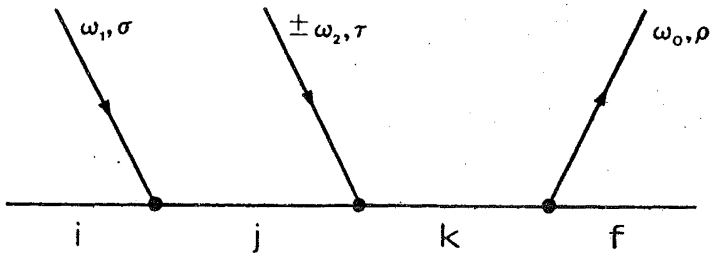

Fig. 2.2 Perturbation diagram describing a term contributing to the β Raman tensor.

The other five diagrams are obtained by permuting the order of the interaction vertices in Figure 2.2.

If we take the frequencies of the incident photons ω_1 and ω_2 to be equal, as is usually the case in practice, and choose the plus sign, then equation (2.4) describes the interaction tensor for the three-photon Raman effect with emitted frequency $\omega_0 = 2\omega_1 + \omega_{if}$. Choosing the minus sign, the process becomes induced emission at a frequency $\omega_0 = \omega_{if}$. This interaction is the inelastic process which derives from the elastic optical rectification interaction in which a dc electric field is produced. We must, in this case, add another equivalent set of terms to those of equation (2.4), as the two processes described by $\beta_{\rho\sigma\tau}^{if}(\omega_0,\omega_1,-\omega_1)$ and $\beta_{\rho\sigma\tau}^{if}(\omega_0,-\omega_1,\omega_1)$ are inseparable. The induced emission process involves a transition from state i to state f. The tensor for the corresponding absorption, involving a transition from state f to state i, is merely the complex conjugate of that for the emission process (so that the transition probabilities of the two processes are the same). When $\omega_1 \neq \omega_2$, three-photon Raman emission occurs at a frequency given by $\omega_0 = |\omega_1 \pm \omega_2| + \omega_{if}$.

Inspection of equation (2.4) shows that when $\omega_1 = \omega_2$, the β tensor is symmetric in the indices σ and τ. That is, $\beta_{\rho\sigma\tau}^{if}(\omega_0,\omega_1,\omega_1) = \beta_{\rho\tau\sigma}^{if}(\omega_0,\omega_1,\omega_1)$. This is also true for induced emission and absorption processes since, as has been mentioned, the tensors $\beta(\omega_0,\omega_1,-\omega_1)$ and $\beta(\omega_0,-\omega_1,\omega_1)$ are indistinguishable. If $\omega_1 \neq \omega_2$, then, as in the case of the α tensor, the β tensor does not exhibit any symmetry.

2.4 FOUR-PHOTON INTERACTIONS

The γ term in the polarizability expansion corresponds to a fourth-order scattering process involving three incident photons of frequency ω_1, ω_2 and ω_3, and is illustrated in Figure 2.3.

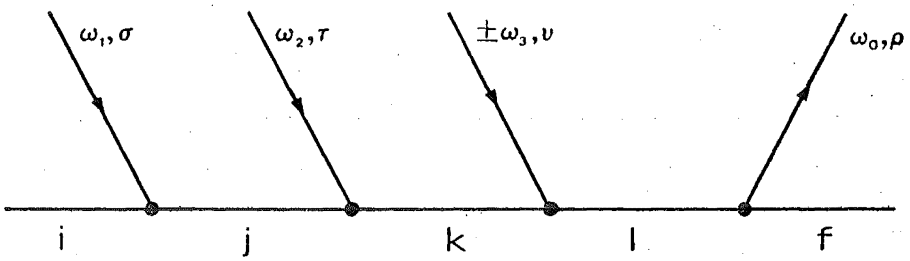

Fig. 2.3 Perturbation diagram describing a term contributing to the γ Raman tensor.

The quantum-mechanical expression for the tensor component $\gamma_{\rho\sigma\tau\nu}^{if}$ has been derived by the method of diagrammatic perturbation theory, and is found to be:

$$\gamma_{\rho\sigma\tau\nu}{}^{if} = \frac{1}{\hbar^3} \sum_{j,k,l} \Bigg(\frac{\langle f|M_\rho|l\rangle\langle l|M_\nu|k\rangle\langle k|M_\tau|j\rangle\langle j|M_\sigma|i\rangle}{(\omega_{ji}-\omega_1)(\omega_{ki}-\omega_1-\omega_2)(\omega_{lf}-\omega_0)} + \frac{\langle f|M_\rho|l\rangle\langle l|M_\tau|k\rangle\langle k|M_\nu|j\rangle\langle j|M_\sigma|i\rangle}{(\omega_{ji}-\omega_1)(\omega_{ki}-\omega_1\mp\omega_3)(\omega_{lf}-\omega_0)}$$

$$+ \frac{\langle f|M_\rho|l\rangle\langle l|M_\nu|k\rangle\langle k|M_\sigma|j\rangle\langle j|M_\tau|i\rangle}{(\omega_{ji}-\omega_2)(\omega_{ki}-\omega_1-\omega_2)(\omega_{lf}-\omega_0)} + \frac{\langle f|M_\rho|l\rangle\langle l|M_\tau|k\rangle\langle k|M_\sigma|j\rangle\langle j|M_\nu|i\rangle}{(\omega_{ji}\mp\omega_3)(\omega_{ki}-\omega_1\mp\omega_3)(\omega_{lf}-\omega_0)}$$

$$+ \frac{\langle f|M_\rho|l\rangle\langle l|M_\sigma|k\rangle\langle k|M_\nu|j\rangle\langle j|M_\tau|i\rangle}{(\omega_{ji}-\omega_2)(\omega_{ki}-\omega_2\mp\omega_3)(\omega_{lf}-\omega_0)} + \frac{\langle f|M_\rho|l\rangle\langle l|M_\sigma|k\rangle\langle k|M_\tau|j\rangle\langle j|M_\nu|i\rangle}{(\omega_{ji}\mp\omega_3)(\omega_{ki}-\omega_2\mp\omega_3)(\omega_{lf}-\omega_0)}$$

$$+ \frac{\langle f|M_\nu|l\rangle\langle l|M_\rho|k\rangle\langle k|M_\tau|j\rangle\langle j|M_\sigma|i\rangle}{(\omega_{ji}-\omega_1)(\omega_{ki}-\omega_1-\omega_2)(\omega_{lf}\pm\omega_3)} + \frac{\langle f|M_\tau|l\rangle\langle l|M_\rho|k\rangle\langle k|M_\nu|j\rangle\langle j|M_\sigma|i\rangle}{(\omega_{ji}-\omega_1)(\omega_{ki}-\omega_1\mp\omega_3)(\omega_{lf}+\omega_2)}$$

$$+ \frac{\langle f|M_\nu|l\rangle\langle l|M_\rho|k\rangle\langle k|M_\sigma|j\rangle\langle j|M_\tau|i\rangle}{(\omega_{ji}-\omega_2)(\omega_{ki}-\omega_1-\omega_2)(\omega_{lf}\pm\omega_3)} + \frac{\langle f|M_\tau|l\rangle\langle l|M_\rho|k\rangle\langle k|M_\sigma|j\rangle\langle j|M_\nu|i\rangle}{(\omega_{ji}\mp\omega_3)(\omega_{ki}-\omega_1\mp\omega_3)(\omega_{lf}+\omega_2)}$$

$$+ \frac{\langle f|M_\sigma|l\rangle\langle l|M_\rho|k\rangle\langle k|M_\nu|j\rangle\langle j|M_\tau|i\rangle}{(\omega_{ji}-\omega_2)(\omega_{ki}-\omega_1\mp\omega_3)(\omega_{lf}+\omega_1)} + \frac{\langle f|M_\sigma|l\rangle\langle l|M_\rho|k\rangle\langle k|M_\tau|j\rangle\langle j|M_\nu|i\rangle}{(\omega_{ji}\mp\omega_3)(\omega_{ki}-\omega_2\mp\omega_3)(\omega_{lf}+\omega_1)}$$

$$+ \frac{\langle f|M_\nu|l\rangle\langle l|M_\tau|k\rangle\langle k|M_\rho|j\rangle\langle j|M_\sigma|i\rangle}{(\omega_{ji}-\omega_1)(\omega_{kf}+\omega_2\pm\omega_3)(\omega_{lf}\pm\omega_3)} + \frac{\langle f|M_\tau|l\rangle\langle l|M_\nu|k\rangle\langle k|M_\rho|j\rangle\langle j|M_\sigma|i\rangle}{(\omega_{ji}-\omega_1)(\omega_{kf}+\omega_2\pm\omega_3)(\omega_{lf}+\omega_2)}$$

$$+ \frac{\langle f|M_\nu|l\rangle\langle l|M_\sigma|k\rangle\langle k|M_\rho|j\rangle\langle j|M_\tau|i\rangle}{(\omega_{ji}-\omega_2)(\omega_{kf}+\omega_1\pm\omega_3)(\omega_{lf}\pm\omega_3)} + \frac{\langle f|M_\tau|l\rangle\langle l|M_\sigma|k\rangle\langle k|M_\rho|j\rangle\langle j|M_\nu|i\rangle}{(\omega_{ji}\mp\omega_3)(\omega_{kf}+\omega_1+\omega_2)(\omega_{lf}+\omega_2)}$$

$$+ \frac{\langle f|M_\sigma|l\rangle\langle l|M_\nu|k\rangle\langle k|M_\rho|j\rangle\langle j|M_\tau|i\rangle}{(\omega_{ji}-\omega_2)(\omega_{kf}+\omega_1\pm\omega_3)(\omega_{lf}+\omega_1)} + \frac{\langle f|M_\sigma|l\rangle\langle l|M_\tau|k\rangle\langle k|M_\rho|j\rangle\langle j|M_\nu|i\rangle}{(\omega_{ji}\mp\omega_3)(\omega_{kf}+\omega_1+\omega_2)(\omega_{lf}+\omega_1)}$$

$$+ \frac{\langle f|M_\nu|l\rangle\langle l|M_\tau|k\rangle\langle k|M_\sigma|j\rangle\langle j|M_\rho|i\rangle}{(\omega_{ji}+\omega_0)(\omega_{kf}+\omega_2\pm\omega_3)(\omega_{lf}\pm\omega_3)} + \frac{\langle f|M_\tau|l\rangle\langle l|M_\nu|k\rangle\langle k|M_\sigma|j\rangle\langle j|M_\rho|i\rangle}{(\omega_{ji}+\omega_0)(\omega_{kf}+\omega_2\pm\omega_3)(\omega_{lf}+\omega_2)}$$

$$+ \frac{\langle f|M_\nu|l\rangle\langle l|M_\sigma|k\rangle\langle k|M_\tau|j\rangle\langle j|M_\rho|i\rangle}{(\omega_{ji}+\omega_0)(\omega_{kf}+\omega_1\pm\omega_3)(\omega_{lf}\pm\omega_3)} + \frac{\langle f|M_\tau|l\rangle\langle l|M_\sigma|k\rangle\langle k|M_\nu|j\rangle\langle j|M_\rho|i\rangle}{(\omega_{ji}+\omega_0)(\omega_{kf}+\omega_1+\omega_2)(\omega_{lf}+\omega_2)}$$

$$+ \frac{\langle f|M_\sigma|l\rangle\langle l|M_\nu|k\rangle\langle k|M_\tau|j\rangle\langle j|M_\rho|i\rangle}{(\omega_{ji}+\omega_0)(\omega_{kf}+\omega_1\pm\omega_3)(\omega_{lf}+\omega_1)} + \frac{\langle f|M_\sigma|l\rangle\langle l|M_\tau|k\rangle\langle k|M_\nu|j\rangle\langle j|M_\rho|i\rangle}{(\omega_{ji}+\omega_0)(\omega_{kf}+\omega_1+\omega_2)(\omega_{lf}+\omega_1)} \Bigg). \tag{2.5}$$

The first term inside the summation is obtained from the diagram given in Figure 2.3.

The tensor $\gamma(\omega_0,\omega_1,\omega_2,\pm\omega_3)$ describes four-photon Raman scattering with the emission frequency $\omega_0 = \omega_1+\omega_2\pm\omega_3+\omega_{if}$. If $\omega_1 \neq \omega_2 \neq \omega_3$, then γ is completely unsymmetric. If any two of the frequencies ω_1, ω_2 and ω_3 are equal, then the tensor is symmetric in the indices with which these frequencies are associated. For example,

$$\gamma_{\rho\sigma\tau\nu}^{if}(\omega_0,\omega_1,\omega_1,\omega_3) = \gamma_{\rho\tau\sigma\nu}^{if}(\omega_0,\omega_1,\omega_1,\omega_3).$$

However, if we choose the minus sign and $|\omega_3| = \omega_1$ or ω_2, we must add two tensors, as in the case of β, and the tensor retains permutation symmetry in the appropriate indices. The experimentally interesting case is that in which $\omega_1 = \omega_2 = \omega_3$. Choosing the plus sign associated with frequency ω_3 gives four-photon Raman scattering at a frequency $\omega_0 = 3\omega_1+\omega_{if}$, and the tensor is symmetric in σ, τ and ν. If the minus sign is chosen, γ is still symmetric in σ, τ, and ν, because the tensor comprises three equivalent parts $\gamma(\omega_0,\omega_1,\omega_1,-\omega_1)$, $\gamma(\omega_0,\omega_1,-\omega_1,\omega_1)$, and $\gamma(\omega_0,-\omega_1,\omega_1,\omega_1)$. Here the scattered frequency is $\omega_0 = \omega_1+\omega_{if}$, which represents a fourth-order contribution to ordinary Raman scattering. This is the process which was observed by Dumartin et al.[5].

2.5 VIBRATIONAL RAMAN EFFECT

The α, β and γ tensors, in their present forms describe Raman transitions in general. In this section, we will restrict attention to the tensors describing the vibrational Raman effect.

We have noted previously that the α tensor in its general form is unsymmetric. Placzek[14] applied to the linear vibrational Raman tensor a series of approximations which are outlined below[15]:

The wavefunctions of the system are assumed to be separable into a product of two functions, dependent on the nuclear and electronic coordinates:

$$\psi_{n\nu}(x,X) = \chi_{n\nu}(X)\ \phi_n(x,X) \qquad (2.6)$$

where X and x represent the nuclear and electronic coordinates respectively, and n and ν are the quantum numbers for the electronic and nuclear wavefunctions respectively. $\phi_n(x,X)$ is the wave function of the electrons, in which the nuclear configuration X appears as a parameter. Noting that only vibrational transitions are being considered, and that at ordinary temperatures molecular systems are practically always in the lowest electronic state, only expressions of $\alpha_{\rho\sigma}^{if}$ in which states i and f belong to the lowest electronic state of the system need be considered.

If the ground electronic state is non-degenerate, (2.3) can be rewritten:

$$\alpha_{\rho\sigma}^{if} = \frac{1}{\hbar} \sum_{n_j} \sum_{\nu_j} \left\{ \frac{\langle n_0\nu_f|M_\rho|n_j\nu_j\rangle\langle n_j\nu_j|M_\sigma|n_0\nu_i\rangle}{\omega_{n_j\nu_j,n_0\nu_i} - \omega_1} + \frac{\langle n_0\nu_f|M_\sigma|n_j\nu_j\rangle\langle n_j\nu_j|M_\rho|n_0\nu_i\rangle}{\omega_{n_j\nu_j,n_0\nu_i} + \omega_0} \right\} \tag{2.7}$$

where the states are now labelled by pairs of quantum numbers. (2.7) is now split into two parts in which $n_j = n_0$ and $n_j \neq n_0$ respectively. In the second case it is assumed that $\omega_{n_j\nu_j,n_0\nu_i} = \omega_{n_jn_0}$, which will be valid provided ω_1 is not too close to one of the frequencies $\omega_{n_jn_0}$:

$$\begin{aligned}\alpha_{\rho\sigma}^{if} = {} & \frac{1}{\hbar} \sum_{\nu_j} \left\{ \frac{\langle n_0\nu_f|M_\rho|n_0\nu_j\rangle\langle n_0\nu_j|M_\sigma|n_0\nu_i\rangle}{\omega_{\nu_j\nu_i} - \omega_1} + \frac{(\rho \leftrightarrow \sigma)}{\omega_{\nu_j\nu_i} + \omega_0} \right\} \\ & + \frac{1}{\hbar} \sum_{n_j \neq n_0} \left\{ \sum_{\nu_j} \frac{\langle n_0\nu_f|M_\rho|n_j\nu_j\rangle\langle n_j\nu_j|M_\sigma|n_0\nu_i\rangle}{\omega_{n_jn_0} - \omega_1} \right. \\ & \left. + \sum_{\nu_j} \frac{\langle n_0\nu_f|M_\sigma|n_j\nu_j\rangle\langle n_j\nu_j|M_\rho|n_0\nu_i\rangle}{\omega_{n_jn_0} + \omega_0} \right\}\end{aligned} \tag{2.8}$$

where $(\rho \leftrightarrow \sigma)$ represents the $\rho\sigma$ term with indices ρ and σ permuted, and $\omega_{\nu_j \nu_i}$ is the transition frequency between vibrational states of the lowest electronic state. Under the condition $\omega_1 >> \omega_{\nu_j \nu_i}$, the first part of (2.8) is neglected.

Taking a term from the second part of (2.8) and writing it out in explicit form, the following expression is obtained:

$$\frac{1}{\omega_{n_j n_0} - \omega_1} \sum_{\nu_j} \int dx \int dX \int dx' \int dX' \left\{ \phi^*_{n_0}(x,X) \chi^*_{n_0 \nu_f}(X) M_\rho(x,X) \right.$$

$$\left. \times \phi_{n_j}(x,X) \chi_{n_j \nu_j}(X) \phi^*_{n_j}(x',X') \chi^*_{n_j \nu_j}(X') M_\sigma(x',X') \phi_{n_0}(x',X') \chi_{n_0 \nu_i}(X') \right\} \tag{2.9}$$

Since the functions $\chi_{n_j \nu_j}(X)$ form a complete set of functions in X, the relation

$$\sum_{\nu_j} \chi_{n_j \nu_j}(X) \chi^*_{n_j \nu_j}(X') = \delta(X-X')$$

can be used to reduce (2.9):

$$\int \chi^*_{n_0 \nu_f}(X) \left\{ \frac{1}{\omega_{n_j n_0} - \omega_1} \int \phi^*_{n_0}(x,X) M_\rho(x,X) \phi_{n_j}(x,X) dx \right.$$

$$\left. \times \int \phi^*_{n_j}(x',X) M_\sigma(x',X) \phi_{n_0}(x',X) dx' \right\} \chi_{n_0 \nu_i}(X) dX \tag{2.10}$$

All the terms in the second part of (2.8) may be similarly reduced, and (2.8) can thus be written:

$$\alpha_{\rho\sigma}^{if} = \langle f | \alpha_{\rho\sigma} | i \rangle \tag{2.11}$$

where

$$\alpha_{\rho\sigma} = \frac{1}{\hbar} \sum_{n_j \neq n_0} \left\{ \frac{(M_\rho)_{oj} (M_\sigma)_{j0}}{\omega_{n_j n_0} - \omega_1} + \frac{(M_\sigma)_{oj} (M_\rho)_{jo}}{\omega_{n_j n_0} + \omega_1} \right\}, \tag{2.12}$$

and

$$(M_\rho)_{oj} = \int \phi^*_{n_0}(x,X)\ M_\rho(x,X)\ \phi_{n_j}(x,X)\ dx \qquad (2.13)$$

Placzek[14] and Li[10] observe that the matrix elements (2.13) are real provided that the system is not subjected to an external magnetic field, or that the lowest electronic state is not degenerate (note that in this latter case, Placzek's approximation would itself be invalid). Under these conditions, $\alpha_{\rho\sigma}$ is a symmetric tensor, and hence so is the tensor $\alpha_{\rho\sigma}^{if}$.

Li[10] applied Placzek's approximation to $\beta_{\rho\sigma\tau}^{if}(\omega_0,\omega_1,\omega_2)$ and found that the reduced tensor $\beta_{\rho\sigma\tau}(\omega_0,\omega_1,\omega_2)$ (defined in a manner similar to the definition (2.11)) possesses no symmetry in any coordinates, and that $\beta_{\rho\sigma\tau}(\omega_0,\omega_1,\omega_1)$ is symmetric in σ and τ only. Thus the symmetry of β, in the case of vibrational transitions, is not altered under Placzek's approximation, in contrast to that of α.

We have investigated, in the same manner, the tensors describing the various fourth-order scattering processes. It is a simple matter to prove that the reduced γ tensors in the vibrational case do not possess any extra symmetry. Taking, for example, the first term under the summation in (2.5) and applying Placzek's approximation, we obtain the term

$$\frac{(M_\rho)_{o\ell}(M_\nu)_{\ell k}(M_\tau)_{kj}(M_\sigma)_{jo}}{(\omega_{n_j n_0}-\omega_1)(\omega_{n_k n_0}-\omega_1-\omega_2)(\omega_{n_\ell n_0}-\omega_0)}$$

This expression is totally unsymmetric, and there are no other terms possessing the same reduced denominator.

Chu[16] has pointed out that $\beta_{\rho\sigma\tau}(\omega_0,\omega_1,\omega_2)$ becomes symmetric in all of its indices under the condition that

$(\omega_{0,1,2}/\omega_{n_j n_0}) << 1$, and the same is obviously true for γ when $(\omega_{0,1,2,3}/\omega_{n_j n_0}) << 1$. Although these conditions are unlikely to hold under realistic experimental conditions (the minimum $\omega_{n_j n_0}$ is, in general, of the order of 45,000 cm^{-1}, and for a ruby laser source and β scattering, $\omega_0 \approx 30{,}000$ cm^{-1}), the analysis demonstrates the different frequency dependence of the magnitudes of the symmetric and nonsymmetric parts of the β and γ tensors. For both β and γ, the nonsymmetric part of the tensor becomes less significant as the photon energies become smaller. This statement also holds in the case of linear Raman scattering in the general case, as has been demonstrated by Placzek (reference 14, p38).

2.6 THE THEORY OF SELECTION RULES

The Raman selection rules are derived from the matrix element theorem, which may be conveniently expressed in the following form[17]:

Let $\psi^{(\alpha)}$ be a base function of an irreducible representation α of a symmetry group G, and let E be the unit (or totally symmetric) representation.

Then

$$\int \psi^{(\alpha)} dx = 0 \quad \text{unless} \quad \alpha = E, \tag{2.14}$$

where the integration is over all space.

It follows from (2.14) that

$$\int \psi_i^* \theta \psi_j dx = 0$$

unless the representation $\Gamma^{(i)*} \times \Gamma^{\theta} \times \Gamma^{(j)}$ contains the unit representation, where ψ_i transforms according to the

representation $\Gamma^{(i)}$. The scattering amplitude for a vibrational Raman transition is proportional to the term $\langle f|\alpha_{\rho\sigma}|i\rangle$ or $\langle f|\beta_{\rho\sigma\tau}|i\rangle$ as appropriate, and the selection rules can be obtained directly:

A transition intensity will be zero unless the product $\Gamma^{(i)} \times \Gamma^{\text{tensor}} \times \Gamma^{(f)*}$ contains the unit representation (2.15)

In general however, the scattering amplitude is proportional to terms of the form $\alpha_{\rho\sigma}{}^{if}$ (equations (2.3), (2.4) and (2.6)), to which the theorem (2.14) cannot be applied directly. We will now show that the selection rule (2.15) holds for the Raman tensors in their general forms.

Consider the expression $\iint\phi(x,x')dx'dx$, where ϕ is a function of a system whose symmetry is described by group G, and both integrals are over all space.

Now

$$\iint\phi(x,x')dx'dx = \int\psi(x)dx$$

where

$$\psi(x) = \int\phi(x,x')dx' \qquad (2.16)$$

In (2.16), $\phi(x,x')$ is a function of the variable x', and x is simply a parameter. In general ϕ will belong to a reducible representation of G, which can be expressed as a sum of irreducible representations. We may now apply the matrix element theorem to (2.16), and conclude that:

$\iint\phi(x,x')dx'dx = 0$ unless ϕ is the basis function of a representation containing the unit representation. (2.17)

Equation (2.3) may be expressed in the following explicit form:

$$\alpha_{\rho\sigma}^{if} =$$

$$\frac{1}{\hbar}\Big\{\sum_j [(\omega_{ji}-\omega_1)^{-1}\int\psi_f^*(x)M_\rho(x)\psi_j(x)dx \int\psi_j^*(x')M_\sigma(x')\psi_i(x')dx'$$

$$+ (\omega_{ji}+\omega_0)^{-1}(\rho \leftrightarrow \sigma)]\Big\}.$$

Therefore,

$$\alpha_{\rho\sigma}^{if} =$$

$$\iint\psi_f^*(x)\Big\{\frac{1}{\hbar}\sum_j [(\omega_{ji}-\omega_1)^{-1}(M_\rho(x)\psi_j(x))\psi_j^*(x')M_\sigma(x')$$

$$+ (\omega_{ji}+\omega_0)^{-1}(\rho \leftrightarrow \sigma)]\Big\}\psi_i(x')dx'dx \qquad (2.18)$$

$$= \iint\psi_f^*(x)\theta_{\rho\sigma}(x,x')\ \psi_i(x')dx'dx, \qquad (2.19)$$

where $\theta_{\rho\sigma}(x,x')$ represents the contents of the curly brackets in (2.18). Applying the result (2.17), we conclude that $\alpha_{\rho\sigma}^{if} = 0$, unless the representation $\Gamma^{(i)} \times \Gamma^{\theta} \times \Gamma^{(f)}$* contains the unit representation. $\theta_{\rho\sigma}$ will transform under the group operations as a nonsymmetric second-rank tensor, and thus the theorem (2.15) also holds for all linear Raman transitions. The treatment can simply and obviously be extended to show that (2.15) also applies to interactions described by $\beta_{\rho\sigma\tau}^{if}$ and $\gamma_{\rho\sigma\tau\nu}^{if}$.

It is interesting to note that, as a consequence of the matrix element theorem, an intermediate state j can contribute to the summation (2.3) only if transitions from j to the initial and final Raman states are allowed by the selection rules for first order absorption and emission. This means, for example, that the resonance Raman effect will not be

observed in the case $\omega_{ji} \approx \omega_l$ if the states j and i are of the same parity (electric quadrupole and magnetic dipole terms assumed to be negligible).

In order to be able to calculate selection rules for Raman interactions, the transformation properties of the appropriate tensors must be known for the relevant symmetry group. In the general case, the equation (3.1) in Chapter 3 may be used to analyse the product representation given in (2.15). However, for the vibrational Raman effect, the initial state i is nearly always the ground state of the system, and consequently possesses all the group symmetry (i.e. it belongs to the unit representation). It may be simply shown, by application of group representation theory, that the product of two irreducible representations will only contain the unit representation if the two representations are complex conjugate representations. We may now state the vibrational Raman selection rule theorem in its most useful form: a Raman transition is allowed if the final state ψ_f transforms according to the same irreducible representation as the appropriate Raman tensor.

CHAPTER 3

CALCULATION OF SELECTION RULES

3.1 SYMMETRIZED RAMAN TENSORS

In Chapter 2, the symmetry of the β and of the γ Raman tensors was discussed, and it was shown that, under conditions of single-frequency excitation, $\beta_{\rho\sigma\tau}^{if}$ is symmetric with respect to permutation of the indices σ and τ, and that $\gamma_{\rho\sigma\tau\nu}^{if}$ is symmetric in the indices σ, τ and ν. We will now make a systematic analysis of these symmetries.

As is well known, the sets of all permutation operations on n symbols form the symmetric groups, S_n. Tensors whose components transform according to irreducible representations of the symmetric groups are labelled "symmetrized tensors". Since the indices of a general n^{th} rank tensor transform among themselves under the operations of S_n, the components of the tensor will form the basis of a representation of S_n, and thus the tensor can always be reduced to a sum of symmetrized tensors.

Let us now consider the case of the Raman tensor $\beta_{\rho\sigma\tau}^{if}$. The appropriate symmetric group, S_3, has the following character table[18]:

S_3	(1^3)	(12)	(3)
{3}	1	1	1
{21}	2	0	-1
$\{1^3\}$	1	-1	1

where (1^3) denotes the identity operator E; (12) the class of

operators (12), (13) and (23), defined in the conventional manner; and (3) the operators (123) and (132). The representations are labelled according to the corresponding partition of the integer 3.[19]

When the group elements operate on the indices ρ, σ and τ, the tensor components $\beta_{\rho\sigma\tau}$, $\beta_{\tau\rho\sigma}$ and $\beta_{\sigma\tau\rho}$ form a closed set under the transformations, and thus form the basis of a representation of S_3. The character, $\chi^{(\beta)}$, of the representation may be simply obtained by applying the group operations to the vector $(\beta_{\rho\sigma\tau}, \beta_{\tau\rho\sigma}, \beta_{\sigma\tau\rho})$ and extracting the trace of the transformation matrix. Note that, for example, the operator (23) interchanges the indices σ and τ, and not simply the last two indices of each tensor component. Following the form of the character table for S_3, we have then,

$$\chi^{(\beta)} = 3 \qquad 1 \qquad 0 \ .$$

Any reducible representation, whose character is χ, may be analyzed by means of the expression[20]

$$N^{(i)} = \frac{1}{g} \sum_{G} \chi^{(i)}(G)^* \ \chi(G) \tag{3.1}$$

where, if g is the order of the group, $\chi^{(i)}$ the character of the i^{th} irreducible representation and the summation is over all elements of the group, then $N^{(i)}$ is the number of times that the irreducible representation i appears in the reducible representation.

Applying (3.1) to the tensor representation $\beta_{\rho\sigma\tau}$, we see that $\chi^{(\beta)} = \chi^{\{3\}} + \chi^{\{21\}}$. $\beta_{\rho\sigma\tau}$ if thus reduces to a sum of three symmetrized tensors, since {21} is doubly degenerate.

In order to calculate the forms of the symmetrized tensors, we will introduce at this stage a very useful class of operators called "projection operators", which are defined as follows:

$$P_j^{(i)} = \frac{\ell^{(i)}}{g} \sum_G \Gamma^{(i)}(G)^*_{jj} \hat{G} \tag{3.2}$$

where $\Gamma^{(i)}(G)_{jj}$ is the j^{th} element of the j^{th} row in the matrix corresponding to the group operator $\hat{G}$ in the i^{th} irreducible representation, and $\ell^{(i)}$ is the dimension of the representation i. When $P_j^{(i)}$ operates on a function, it puts to zero any part of the function which does not belong to row j of representation i. The symmetrized Raman tensors are obtained by applying (3.2) to the general Raman tensors for the appropriate symmetric group.

Since the two β tensors transforming according to the representation {21} are physically indistinguishable, there is no reason to maintain a distinction between them, and we will therefore reduce $\beta_{\rho\sigma\tau}$ if to two tensors only, namely $\beta^{\{3\}}$ and $\beta^{\{21\}}$, where $\beta^{\{21\}}$ is the sum of the two degenerate tensors:

$$\beta^{\{21\}}_{\rho\sigma\tau} = P_1^{\{21\}}\beta_{\rho\sigma\tau} + P_2^{\{21\}}\beta_{\rho\sigma\tau} = P^{\{21\}}\beta_{\rho\sigma\tau}$$

where

$$P^{\{21\}} = \frac{\ell^{\{21\}}}{g} \sum_G \chi^{\{21\}}(G)^* \hat{G} \tag{3.3}$$

Therefore

$$\beta^{\{21\}}_{\rho\sigma\tau} = \frac{1}{3}(2\beta_{\rho\sigma\tau} - \beta_{\tau\rho\sigma} - \beta_{\sigma\tau\rho}) \tag{3.4}$$

where use is made of the character table for S_3. For one-dimensional representations, the values of $\Gamma^{(i)}(G)^*_{jj}$ in (3.2) are given in the character tables. We have therefore,

$$\beta^{\{3\}}_{\rho\sigma\tau} = \frac{1}{3}(\beta_{\rho\sigma\tau} + \beta_{\tau\rho\sigma} + \beta_{\sigma\tau\rho}). \tag{3.5}$$

Equations (3.4) and (3.5) give the forms of the "symmetrized" β tensors, where we note that $\beta^{\{21\}}$ is not a symmetrized tensor in the usual definition of the word. Using (3.2) for the representation $\{1^3\}$, it is found that, as predicted, $P^{\{1^3\}}\beta_{\rho\sigma\tau} = 0$.

It is instructive at this stage to compare these results with those for the more familiar second-rank tensor $\alpha_{\rho\sigma}$ if. The character table for S_2 is

S_2	(1^2)	(2)
$\{2\}$	1	1
$\{1^2\}$	1	-1

Making use of the projection operator form (3.3) we obtain

$$\alpha^{\{2\}}_{\rho\sigma} = \tfrac{1}{2}(\alpha_{\rho\sigma} + \alpha_{\sigma\rho})$$

and

$$\alpha^{\{1^2\}}_{\rho\sigma} = \tfrac{1}{2}(\alpha_{\rho\sigma} - \alpha_{\sigma\rho})$$

i.e. the symmetrized tensors in this case are the "symmetric" and "antisymmetric" tensors. Similarly we note that $\beta^{\{3\}}$ is a "symmetric" tensor, and that $\beta^{\{21\}}$ is the "nonsymmetric" tensor which disappears in the low frequency limit of three-photon Raman scattering.

The analysis of the symmetry properties of $\gamma_{\rho\sigma\tau\nu}{}^{if}$ closely follows that of $\beta_{\rho\sigma\tau}{}^{if}$.

The character table of S_4 is[18]

S_4	(1^4)	$(1^2 2)$	(13)	(4)	(2^2)
$\{4\}$	1	1	1	1	1
$\{31\}$	3	1	0	-1	-1
$\{2^2\}$	2	0	-1	0	2
$\{21^2\}$	3	-1	0	1	-1
$\{1^4\}$	1	-1	1	-1	1

We form a reducible representation of S_4 on the basis vector $(\gamma_{\rho\sigma\tau\nu}, \gamma_{\nu\rho\sigma\tau}, \gamma_{\tau\nu\rho\sigma}, \gamma_{\sigma\tau\nu\rho})$; the character of this representation is

$$\chi^{(\gamma)} = 4 \qquad 2 \qquad 1 \qquad 0 \qquad 0 .$$

Applying (3.1), we deduce

$$\chi^{(\gamma)} = \chi^{\{4\}} + \chi^{\{31\}}$$

and hence that $\gamma_{\rho\sigma\tau\nu}{}^{if}$ reduces to four tensors, three of which are degenerate. As in the previous case, it is only necessary to evaluate the sum of the degenerate tensors, which will again, in the interests of simplicity, be termed a symmetrized tensor. These tensors are found, with the help of the projection operators $P^{\{4\}}$ and $P^{\{31\}}$, to be:

$$\gamma^{\{4\}}_{\rho\sigma\tau\nu} = \tfrac{1}{4}(\gamma_{\rho\sigma\tau\nu} + \gamma_{\nu\rho\sigma\tau} + \gamma_{\tau\nu\rho\sigma} + \gamma_{\sigma\tau\nu\rho}) \tag{3.6}$$

which is a "symmetric" tensor; and

$$\gamma^{\{31\}}_{\rho\sigma\tau\nu} = \tfrac{1}{4}(3\gamma_{\rho\sigma\tau\nu} - \gamma_{\nu\rho\sigma\tau} - \gamma_{\tau\nu\rho\sigma} - \gamma_{\sigma\tau\nu\rho}) \tag{3.7}$$

The results (3,4), (3.5), (3.6) and (3.7) have been obtained in a previous work[21]† by a different technique in which the symmetry analyses are based on subgroups of S_3 and S_4, rather than on the symmetric groups themselves.

3.2 THE SYMMETRIZED RAMAN TENSORS: DISCUSSION

In Chapter 2 it was shown that there existed at least two symmetry species for both the β and the γ Raman tensors which were physically distinct. The results of the previous section show that there are only two species in each case. Neither of the species can be further reduced in terms of a physical property.

The two tensors $\beta^{\{3\}}$ and $\gamma^{\{4\}}$ are tensors which are commonly termed "symmetric" tensors; that is, their components are invariant with respect to any permutation of their indices. It is, with one exception[10], on the basis of these tensors that the previously published selection rule tables[1,6,7] for nonlinear Raman scattering have been calculated. Strictly speaking, this other work is not correct, as the complete selection rules are determined by the properties of the complete tensors, which, as has been shown, are not "symmetric". When the exciting radiation is of low frequency and far away from resonance, it may be that only the symmetric parts are significant in the vibrational Raman effect; but under practical conditions, with excitation at optical frequencies ($\omega_{0,1,2,3} \sim 0.3\omega_{n_j n_0}$), the "non-symmetric" parts cannot be neglected.

From equations (3.4) and (3.7) we can deduce equations which describe the relationships between the components of the

†See Appendix IV .

tensors $\beta^{\{21\}}$ and $\gamma^{\{31\}}$:

$$\beta^{\{21\}}_{\rho\sigma\tau} + \beta^{\{21\}}_{\tau\rho\sigma} + \beta^{\{21\}}_{\sigma\tau\rho} = 0$$

and

$$\gamma^{\{31\}}_{\rho\sigma\tau\nu} + \gamma^{\{31\}}_{\nu\rho\sigma\tau} + \gamma^{\{31\}}_{\tau\nu\rho\sigma} + \gamma^{\{31\}}_{\sigma\tau\nu\rho} = 0$$

These equations are an expression of the obvious fact that neither tensor contains a totally symmetric part. From these equations, detailed relations between the components may be found. For example, $\beta^{\{21\}}_{ijj} + 2\beta^{\{21\}}_{jji} = 0$ and $\beta^{\{21\}}_{iii} = 0$. All of the symmetrized tensors retain symmetry properties of the parent tensors, which may, of course, be reconstituted by addition of symmetrized tensors.

For practical purposes, it is useful to know the number of independent components possessed by each of the symmetrized tensors. These numbers, which may be obtained either empirically or with the help of (3.1), are for $\beta^{\{3\}}$, $\beta^{\{21\}}$, $\gamma^{\{4\}}$, $\gamma^{\{31\}}$ respectively: 10, 8, 15, 15.

3.3 THE SELECTION RULES

The transformation properties of the $\beta^{\{3\}}$, $\beta^{\{21\}}$, $\gamma^{\{4\}}$ and $\gamma^{\{31\}}$ tensors have been calculated for the important molecular point groups, including the 32 crystallographic point groups, by the method of projection operators (see equation (3.2)). The distinction between the symmetrized tensors has been maintained firstly because the frequency dependence of the scattered intensity differs for processes involving different tensors, and secondly to allow comparison with and show deviations from the work of other authors. As

one would expect, the selection rules for the complete tensors may be obtained by adding, for each point group representation, the components of the symmetrized tensors transforming according to that representation. It should be noted that since the selection rules depend only on the rank and symmetry properties of the β and γ tensors, they are applicable to any process described by such tensors.

The selection rules for the nonlinear Raman effects are tabulated in Table I, together with those for ordinary Raman scattering. Two simplifications have been made in the presentation. Firstly, the symmetrized tensors have been represented as follows: $\alpha^{\{2\}}$, $\beta^{\{3\}}$ and $\gamma^{\{4\}}$ by α, β and γ; $\alpha^{\{1^2\}}$, $\beta^{\{21\}}$ and $\gamma^{\{31\}}$ by $\bar{\alpha}$, $\bar{\beta}$ and $\bar{\gamma}$. We will use this notation from here onwards. Secondly, the various linear combinations of the β, $\bar{\beta}$, γ and $\bar{\gamma}$ tensor components have been replaced by numerically subscripted symbols. The correspondence between these two representations is given in Table II, which immediately follows Table I.

To further simplify Table I, groups which contain inversion symmetry have been omitted. These groups are always equal to the direct product of the group C_i and another (parent) point group; the selection rules for centrosymmetric groups may be obtained from the parent group by application of the following rules:

(1) The α, $\bar{\alpha}$, γ and $\bar{\gamma}$ tensors always transform according to the even (or g) representations and the β and $\bar{\beta}$ tensors according to the odd (or u) representations;

(2) the linear combinations of tensor components are not altered by the addition of inversion symmetry;

TABLE I

Transformation properties of the tensors describing two-, three-, and four-photon Raman scattering.

A. The groups C_s and C_n ($n=2, 3, 4, 5, 6$)

C_s	A'	$\alpha_{xx}, \alpha_{yy}, \alpha_{zz}, \alpha_{xy}$	$\bar{\alpha}_{xy}$	$\beta_1, \beta_2, \beta_4, \beta_6, \beta_8, \beta_9$	$\bar{\beta}_1, \bar{\beta}_3, \bar{\beta}_5, \bar{\beta}_6$	$\gamma_1, \gamma_2, \gamma_3, \gamma_4, \gamma_5, \gamma_6, \gamma_7, \gamma_9, \gamma_{15}$	$\bar{\gamma}_1, \bar{\gamma}_3, \bar{\gamma}_7, \bar{\gamma}_8, \bar{\gamma}_9, \bar{\gamma}_{10}, \bar{\gamma}_{11}$
	A''	α_{yz}, α_{zx}	$\bar{\alpha}_{yz}, \bar{\alpha}_{zx}$	$\beta_3, \beta_5, \beta_7, \beta_{10}$	$\bar{\beta}_2, \bar{\beta}_4, \bar{\beta}_7, \bar{\beta}_8$	$\gamma_8, \gamma_{10}, \gamma_{11}, \gamma_{12}, \gamma_{13}, \gamma_{14}$	$\bar{\gamma}_2, \bar{\gamma}_4, \bar{\gamma}_5, \bar{\gamma}_6, \bar{\gamma}_{12}, \bar{\gamma}_{13}, \bar{\gamma}_{14}, \bar{\gamma}_{15}$
C_2	A	$\alpha_{xx}, \alpha_{yy}, \alpha_{zz}, \alpha_{xy}$	$\bar{\alpha}_{xy}$	$\beta_3, \beta_5, \beta_7, \beta_{10}$	$\bar{\beta}_2, \bar{\beta}_4, \bar{\beta}_7, \bar{\beta}_8$	$\gamma_1, \gamma_2, \gamma_3, \gamma_4, \gamma_5, \gamma_6, \gamma_7, \gamma_9, \gamma_{15}$	$\bar{\gamma}_1, \bar{\gamma}_3, \bar{\gamma}_7, \bar{\gamma}_8, \bar{\gamma}_9, \bar{\gamma}_{10}, \bar{\gamma}_{11}$
	B	α_{yz}, α_{zx}	$\bar{\alpha}_{yz}, \bar{\alpha}_{zx}$	$\beta_1, \beta_2, \beta_4, \beta_6, \beta_8, \beta_9$	$\bar{\beta}_1, \bar{\beta}_3, \bar{\beta}_5, \bar{\beta}_6$	$\gamma_8, \gamma_{10}, \gamma_{11}, \gamma_{12}, \gamma_{13}, \gamma_{14}$	$\bar{\gamma}_2, \bar{\gamma}_4, \bar{\gamma}_5, \bar{\gamma}_6, \bar{\gamma}_{12}, \bar{\gamma}_{13}, \bar{\gamma}_{14}, \bar{\gamma}_{15}$
C_3	A	$\alpha_{xx}+\alpha_{yy}, \alpha_{zz}$	$\bar{\alpha}_{xy}$	$\beta_3, \beta_{13}, \beta_{19}, \beta_{20}$	$\bar{\beta}_{11}, \bar{\beta}_{16}$	$\gamma_3, \gamma_{20}, \gamma_{22}, \gamma_{34}, \gamma_{35}$	$\bar{\gamma}_{19}, \bar{\gamma}_{23}, \bar{\gamma}_{29}, \bar{\gamma}_{34}, \bar{\gamma}_{35}$
	E	$(\alpha_{xx}-\alpha_{yy}, \alpha_{xy})$, $(\alpha_{yz}, \alpha_{zx})$	$(\bar{\alpha}_{yz}, \bar{\alpha}_{zx})$	(β_8, β_9), (β_{10}, β_{16}), (β_{17}, β_{18})	$(\bar{\beta}_1, \bar{\beta}_3)$, $(\bar{\beta}_5, \bar{\beta}_6)$, $(\bar{\beta}_{14}, \bar{\beta}_{15})$	$(\gamma_{11}, \gamma_{12})$, $(\gamma_{15}, \gamma_{23})$, $(\gamma_{17}, \gamma_{26})$, $(\gamma_{21}, \gamma_{29})$, $(\gamma_{32}, \gamma_{33})$	$(\bar{\gamma}_5, \bar{\gamma}_6)$, $(\bar{\gamma}_7, \bar{\gamma}_{16})$, $(\bar{\gamma}_{12}, \bar{\gamma}_{15})$, $(\bar{\gamma}_{22}, \bar{\gamma}_{26})$, $(\bar{\gamma}_{32}, \bar{\gamma}_{33})$
C_4	A	$\alpha_{xx}+\alpha_{yy}, \alpha_{zz}$	$\bar{\alpha}_{xy}$	β_3, β_{13}	$\bar{\beta}_{11}, \bar{\beta}_{16}$	$\gamma_3, \gamma_4, \gamma_{16}, \gamma_{22}, \gamma_{29}$	$\bar{\gamma}_{19}, \bar{\gamma}_{23}, \bar{\gamma}_{29}$
	B	$\alpha_{xx}-\alpha_{yy}, \alpha_{xy}$		β_{10}, β_{16}	$\bar{\beta}_{14}, \bar{\beta}_{15}$	$\gamma_{15}, \gamma_{17}, \gamma_{23}, \gamma_{26}$	$\bar{\gamma}_7, \bar{\gamma}_{16}, \bar{\gamma}_{22}, \bar{\gamma}_{26}$
	E	$(\alpha_{yz}, \alpha_{zx})$	$(\bar{\alpha}_{yz}, \bar{\alpha}_{zx})$	(β_1, β_2), (β_4, β_6), (β_8, β_9)	$(\bar{\beta}_1, \bar{\beta}_3)$, $(\bar{\beta}_5, \bar{\beta}_6)$	(γ_8, γ_{10}), $(\gamma_{11}, \gamma_{12})$, $(\gamma_{13}, \gamma_{14})$	$(\bar{\gamma}_2, \bar{\gamma}_4)$, $(\bar{\gamma}_5, \bar{\gamma}_6)$, $(\bar{\gamma}_{12}, \bar{\gamma}_{15})$, $(\bar{\gamma}_{13}, \bar{\gamma}_{14})$
C_5	A	$\alpha_{xx}+\alpha_{yy}, \alpha_{zz}$	$\bar{\alpha}_{xy}$	β_3, β_{13}	$\bar{\beta}_{11}, \bar{\beta}_{16}$	$\gamma_3, \gamma_{20}, \gamma_{22}$	$\bar{\gamma}_{19}, \bar{\gamma}_{23}, \bar{\gamma}_{29}$
	E_1	$(\alpha_{yz}, \alpha_{zx})$	$(\bar{\alpha}_{yz}, \bar{\alpha}_{zx})$	(β_8, β_9), (β_{17}, β_{18})	$(\bar{\beta}_1, \bar{\beta}_3)$, $(\bar{\beta}_5, \bar{\beta}_6)$	$(\gamma_{11}, \gamma_{12})$, $(\gamma_{21}, \gamma_{29})$, $(\gamma_{32}, \gamma_{33})$	$(\bar{\gamma}_5, \bar{\gamma}_6)$, $(\bar{\gamma}_{12}, \bar{\gamma}_{15})$, $(\bar{\gamma}_{32}, \bar{\gamma}_{33})$
	E_2	$(\alpha_{xx}-\alpha_{yy}, \alpha_{xy})$		(β_{10}, β_{16}), (β_{19}, β_{20})	$(\bar{\beta}_{14}, \bar{\beta}_{15})$	$(\gamma_{15}, \gamma_{23})$, $(\gamma_{17}, \gamma_{26})$, $(\gamma_{34}, \gamma_{35})$	$(\bar{\gamma}_7, \bar{\gamma}_{16})$, $(\bar{\gamma}_{22}, \bar{\gamma}_{26})$, $(\bar{\gamma}_{34}, \bar{\gamma}_{35})$
C_6	A	$\alpha_{xx}+\alpha_{yy}, \alpha_{zz}$	$\bar{\alpha}_{xy}$	β_3, β_{13}	$\bar{\beta}_{11}, \bar{\beta}_{16}$	$\gamma_3, \gamma_{20}, \gamma_{22}$	$\bar{\gamma}_{19}, \bar{\gamma}_{23}, \bar{\gamma}_{29}$
	B			β_{19}, β_{20}		γ_{34}, γ_{35}	$\bar{\gamma}_{34}, \bar{\gamma}_{35}$
	E_1	$(\alpha_{yz}, \alpha_{zx})$	$(\bar{\alpha}_{yz}, \bar{\alpha}_{zx})$	(β_8, β_9), (β_{17}, β_{18})	$(\bar{\beta}_1, \bar{\beta}_3)$, $(\bar{\beta}_5, \bar{\beta}_6)$	$(\gamma_{11}, \gamma_{12})$, $(\gamma_{32}, \gamma_{33})$	$(\bar{\gamma}_5, \bar{\gamma}_6)$, $(\bar{\gamma}_{12}, \bar{\gamma}_{15})$, $(\bar{\gamma}_{32}, \bar{\gamma}_{33})$
	E_2	$(\alpha_{xx}-\alpha_{yy}, \alpha_{xy})$		(β_{10}, β_{16})	$(\bar{\beta}_{14}, \bar{\beta}_{15})$	$(\gamma_{15}, \gamma_{23})$, $(\gamma_{17}, \gamma_{26})$, $(\gamma_{21}, \gamma_{29})$	$(\bar{\gamma}_7, \bar{\gamma}_{16})$, $(\bar{\gamma}_{22}, \bar{\gamma}_{26})$

B. The groups D_n ($n=2, 3, 4, 5, 6$)

D_2	A	$\alpha_{xx}, \alpha_{yy}, \alpha_{zz}$		β_{10}	$\bar{\beta}_7, \bar{\beta}_8$	$\gamma_1, \gamma_2, \gamma_3, \gamma_4, \gamma_5, \gamma_6$	$\bar{\gamma}_7, \bar{\gamma}_8, \bar{\gamma}_9$
	B_1	α_{xy}	$\bar{\alpha}_{xy}$	$\beta_3, \beta_5, \beta_7$	$\bar{\beta}_2, \bar{\beta}_4$	$\gamma_7, \gamma_9, \gamma_{15}$	$\bar{\gamma}_1, \bar{\gamma}_3, \bar{\gamma}_{10}, \bar{\gamma}_{11}$
	B_2	α_{zx}	$\bar{\alpha}_{zx}$	$\beta_2, \beta_4, \beta_9$	$\bar{\beta}_1, \bar{\beta}_6$	$\gamma_8, \gamma_{11}, \gamma_{14}$	$\bar{\gamma}_2, \bar{\gamma}_5, \bar{\gamma}_{14}, \bar{\gamma}_{15}$
	B_3	α_{yz}	$\bar{\alpha}_{yz}$	$\beta_1, \beta_6, \beta_8$	$\bar{\beta}_3, \bar{\beta}_5$	$\gamma_{10}, \gamma_{12}, \gamma_{13}$	$\bar{\gamma}_4, \bar{\gamma}_6, \bar{\gamma}_{12}, \bar{\gamma}_{13}$
D_3	A_1[a]	$\alpha_{xx}+\alpha_{yy}, \alpha_{zz}$		β_{19}	$\bar{\beta}_{16}$	$\gamma_3, \gamma_{20}, \gamma_{22}, \gamma_{35}$	$\bar{\gamma}_{23}, \bar{\gamma}_{35}$
	A_2[a]		$\bar{\alpha}_{xy}$	$\beta_3, \beta_{13}, \beta_{20}$	$\bar{\beta}_{11}$	γ_{34}	$\bar{\gamma}_{19}, \bar{\gamma}_{29}, \bar{\gamma}_{34}$
	E	$(\alpha_{xx}-\alpha_{yy}, \alpha_{xy})$, $(\alpha_{yz}, \alpha_{zx})$	$(\bar{\alpha}_{yz}, \bar{\alpha}_{zx})$	(β_8, β_9), (β_{10}, β_{16}), (β_{17}, β_{18})	$(\bar{\beta}_1, \bar{\beta}_3)$, $(\bar{\beta}_5, \bar{\beta}_6)$, $(\bar{\beta}_{14}, \bar{\beta}_{15})$	$(\gamma_{11}, \gamma_{12})$, $(\gamma_{15}, \gamma_{23})$, $(\gamma_{17}, \gamma_{26})$, $(\gamma_{21}, \gamma_{29})$, $(\gamma_{32}, \gamma_{33})$	$(\bar{\gamma}_5, \bar{\gamma}_6)$, $(\bar{\gamma}_7, \bar{\gamma}_{16})$, $(\bar{\gamma}_{12}, \bar{\gamma}_{15})$, $(\bar{\gamma}_{22}, \bar{\gamma}_{26})$, $(\bar{\gamma}_{32}, \bar{\gamma}_{33})$
D_4	A_1	$\alpha_{xx}+\alpha_{yy}, \alpha_{zz}$			$\bar{\beta}_{16}$	$\gamma_3, \gamma_4, \gamma_{16}, \gamma_{22}$	$\bar{\gamma}_{23}$
	A_2		$\bar{\alpha}_{xy}$	β_3, β_{13}	$\bar{\beta}_{11}$	γ_{29}	$\bar{\gamma}_{19}, \bar{\gamma}_{29}$
	B_1	$\alpha_{xx}-\alpha_{yy}$		β_{10}	$\bar{\beta}_{15}$	γ_{17}, γ_{23}	$\bar{\gamma}_7, \bar{\gamma}_{22}$
	B_2	α_{xy}		β_{16}	$\bar{\beta}_{14}$	γ_{15}, γ_{26}	$\bar{\gamma}_{16}, \bar{\gamma}_{26}$
	E	$(\alpha_{yz}, \alpha_{zx})$	$(\bar{\alpha}_{yz}, \bar{\alpha}_{zx})$	(β_1, β_2), (β_4, β_6), (β_8, β_9)	$(\bar{\beta}_1, \bar{\beta}_3)$, $(\bar{\beta}_5, \bar{\beta}_6)$	(γ_8, γ_{10}), $(\gamma_{11}, \gamma_{12})$, $(\gamma_{13}, \gamma_{14})$	$(\bar{\gamma}_2, \bar{\gamma}_4)$, $(\bar{\gamma}_5, \bar{\gamma}_6)$, $(\bar{\gamma}_{12}, \bar{\gamma}_{15})$, $(\bar{\gamma}_{13}, \bar{\gamma}_{14})$
D_5	A_1	$\alpha_{xx}+\alpha_{yy}, \alpha_{zz}$			$\bar{\beta}_{16}$	$\gamma_3, \gamma_{20}, \gamma_{22}$	$\bar{\gamma}_{23}$
	A_2		$\bar{\alpha}_{xy}$	β_3, β_{13}	$\bar{\beta}_{11}$		$\bar{\gamma}_{19}, \bar{\gamma}_{29}$
	E_1	$(\alpha_{yz}, \alpha_{zx})$	$(\bar{\alpha}_{yz}, \bar{\alpha}_{zx})$	(β_8, β_9), (β_{17}, β_{18})	$(\bar{\beta}_1, \bar{\beta}_3)$, $(\bar{\beta}_5, \bar{\beta}_6)$	$(\gamma_{11}, \gamma_{12})$, $(\gamma_{21}, \gamma_{29})$, $(\gamma_{32}, \gamma_{33})$	$(\bar{\gamma}_5, \bar{\gamma}_6)$, $(\bar{\gamma}_{12}, \bar{\gamma}_{15})$, $(\bar{\gamma}_{32}, \bar{\gamma}_{33})$
	E_2	$(\alpha_{xx}-\alpha_{yy}, \alpha_{xy})$		(β_{10}, β_{16}), (β_{19}, β_{20})	$(\bar{\beta}_{14}, \bar{\beta}_{15})$	$(\gamma_{15}, \gamma_{23})$, $(\gamma_{17}, \gamma_{26})$, $(\gamma_{34}, \gamma_{35})$	$(\bar{\gamma}_7, \bar{\gamma}_{16})$, $(\bar{\gamma}_{22}, \bar{\gamma}_{26})$, $(\bar{\gamma}_{34}, \bar{\gamma}_{35})$

D_6	A_1	$\alpha_{xx}+\alpha_{yy}, \alpha_{zz}$			$\bar{\beta}_{16}$	$\gamma_3, \gamma_{20}, \gamma_{22}$	$\bar{\gamma}_{23}$
	A_2		$\bar{\alpha}_{xy}$	β_3, β_{13}	$\bar{\beta}_{11}$		$\bar{\gamma}_{19}, \bar{\gamma}_{29}$
	B_1[b]			β_{19}		γ_{35}	$\bar{\gamma}_{35}$
	B_2[b]			β_{20}		γ_{34}	$\bar{\gamma}_{34}$
	E_1	$(\alpha_{yz}, \alpha_{zx})$	$(\bar{\alpha}_{yz}, \bar{\alpha}_{zx})$	$(\beta_8, \beta_9), (\beta_{17}, \beta_{18})$	$(\bar{\beta}_1, \bar{\beta}_3), (\bar{\beta}_5, \bar{\beta}_6)$	$(\gamma_{11}, \gamma_{12}), (\gamma_{32}, \gamma_{33})$	$(\bar{\gamma}_5, \bar{\gamma}_6), (\bar{\gamma}_{12}, \bar{\gamma}_{15}), (\bar{\gamma}_{32}, \bar{\gamma}_{33})$
	E_2	$(\alpha_{xx}-\alpha_{yy}, \alpha_{xy})$		(β_{10}, β_{16})	$(\bar{\beta}_{14}, \bar{\beta}_{15})$	$(\gamma_{15}, \gamma_{23}), (\gamma_{17}, \gamma_{26}), (\gamma_{21}, \gamma_{29})$	$(\bar{\gamma}_7, \bar{\gamma}_{16}), (\bar{\gamma}_{22}, \bar{\gamma}_{26})$
				C. The groups C_{nv} ($n=2, 3, 4, 5, 6$)			
C_{2v}	A_1	$\alpha_{xx}, \alpha_{yy}, \alpha_{zz}$		$\beta_3, \beta_5, \beta_7$	$\bar{\beta}_2, \bar{\beta}_4$	$\gamma_1, \gamma_2, \gamma_3, \gamma_4, \gamma_5, \gamma_6$	$\bar{\gamma}_7, \bar{\gamma}_8, \bar{\gamma}_9$
	A_2	α_{xy}	$\bar{\alpha}_{xy}$	β_{10}	$\bar{\beta}_7, \bar{\beta}_8$	$\gamma_7, \gamma_9, \gamma_{15}$	$\bar{\gamma}_1, \bar{\gamma}_3, \bar{\gamma}_{10}, \bar{\gamma}_{11}$
	B_1	α_{zx}	$\bar{\alpha}_{zx}$	$\beta_1, \beta_6, \beta_8$	$\bar{\beta}_3, \bar{\beta}_5$	$\gamma_8, \gamma_{11}, \gamma_{14}$	$\bar{\gamma}_2, \bar{\gamma}_5, \bar{\gamma}_{14}, \bar{\gamma}_{15}$
	B_2	α_{yz}	$\bar{\alpha}_{yz}$	$\beta_2, \beta_4, \beta_9$	$\bar{\beta}_1, \bar{\beta}_6$	$\gamma_{10}, \gamma_{12}, \gamma_{13}$	$\bar{\gamma}_4, \bar{\gamma}_6, \bar{\gamma}_{12}, \bar{\gamma}_{13}$
C_{3v}	A_1[c]	$\alpha_{xx}+\alpha_{yy}, \alpha_{zz}$		$\beta_3, \beta_{13}, \beta_{19}$	$\bar{\beta}_{11}$	$\gamma_3, \gamma_{20}, \gamma_{22}, \gamma_{34}$	$\bar{\gamma}_{23}, \bar{\gamma}_{34}$
	A_2[c]		$\bar{\alpha}_{xy}$	β_{20}	$\bar{\beta}_{16}$	γ_{35}	$\bar{\gamma}_{19}, \bar{\gamma}_{29}, \bar{\gamma}_{35}$
	E	$(\alpha_{xx}-\alpha_{yy}, \alpha_{xy}), (\alpha_{yz}, \alpha_{zx})$	$(\bar{\alpha}_{yz}, \bar{\alpha}_{zx})$	$(\beta_8, \beta_9), (\beta_{10}, \beta_{16}), (\beta_{17}, \beta_{18})$	$(\bar{\beta}_1, \bar{\beta}_3), (\bar{\beta}_5, \bar{\beta}_6), (\bar{\beta}_{14}, \bar{\beta}_{15})$	$(\gamma_{11}, \gamma_{12}), (\gamma_{15}, \gamma_{23}), (\gamma_{17}, \gamma_{26}), (\gamma_{21}, \gamma_{29}), (\gamma_{32}, \gamma_{33})$	$(\bar{\gamma}_5, \bar{\gamma}_6), (\bar{\gamma}_7, \bar{\gamma}_{16}), (\bar{\gamma}_{12}, \bar{\gamma}_{15}), (\bar{\gamma}_{22}, \bar{\gamma}_{26}), (\bar{\gamma}_{32}, \bar{\gamma}_{33})$
C_{4v}	A_1	$\alpha_{xx}+\alpha_{yy}, \alpha_{zz}$		β_3, β_{13}	$\bar{\beta}_{11}$	$\gamma_3, \gamma_4, \gamma_{16}, \gamma_{22}$	$\bar{\gamma}_{23}$
	A_2		$\bar{\alpha}_{xy}$		$\bar{\beta}_{16}$	γ_{29}	$\bar{\gamma}_{19}, \bar{\gamma}_{29}$
	B_1	$\alpha_{xx}-\alpha_{yy}$		β_{16}	$\bar{\beta}_{14}$	γ_{17}, γ_{23}	$\bar{\gamma}_7, \bar{\gamma}_{22}$
	B_2	α_{xy}		β_{10}	$\bar{\beta}_{15}$	γ_{15}, γ_{26}	$\bar{\gamma}_{16}, \bar{\gamma}_{26}$
	E	$(\alpha_{yz}, \alpha_{zx})$	$(\bar{\alpha}_{yz}, \bar{\alpha}_{zx})$	$(\beta_1, \beta_2), (\beta_4, \beta_6), (\beta_8, \beta_9)$	$(\bar{\beta}_1, \bar{\beta}_3), (\bar{\beta}_5, \bar{\beta}_6)$	$(\gamma_8, \gamma_{10}), (\gamma_{11}, \gamma_{12}), (\gamma_{13}, \gamma_{14})$	$(\bar{\gamma}_2, \bar{\gamma}_4), (\bar{\gamma}_5, \bar{\gamma}_6), (\bar{\gamma}_{12}, \bar{\gamma}_{15}), (\bar{\gamma}_{13}, \bar{\gamma}_{14})$
C_{5v}	A_1	$\alpha_{xx}+\alpha_{yy}, \alpha_{zz}$		β_3, β_{13}	$\bar{\beta}_{11}$	$\gamma_3, \gamma_{20}, \gamma_{22}$	$\bar{\gamma}_{23}$
	A_2		$\bar{\alpha}_{xy}$		$\bar{\beta}_{16}$		$\bar{\gamma}_{19}, \bar{\gamma}_{29}$
	E_1	$(\alpha_{yz}, \alpha_{zx})$	$(\bar{\alpha}_{yz}, \bar{\alpha}_{zx})$	$(\beta_8, \beta_9), (\beta_{17}, \beta_{18})$	$(\bar{\beta}_1, \bar{\beta}_3), (\bar{\beta}_5, \bar{\beta}_6)$	$(\gamma_{11}, \gamma_{12}), (\gamma_{21}, \gamma_{29}), (\gamma_{32}, \gamma_{33})$	$(\bar{\gamma}_5, \bar{\gamma}_6), (\bar{\gamma}_{12}, \bar{\gamma}_{15}), (\bar{\gamma}_{32}, \bar{\gamma}_{33})$
	E_2	$(\alpha_{xx}-\alpha_{yy}, \alpha_{xy})$		$(\beta_{10}, \beta_{16}), (\beta_{19}, \beta_{20})$	$(\bar{\beta}_{14}, \bar{\beta}_{15})$	$(\gamma_{15}, \gamma_{23}), (\gamma_{17}, \gamma_{26}), (\gamma_{34}, \gamma_{35})$	$(\bar{\gamma}_7, \bar{\gamma}_{16}), (\bar{\gamma}_{22}, \bar{\gamma}_{26}), (\bar{\gamma}_{34}, \bar{\gamma}_{35})$
C_{6v}	A_1	$\alpha_{xx}+\alpha_{yy}, \alpha_{zz}$		β_3, β_{13}	$\bar{\beta}_{11}$	$\gamma_3, \gamma_{20}, \gamma_{22}$	$\bar{\gamma}_{23}$
	A_2		$\bar{\alpha}_{xy}$		$\bar{\beta}_{16}$		$\bar{\gamma}_{19}, \bar{\gamma}_{29}$
	B_1[c]			β_{19}		γ_{34}	$\bar{\gamma}_{34}$
	B_2[c]			β_{20}		γ_{35}	$\bar{\gamma}_{35}$
	E_1	$(\alpha_{yz}, \alpha_{zx})$	$(\bar{\alpha}_{yz}, \bar{\alpha}_{zx})$	$(\beta_8, \beta_9), (\beta_{17}, \beta_{18})$	$(\bar{\beta}_1, \bar{\beta}_3), (\bar{\beta}_5, \bar{\beta}_6)$	$(\gamma_{11}, \gamma_{12}), (\gamma_{32}, \gamma_{33})$	$(\bar{\gamma}_5, \bar{\gamma}_6), (\bar{\gamma}_{12}, \bar{\gamma}_{15}), (\bar{\gamma}_{32}, \bar{\gamma}_{33})$
	E_2	$(\alpha_{xx}-\alpha_{yy}, \alpha_{xy})$		(β_{10}, β_{16})	$(\bar{\beta}_{14}, \bar{\beta}_{15})$	$(\gamma_{15}, \gamma_{23}), (\gamma_{17}, \gamma_{26}), (\gamma_{21}, \gamma_{29})$	$(\bar{\gamma}_7, \bar{\gamma}_{16}), (\bar{\gamma}_{22}, \bar{\gamma}_{26})$
				D. The groups C_{nh} ($n=3, 5$)			
C_{3h}	A'	$\alpha_{xx}+\alpha_{yy}, \alpha_{zz}$	$\bar{\alpha}_{xy}$	β_{19}, β_{20}		$\gamma_3, \gamma_{20}, \gamma_{22}$	$\bar{\gamma}_{19}, \bar{\gamma}_{23}, \bar{\gamma}_{29}$
	E'	$(\alpha_{xx}-\alpha_{yy}, \alpha_{xy})$		$(\beta_8, \beta_9), (\beta_{17}, \beta_{18})$	$(\bar{\beta}_1, \bar{\beta}_3), (\bar{\beta}_5, \bar{\beta}_6)$	$(\gamma_{15}, \gamma_{23}), (\gamma_{17}, \gamma_{26}), (\gamma_{21}, \gamma_{29})$	$(\bar{\gamma}_7, \bar{\gamma}_{16}), (\bar{\gamma}_{22}, \bar{\gamma}_{26})$
	A''			β_3, β_{13}	$\bar{\beta}_{11}, \bar{\beta}_{16}$	γ_{34}, γ_{35}	$\bar{\gamma}_{34}, \bar{\gamma}_{35}$
	E''	$(\alpha_{yz}, \alpha_{zx})$	$(\bar{\alpha}_{yz}, \bar{\alpha}_{zx})$	(β_{10}, β_{16})	$(\bar{\beta}_{14}, \bar{\beta}_{15})$	$(\gamma_{11}, \gamma_{12}), (\gamma_{32}, \gamma_{33})$	$(\bar{\gamma}_5, \bar{\gamma}_6), (\bar{\gamma}_{12}, \bar{\gamma}_{15}), (\bar{\gamma}_{32}, \bar{\gamma}_{33})$
C_{5h}	A'	$\alpha_{xx}+\alpha_{yy}, \alpha_{zz}$	$\bar{\alpha}_{xy}$			$\gamma_3, \gamma_{20}, \gamma_{22}$	$\bar{\gamma}_{19}, \bar{\gamma}_{23}, \bar{\gamma}_{29}$
	E_1'			$(\beta_8, \beta_9), (\beta_{17}, \beta_{18})$	$(\bar{\beta}_1, \bar{\beta}_3), (\bar{\beta}_5, \bar{\beta}_6)$	$(\gamma_{21}, \gamma_{29})$	
	E_2'	$(\alpha_{xx}-\alpha_{yy}, \alpha_{xy})$		(β_{19}, β_{20})		$(\gamma_{15}, \gamma_{23}), (\gamma_{17}, \gamma_{26})$	$(\bar{\gamma}_7, \bar{\gamma}_{16}), (\bar{\gamma}_{22}, \bar{\gamma}_{26})$

TABLE I (*Continued*)

	A''			β_3, β_{13}	$\bar{\beta}_{11}, \bar{\beta}_{16}$		
	E_1''	$(\alpha_{yz}, \alpha_{zx})$	$(\bar{\alpha}_{yz}, \bar{\alpha}_{zx})$			$(\gamma_{11}, \gamma_{12}), (\gamma_{32}, \gamma_{33})$	$(\bar{\gamma}_5, \bar{\gamma}_6), (\bar{\gamma}_{12}, \bar{\gamma}_{15}), (\bar{\gamma}_{32}, \bar{\gamma}_{33})$
	E_2''			(β_{10}, β_{16})	$(\bar{\beta}_{14}, \bar{\beta}_{15})$	$(\gamma_{34}, \gamma_{35})$	$(\bar{\gamma}_{34}, \bar{\gamma}_{35})$
			E. The groups D_{nh} $(n=3, 5)$				
D_{3h}	A_1' [a]	$\alpha_{xx}+\alpha_{yy}, \alpha_{zz}$		β_{19}		$\gamma_3, \gamma_{20}, \gamma_{22}$	$\bar{\gamma}_{23}$
	A_2' [a]		$\bar{\alpha}_{xy}$	β_{20}			$\bar{\gamma}_{19}, \bar{\gamma}_{29}$
	E'	$(\alpha_{xx}-\alpha_{yy}, \alpha_{xy})$		$(\beta_8, \beta_9), (\beta_{17}, \beta_{18})$	$(\bar{\beta}_1, \bar{\beta}_3), (\bar{\beta}_5, \bar{\beta}_6)$	$(\gamma_{15}, \gamma_{23}), (\gamma_{17}, \gamma_{26}), (\gamma_{21}, \gamma_{29})$	$(\bar{\gamma}_7, \bar{\gamma}_{16}), (\bar{\gamma}_{22}, \bar{\gamma}_{26})$
	A_1''				$\bar{\beta}_{16}$	γ_{35}	$\bar{\gamma}_{35}$
	A_2''			β_3, β_{13}	$\bar{\beta}_{11}$	γ_{34}	$\bar{\gamma}_{34}$
	E''	$(\alpha_{yz}, \alpha_{zx})$	$(\bar{\alpha}_{yz}, \bar{\alpha}_{zx})$	(β_{10}, β_{16})	$(\bar{\beta}_{14}, \bar{\beta}_{15})$	$(\gamma_{11}, \gamma_{12}), (\gamma_{32}, \gamma_{33})$	$(\bar{\gamma}_5, \bar{\gamma}_6), (\bar{\gamma}_{12}, \bar{\gamma}_{15}), (\bar{\gamma}_{32}, \bar{\gamma}_{33})$
D_{5h}	A_1'	$\alpha_{xx}+\alpha_{yy}, \alpha_{zz}$				$\gamma_3, \gamma_{20}, \gamma_{22}$	$\bar{\gamma}_{23}$
	A_2'		$\bar{\alpha}_{xy}$				$\bar{\gamma}_{19}, \bar{\gamma}_{29}$
	E_1'			$(\beta_8, \beta_9), (\beta_{17}, \beta_{18})$	$(\bar{\beta}_1, \bar{\beta}_3), (\bar{\beta}_5, \bar{\beta}_6)$	$(\gamma_{21}, \gamma_{29})$	
	E_2'	$(\alpha_{xx}-\alpha_{yy}, \alpha_{xy})$		(β_{19}, β_{20})		$(\gamma_{15}, \gamma_{23}), (\gamma_{17}, \gamma_{26})$	$(\bar{\gamma}_7, \bar{\gamma}_{16}), (\bar{\gamma}_{22}, \bar{\gamma}_{26})$
	A_1''				$\bar{\beta}_{16}$		
	A_2''			β_3, β_{13}	$\bar{\beta}_{11}$		
	E_1''	$(\alpha_{yz}, \alpha_{zx})$	$(\bar{\alpha}_{yz}, \bar{\alpha}_{zx})$			$(\gamma_{11}, \gamma_{12}), (\gamma_{32}, \gamma_{33})$	$(\bar{\gamma}_5, \bar{\gamma}_6), (\bar{\gamma}_{12}, \bar{\gamma}_{15}), (\bar{\gamma}_{32}, \bar{\gamma}_{33})$
	E_2''			(β_{10}, β_{16})	$(\bar{\beta}_{14}, \bar{\beta}_{15})$	$(\gamma_{34}, \gamma_{35})$	$(\bar{\gamma}_{34}, \bar{\gamma}_{35})$
			F. The groups D_{nd} $(n=2, 4, 6)$				
D_{2d}	A_1	$\alpha_{xx}+\alpha_{yy}, \alpha_{zz}$		β_{10}	$\bar{\beta}_{15}$	$\gamma_3, \gamma_4, \gamma_{16}, \gamma_{22}$	$\bar{\gamma}_{23}$
	A_2		$\bar{\alpha}_{xy}$	β_{16}	$\bar{\beta}_{14}$	γ_{29}	$\bar{\gamma}_{19}, \bar{\gamma}_{29}$
	B_1	$\alpha_{xx}-\alpha_{yy}$			$\bar{\beta}_{16}$	γ_{17}, γ_{23}	$\bar{\gamma}_7, \bar{\gamma}_{22}$
	B_2	α_{xy}		β_3, β_{13}	$\bar{\beta}_{11}$	γ_{15}, γ_{26}	$\bar{\gamma}_{16}, \bar{\gamma}_{26}$
	E	$(\alpha_{yz}, \alpha_{zx})$	$(\bar{\alpha}_{yz}, \bar{\alpha}_{zx})$	$(\beta_1, \beta_2), (\beta_4, \beta_6), (\beta_8, \beta_9)$	$(\bar{\beta}_1, \bar{\beta}_3), (\bar{\beta}_5, \bar{\beta}_6)$	$(\gamma_8, \gamma_{10}), (\gamma_{11}, \gamma_{12}), (\gamma_{13}, \gamma_{14})$	$(\bar{\gamma}_2, \bar{\gamma}_4), (\bar{\gamma}_5, \bar{\gamma}_6), (\bar{\gamma}_{12}, \bar{\gamma}_{15}), (\bar{\gamma}_{13}, \bar{\gamma}_{14})$
D_{4d}	A_1	$\alpha_{xx}+\alpha_{yy}, \alpha_{zz}$				$\gamma_3, \gamma_{20}, \gamma_{22}$	$\bar{\gamma}_{23}$
	A_2		$\bar{\alpha}_{xy}$				$\bar{\gamma}_{19}, \bar{\gamma}_{29}$
	B_1				$\bar{\beta}_{16}$	γ_{21}	
	B_2			β_3, β_{13}	$\bar{\beta}_{11}$	γ_{29}	
	E_1			$(\beta_8, \beta_9), (\beta_{17}, \beta_{18})$	$(\bar{\beta}_1, \bar{\beta}_3), (\bar{\beta}_5, \bar{\beta}_6)$	$(\gamma_{34}, \gamma_{35})$	$(\bar{\gamma}_{34}, \bar{\gamma}_{35})$
	E_2	$(\alpha_{xx}-\alpha_{yy}, \alpha_{xy})$		(β_{10}, β_{16})	$(\bar{\beta}_{14}, \bar{\beta}_{15})$	$(\gamma_{15}, \gamma_{23}), (\gamma_{17}, \gamma_{26})$	$(\bar{\gamma}_7, \bar{\gamma}_{16}), (\bar{\gamma}_{22}, \bar{\gamma}_{26})$
	E_3	$(\alpha_{yz}, \alpha_{zx})$	$(\bar{\alpha}_{yz}, \bar{\alpha}_{zx})$	(β_{19}, β_{20})		$(\gamma_{11}, \gamma_{12}), (\gamma_{32}, \gamma_{33})$	$(\bar{\gamma}_5, \bar{\gamma}_6), (\bar{\gamma}_{12}, \bar{\gamma}_{15}), (\bar{\gamma}_{32}, \bar{\gamma}_{33})$
D_{6d}	A_1	$\alpha_{xx}+\alpha_{yy}, \alpha_{zz}$				$\gamma_3, \gamma_{20}, \gamma_{22}$	$\bar{\gamma}_{23}$
	A_2		$\bar{\alpha}_{xy}$				$\bar{\gamma}_{19}, \bar{\gamma}_{29}$
	B_1				$\bar{\beta}_{16}$		
	B_2			β_3, β_{13}	$\bar{\beta}_{11}$		
	E_1			$(\beta_8, \beta_9), (\beta_{17}, \beta_{18})$	$(\bar{\beta}_1, \bar{\beta}_3), (\bar{\beta}_5, \bar{\beta}_6)$		
	E_2	$(\alpha_{xx}-\alpha_{yy}, \alpha_{xy})$				$(\gamma_{15}, \gamma_{23}), (\gamma_{17}, \gamma_{26})$	$(\bar{\gamma}_7, \bar{\gamma}_{16}), (\bar{\gamma}_{22}, \bar{\gamma}_{26})$
	E_3			(β_{19}, β_{20})		$(\gamma_{34}, \gamma_{35})$	$(\bar{\gamma}_{34}, \bar{\gamma}_{35})$

TABLE I (*Continued*)

	E_4			(β_{10}, β_{16})	$(\bar{\beta}_{14}, \bar{\beta}_{15})$	$(\gamma_{21}, \gamma_{29})$	
	E_5	$(\alpha_{yz}, \alpha_{zx})$	$(\bar{\alpha}_{yz}, \bar{\alpha}_{zx})$			$(\gamma_{11}, \gamma_{12})$, $(\gamma_{32}, \gamma_{33})$	$(\bar{\gamma}_5, \bar{\gamma}_6)$, $(\bar{\gamma}_{12}, \bar{\gamma}_{15})$, $(\bar{\gamma}_{32}, \bar{\gamma}_{33})$
				G. The groups S_n ($n=4, 8$)			
S_4	A	$\alpha_{xx}+\alpha_{yy}, \alpha_{zz}$	$\bar{\alpha}_{xy}$	β_{10}, β_{16}	$\bar{\beta}_{14}, \bar{\beta}_{15}$	$\gamma_3, \gamma_4, \gamma_{16}, \gamma_{22}, \gamma_{29}$	$\bar{\gamma}_{19}, \bar{\gamma}_{23}, \bar{\gamma}_{29}$
	B	$\alpha_{xx}-\alpha_{yy}, \alpha_{xy}$		β_3, β_{13}	$\bar{\beta}_{11}, \bar{\beta}_{16}$	$\gamma_{15}, \gamma_{17}, \gamma_{23}, \gamma_{26}$	$\bar{\gamma}_7, \bar{\gamma}_{16}, \bar{\gamma}_{22}, \bar{\gamma}_{26}$
	E	$(\alpha_{yz}, \alpha_{zx})$	$(\bar{\alpha}_{yz}, \bar{\alpha}_{zx})$	(β_1, β_2), (β_4, β_6), (β_8, β_9)	$(\bar{\beta}_1, \bar{\beta}_3)$, $(\bar{\beta}_5, \bar{\beta}_6)$	(γ_8, γ_{10}), $(\gamma_{11}, \gamma_{12})$, $(\gamma_{13}, \gamma_{14})$	$(\bar{\gamma}_2, \bar{\gamma}_7)$, $(\bar{\gamma}_5, \bar{\gamma}_6)$, $(\bar{\gamma}_{12}, \bar{\gamma}_{15})$, $(\bar{\gamma}_{13}, \bar{\gamma}_{14})$
S_8	A	$\alpha_{xx}+\alpha_{yy}, \alpha_{zz}$	$\bar{\alpha}_{xy}$			$\gamma_3, \gamma_{20}, \gamma_{22}$	$\bar{\gamma}_{19}, \bar{\gamma}_{23}, \bar{\gamma}_{29}$
	B			β_3, β_{13}	$\bar{\beta}_{11}, \bar{\beta}_{16}$	γ_{21}, γ_{29}	
	E_1			(β_8, β_9), (β_{17}, β_{18})	$(\bar{\beta}_1, \bar{\beta}_3)$, $(\bar{\beta}_5, \bar{\beta}_6)$	$(\gamma_{34}, \gamma_{35})$	$(\bar{\gamma}_{34}, \bar{\gamma}_{35})$
	E_2	$(\alpha_{xx}-\alpha_{yy}, \alpha_{xy})$		(β_{10}, β_{16})	$(\bar{\beta}_{14}, \bar{\beta}_{15})$	$(\gamma_{15}, \gamma_{23})$, (γ_1, γ_{26})	$(\bar{\gamma}_7, \bar{\gamma}_{16})$, $(\bar{\gamma}_{22}, \bar{\gamma}_{26})$
	E_3	$(\alpha_{yz}, \alpha_{zx})$	$(\bar{\alpha}_{yz}, \bar{\alpha}_{zx})$	(β_{19}, β_{20})		$(\gamma_{11}, \gamma_{12})$, $(\gamma_{32}, \gamma_{33})$	$(\bar{\gamma}_5, \bar{\gamma}_6)$, $(\bar{\gamma}_{12}, \bar{\gamma}_{15})$, $(\bar{\gamma}_{32}, \bar{\gamma}_{33})$
				H. The groups T, T_d and O			
T	A	$\alpha_{xx}+\alpha_{yy}+\alpha_{zz}$		β_{10}		γ_{18}, γ_{24}	$\bar{\gamma}_{24}$
	E	$(\alpha_{xx}+\alpha_{yy}-2\alpha_{zz}, \alpha_{xx}-\alpha_{yy})$			$(\bar{\beta}_{15}, \bar{\beta}_{16})$	$(\gamma_{17}, \gamma_{19})$, $(\gamma_{23}, \gamma_{25})$	$(\bar{\gamma}_{23}, \bar{\gamma}_{25})$
	F	$(\alpha_{xy}, \alpha_{yz}, \alpha_{zx})$	$(\bar{\alpha}_{xy}, \bar{\alpha}_{yz}, \bar{\alpha}_{zx})$	$(\beta_1, \beta_2, \beta_3)$, $(\beta_5, \beta_6, \beta_9)$, $(\beta_4, \beta_7, \beta_8)$	$(\bar{\beta}_2, \bar{\beta}_3, \bar{\beta}_6)$, $(\bar{\beta}_1, \bar{\beta}_4, \bar{\beta}_5)$	$(\gamma_7, \gamma_{10}, \gamma_{11})$, $(\gamma_8, \gamma_9, \gamma_{12})$, $(\gamma_{13}, \gamma_{14}, \gamma_{15})$	$(\bar{\gamma}_1, \bar{\gamma}_4, \bar{\gamma}_5)$, $(\bar{\gamma}_2, \bar{\gamma}_3, \bar{\gamma}_6)$, $(\bar{\gamma}_{10}, \bar{\gamma}_{12}, \bar{\gamma}_{14})$, $(\bar{\gamma}_{11}, \bar{\gamma}_{13}, \bar{\gamma}_{15})$
T_d	A_1	$\alpha_{xx}+\alpha_{yy}+\alpha_{zz}$		β_{10}		γ_{18}, γ_{24}	
	A_2						$\bar{\gamma}_{24}$
	E	$(\alpha_{xx}+\alpha_{yy}-2\alpha_{zz}, \alpha_{xx}-\alpha_{yy})$			$(\bar{\beta}_{15}, \bar{\beta}_{16})$	$(\gamma_{17}, \gamma_{19})$, $(\gamma_{23}, \gamma_{25})$	$(\bar{\gamma}_{23}, \bar{\gamma}_{25})$
	F_1		$(\bar{\alpha}_{xy}, \bar{\alpha}_{yz}, \bar{\alpha}_{zx})$	$(\beta_{14}, \beta_{15}, \beta_{16})$	$(\bar{\beta}_{12}, \bar{\beta}_{13}, \bar{\beta}_{14})$	$(\gamma_{29}, \gamma_{30}, \gamma_{31})$	$(\bar{\gamma}_{19}, \bar{\gamma}_{20}, \bar{\gamma}_{21})$, $(\bar{\gamma}_{29}, \bar{\gamma}_{30}, \bar{\gamma}_{31})$
	F_2	$(\alpha_{xy}, \alpha_{yz}, \alpha_{zx})$		$(\beta_1, \beta_2, \beta_3)$, $(\beta_{11}, \beta_{12}, \beta_{13})$	$(\bar{\beta}_9, \bar{\beta}_{10}, \bar{\beta}_{11})$	$(\gamma_{13}, \gamma_{14}, \gamma_{15})$, $(\gamma_{26}, \gamma_{27}, \gamma_{28})$	$(\bar{\gamma}_{16}, \bar{\gamma}_{17}, \bar{\gamma}_{18})$, $(\bar{\gamma}_{26}, \bar{\gamma}_{27}, \bar{\gamma}_{28})$
O	A_1	$\alpha_{xx}+\alpha_{yy}+\alpha_{zz}$				γ_{18}, γ_{24}	
	A_2			β_{10}			$\bar{\gamma}_{24}$
	E	$(\alpha_{xx}+\alpha_{yy}-2\alpha_{zz}, \alpha_{xx}-\alpha_{yy})$			$(\bar{\beta}_{15}, \bar{\beta}_{16})$	$(\gamma_{17}, \gamma_{19})$, $(\gamma_{23}, \gamma_{25})$	$(\bar{\gamma}_{23}, \bar{\gamma}_{25})$
	F_1		$(\bar{\alpha}_{xy}, \bar{\alpha}_{yz}, \bar{\alpha}_{zx})$	$(\beta_1, \beta_2, \beta_3)$, $(\beta_{11}, \beta_{12}, \beta_{13})$	$(\bar{\beta}_9, \bar{\beta}_{10}, \bar{\beta}_{11})$	$(\gamma_{29}, \gamma_{30}, \gamma_{31})$	$(\bar{\gamma}_{19}, \bar{\gamma}_{20}, \bar{\gamma}_{21})$, $(\bar{\gamma}_{29}, \bar{\gamma}_{30}, \bar{\gamma}_{31})$
	F_2	$(\alpha_{xy}, \alpha_{yz}, \alpha_{zx})$		$(\beta_{14}, \beta_{15}, \beta_{16})$	$(\bar{\beta}_{12}, \bar{\beta}_{13}, \bar{\beta}_{14})$	$(\gamma_{13}, \gamma_{14}, \gamma_{15})$, $(\gamma_{26}, \gamma_{27}, \gamma_{28})$	$(\bar{\gamma}_{16}, \bar{\gamma}_{17}, \bar{\gamma}_{18})$, $(\bar{\gamma}_{26}, \bar{\gamma}_{27}, \bar{\gamma}_{28})$
				I. The group $C_{\infty v}$			
$C_{\infty v}$	A_1	$\alpha_{xx}+\alpha_{yy}, \alpha_{zz}$		β_3, β_{13}	$\bar{\beta}_{11}$	$\gamma_3, \gamma_{20}, \gamma_{22}$	$\bar{\gamma}_{23}$
	A_2		$\bar{\alpha}_{xy}$		$\bar{\beta}_{16}$		$\bar{\gamma}_{19}, \bar{\gamma}_{29}$
	E_1	$(\alpha_{yz}, \alpha_{zx})$	$(\bar{\alpha}_{yz}, \bar{\alpha}_{zx})$	(β_8, β_9), (β_{17}, β_{18})	$(\bar{\beta}_1, \bar{\beta}_3)$, $(\bar{\beta}_5, \bar{\beta}_6)$	$(\gamma_{11}, \gamma_{12})$, $(\gamma_{32}, \gamma_{33})$	$(\bar{\gamma}_5, \bar{\gamma}_6)$, $(\bar{\gamma}_{12}, \bar{\gamma}_{15})$, $(\bar{\gamma}_{32}, \bar{\gamma}_{33})$
	E_2	$(\alpha_{xx}-\alpha_{yy}, \alpha_{xy})$		(β_{10}, β_{16})	$(\bar{\beta}_{14}, \bar{\beta}_{15})$	$(\gamma_{15}, \gamma_{23})$, $(\gamma_{17}, \gamma_{26})$	$(\bar{\gamma}_7, \bar{\gamma}_{16})$, $(\bar{\gamma}_{22}, \bar{\gamma}_{26})$
	E_3			(β_{19}, β_{20})		$(\gamma_{34}, \gamma_{35})$	$(\bar{\gamma}_{34}, \bar{\gamma}_{35})$
	E_4					$(\gamma_{21}, \gamma_{29})$	

[a] x axis along C_2. [b] x axis along C_2'. [c] x axis in σ_v.

TABLE II

Definition of the symbols used in Table I.

$\beta_1=\beta_{xxx}$	$\bar{\beta}_1=\bar{\beta}_{xxy}$
$\beta_2=\beta_{yyy}$	$\bar{\beta}_2=\bar{\beta}_{xxz}$
$\beta_3=\beta_{zzz}$	$\bar{\beta}_3=\bar{\beta}_{yyx}$
$\beta_4=\beta_{xxy}$	$\bar{\beta}_4=\bar{\beta}_{yyz}$
$\beta_5=\beta_{xxz}$	$\bar{\beta}_5=\bar{\beta}_{zzx}$
$\beta_6=\beta_{xyy}$	$\bar{\beta}_6=\bar{\beta}_{zzy}$
$\beta_7=\beta_{yyz}$	$\bar{\beta}_7=\bar{\beta}_{xyz}$
$\beta_8=\beta_{zzx}$	$\bar{\beta}_8=\bar{\beta}_{yzx}$
$\beta_9=\beta_{yzz}$	$\bar{\beta}_9=\bar{\beta}_{yyx}+\bar{\beta}_{zzx}$
$\beta_{10}=\beta_{xyz}$	$\bar{\beta}_{10}=\bar{\beta}_{xxy}+\bar{\beta}_{zzy}$
$\beta_{11}=\beta_{xyy}+\beta_{zzx}$	$\bar{\beta}_{11}=\bar{\beta}_{xxz}+\bar{\beta}_{yyz}$
$\beta_{12}=\beta_{xxy}+\beta_{yzz}$	$\bar{\beta}_{12}=\bar{\beta}_{yyx}-\bar{\beta}_{zzx}$
$\beta_{13}=\beta_{zxx}+\beta_{yyz}$	$\bar{\beta}_{13}=\bar{\beta}_{xxy}-\bar{\beta}_{zzy}$
$\beta_{14}=\beta_{xyy}-\beta_{zzx}$	$\bar{\beta}_{14}=\bar{\beta}_{xxz}-\bar{\beta}_{yyz}$
$\beta_{15}=\beta_{xxy}-\beta_{yzz}$	$\bar{\beta}_{15}=\bar{\beta}_{xyz}+\bar{\beta}_{yzx}$
$\beta_{16}=\beta_{zxx}-\beta_{yyz}$	$\bar{\beta}_{16}=\bar{\beta}_{xyz}-\bar{\beta}_{yzx}$
$\beta_{17}=\beta_{xxx}+\beta_{xyy}$	
$\beta_{18}=\beta_{yyy}+\beta_{xxy}$	
$\beta_{19}=\beta_{xxx}-3\beta_{xyy}$	
$\beta_{20}=\beta_{yyy}-3\beta_{xxy}$	
$\gamma_1=\gamma_{xxxx}$	$\bar{\gamma}_1=\bar{\gamma}_{xxxy}$
$\gamma_2=\gamma_{yyyy}$	$\bar{\gamma}_2=\bar{\gamma}_{xxxz}$
$\gamma_3=\gamma_{zzzz}$	$\bar{\gamma}_3=\bar{\gamma}_{yyyx}$
$\gamma_4=\gamma_{xxyy}$	$\bar{\gamma}_4=\bar{\gamma}_{yyyz}$
$\gamma_5=\gamma_{yyzz}$	$\bar{\gamma}_5=\bar{\gamma}_{zzzx}$
$\gamma_6=\gamma_{zzxx}$	$\bar{\gamma}_6=\bar{\gamma}_{zzzy}$
$\gamma_7=\gamma_{xxxy}$	$\bar{\gamma}_7=\bar{\gamma}_{xxyy}$
$\gamma_8=\gamma_{xxxz}$	$\bar{\gamma}_8=\bar{\gamma}_{yyzz}$
$\gamma_9=\gamma_{yyyx}$	$\bar{\gamma}_9=\bar{\gamma}_{zzxx}$
$\gamma_{10}=\gamma_{yyyz}$	$\bar{\gamma}_{10}=\bar{\gamma}_{xyzz}$
$\gamma_{11}=\gamma_{zzzx}$	$\bar{\gamma}_{11}=\bar{\gamma}_{yxzz}$
$\gamma_{12}=\gamma_{zzzy}$	$\bar{\gamma}_{12}=\bar{\gamma}_{yzxx}$
$\gamma_{13}=\gamma_{xxyz}$	$\bar{\gamma}_{13}=\bar{\gamma}_{zyxx}$
$\gamma_{14}=\gamma_{yyzx}$	$\bar{\gamma}_{14}=\bar{\gamma}_{zxyy}$
$\gamma_{15}=\gamma_{zzxy}$	$\bar{\gamma}_{15}=\bar{\gamma}_{xzyy}$
$\gamma_{16}=\gamma_{xxxx}+\gamma_{yyyy}$	$\bar{\gamma}_{16}=\bar{\gamma}_{xxxy}+\bar{\gamma}_{yyyx}$
$\gamma_{17}=\gamma_{xxxx}-\gamma_{yyyy}$	$\bar{\gamma}_{17}=\bar{\gamma}_{yyyz}+\bar{\gamma}_{zzzy}$
$\gamma_{18}=\gamma_{xxxx}+\gamma_{yyyy}+\gamma_{zzzz}$	$\bar{\gamma}_{18}=\bar{\gamma}_{zzzx}+\bar{\gamma}_{xxxz}$
$\gamma_{19}=\gamma_{xxxx}+\gamma_{yyyy}-2\gamma_{zzzz}$	$\bar{\gamma}_{19}=\bar{\gamma}_{xxxy}-\bar{\gamma}_{yyyx}$
$\gamma_{20}=\gamma_{xxxx}+2\gamma_{xxyy}+\gamma_{zzzz}$	$\bar{\gamma}_{20}=\bar{\gamma}_{yyyz}-\bar{\gamma}_{zzzy}$
$\gamma_{21}=\gamma_{xxxx}-6\gamma_{xxyy}+\gamma_{yyyy}$	$\bar{\gamma}_{21}=\bar{\gamma}_{zzzx}-\bar{\gamma}_{xxxz}$
$\gamma_{22}=\gamma_{yyzz}+\gamma_{zzxx}$	$\bar{\gamma}_{22}=\bar{\gamma}_{yyzz}+\bar{\gamma}_{zzxx}$
$\gamma_{23}=\gamma_{yyzz}-\gamma_{zzxx}$	$\bar{\gamma}_{23}=\bar{\gamma}_{yyzz}-\bar{\gamma}_{zzxx}$
$\gamma_{24}=\gamma_{xxyy}+\gamma_{yyzz}+\gamma_{zzxx}$	$\bar{\gamma}_{24}=\bar{\gamma}_{xxyy}+\bar{\gamma}_{yyzz}+\bar{\gamma}_{zzxx}$
$\gamma_{25}=\gamma_{yyzz}+\gamma_{zzxx}-2\gamma_{xxyy}$	$\bar{\gamma}_{25}=\bar{\gamma}_{yyzz}+\bar{\gamma}_{zzxx}-2\bar{\gamma}_{xxyy}$
$\gamma_{26}=\gamma_{xxxy}+\gamma_{yyyx}$	$\bar{\gamma}_{26}=\bar{\gamma}_{xyzz}+\bar{\gamma}_{yxzz}$
$\gamma_{27}=\gamma_{yyyz}+\gamma_{zzzy}$	$\bar{\gamma}_{27}=\bar{\gamma}_{yzxx}+\bar{\gamma}_{zyxx}$
$\gamma_{28}=\gamma_{zzzx}+\gamma_{xxxz}$	$\bar{\gamma}_{28}=\bar{\gamma}_{xzyy}+\bar{\gamma}_{xzyy}$
$\gamma_{29}=\gamma_{xxxy}-\gamma_{yyyx}$	$\bar{\gamma}_{29}=\bar{\gamma}_{xyzz}-\bar{\gamma}_{yxzz}$
$\gamma_{30}=\gamma_{yyyz}-\gamma_{zzzy}$	$\bar{\gamma}_{30}=\bar{\gamma}_{yzxx}-\bar{\gamma}_{zyxx}$
$\gamma_{31}=\gamma_{zzzx}-\gamma_{xxxz}$	$\bar{\gamma}_{31}=\bar{\gamma}_{zxyy}-\bar{\gamma}_{xzyy}$
$\gamma_{32}=\gamma_{xxxz}+\gamma_{yyzz}$	$\bar{\gamma}_{32}=\bar{\gamma}_{xxxz}-\bar{\gamma}_{zzyy}$
$\gamma_{33}=\gamma_{yyyz}+\gamma_{xxyz}$	$\bar{\gamma}_{33}=\bar{\gamma}_{yyyz}-\bar{\gamma}_{zyxx}$
$\gamma_{34}=\gamma_{xxxz}-3\gamma_{yyzz}$	$\bar{\gamma}_{34}=\bar{\gamma}_{xxxz}+3\bar{\gamma}_{zxyy}-\bar{\gamma}_{xzyy}$
$\gamma_{35}=\gamma_{yyyz}-3\gamma_{xxyz}$	$\bar{\gamma}_{35}=\bar{\gamma}_{yyyz}+3\bar{\gamma}_{zyxx}-\bar{\gamma}_{yzxx}$

(3) the distribution of linear combinations among the odd or even representations is identical with the distribution among the representations of the parent group.

The $\bar{\alpha}$ and β selection rules for the group $C_{2h} = C_2 \times C_i$ are given as an example:

C_{2h}	
Ag	$\bar{\alpha}_{xy}$
Bg	$\bar{\alpha}_{yz}$, $\bar{\alpha}_{zx}$
Au	β_3, β_5, β_7, β_{10}
Eu	β_1, β_2, β_4, β_6, β_8, β_9

3.4 CONTROL METHODS

The selection rule calculations were performed by an IBM 360/44 computer, and the complexity of the programs necessitates a confirmation of the results by other means (a description of the programs is given in Appendix I). Two control methods, based on the properties of the point groups, have been used.

The first utilises (3.1) to determine the number of independent linear combinations of tensor components which belong to each of the irreducible representations of the groups. The heart of the problem is to determine, for each group, the character of the representation based on the components of the tensor under investigation, and it is approached as follows[20]: denoting the rotation axis as z', any point group symmetry transformation $\hat{G}$ may be written in the form:

$$\hat{G}\, x' = x' \cos\theta + y' \sin\theta$$

$$\hat{G}\, y' = -x' \sin\theta + y' \cos\theta \qquad (3.8)$$

$$\hat{G}\, z' = \pm z'$$

where θ denotes the angle of rotation about the z' axis, and the upper or lower signs refer to proper and improper rotations respectively. The traces of the transformation matrices which describe the operation of $\hat{G}$ on the β, $\bar{\beta}$, γ and $\bar{\gamma}$ tensor components have been found to be:

$$T^{\beta}(G) = 8\cos^3\theta \pm 4\cos^2\theta - 2\cos\theta$$

$$T^{\bar{\beta}}(G) = \pm 4\cos^2\theta + 4\cos\theta$$

$$T^{\gamma}(G) = 16\cos^4\theta \pm 8\cos^3\theta - 8\cos^2\theta \mp 2\cos\theta + 1 \qquad (3.9)$$

$$T^{\bar{\gamma}}(G) = \pm 8\cos^3\theta + 8\cos^2\theta - 1$$

The characters for each group may now be evaluated by inserting the value of θ and the + or - sign as appropriate for each class of group operations. A reflection is equivalent to an improper rotation of zero radians, and inversion one of π radians. The required numbers, the "symmetric structures" of the groups, are now quickly obtained by substitution into (3.1). The results are completely consistent with those given by the computer.

The results have also been verified by means of correlation tables[22] which describe the relationships between the representations of a group and the representations of its subgroups.

As the projection operator method is not readily applicable to the infinite point groups ($C_{\infty v}$ and $D_{\infty h}$), the selection rules for these groups were calculated from the results for the finite groups by means of the correlation tables, with the first control method being used to confirm the results.

The results of earlier calculations[1,6,7,10] are consistent with those given in Table I, with the exception of two small errors. In reference 1, page 4088, the term β_{zzx} belonging to the representation B_{1u} of D_{2h} should be β_{zxx}; and in reference 7, page 1089, the term $\gamma_{xxxy} + \gamma_{yyyz}$ belonging to the representation F_2 of the octahedral group should be $\gamma_{xxxy} + \gamma_{xyyy}$. Throughout Table I, a rectangular coordinate system has been used. A similar system is used in reference 7 for the subgroups of the group O_h, but not for subgroups of the group D_{6h}, making close comparison with Table I difficult.

Equation (3.1) has been used to analyse the transformation properties of the tensors $\beta(\omega_0,\omega_1,\omega_2)$, $\gamma(\omega_0,\omega_1,\omega_2,\omega_3)$ and $\gamma(\omega_0,\omega_1,\omega_2,\omega_2)$ for the point groups, and the results are given in Appendix II. We note that the first two tensors possess no permutation symmetry, and the third tensor symmetry in two of its last three indices only.

CHAPTER 4

DISCUSSION OF RESULTS

4.1 NONLINEAR RAMAN SELECTION RULES

In addition to giving specific information concerning the possibility of a particular nonlinear Raman transition and the properties of such a transition, the selection rule table (i.e. the table of tensor transformation properties) gives general information which is relevant to all transitions.

As is well known, there is always a portion of the linear Raman tensor that transforms according to the unit or totally symmetric representation. This has two consequences:

(1) all transitions allowed in two-photon Raman scattering are also allowed in four-photon Raman scattering;

(2) all transitions allowed by the selection rules for absorption and emission are allowed in three-photon Raman scattering.

A third consequence of this property of α, which may also be derived directly, is that mentioned previously:

(3) in all systems containing inversion symmetry, the components of third-order (β and $\bar{\beta}$) tensors belong to the odd or u species of representations, and the components of the fourth-order tensors belong to the even g species.

Generally, this will mean that the parities of the final state and of the appropriate tensor for a transition must be the same, but this is not necessarily so.

There are two further properties of Table I which deserve attention. Firstly, we observe that the table describes simply the transformation properties of the β, $\bar{\beta}$, γ and $\bar{\gamma}$ tensors, and it is, therefore, a function of the rank and symmetry of the tensors only. Therefore

(4) Table I may be used to determine the selection rules for any phenomenon for which the quantum mechanical operator is a tensor of the same nature as any of the Raman tensors.

For example, the selection rules for induced emission and for three-photon Raman scattering are identical.

The most important and obvious feature of the table is that

(5) a large number of transitions forbidden by the selection rules for first-order absorption and for linear Raman scattering are allowed in three- and four-photon Raman scattering.

As a convenient example, let us consider the case of benzene. The molecule possesses D_{6h} symmetry, and has 20 fundamental vibrational frequencies distributed as follows: $2A_{1g} + A_{2g} + A_{2u} + 2B_{1u} + 2B_{2g} + 2B_{2u} + E_{1g} + 3E_{1u} + 4E_{2g} + 2E_{2u}$. Only 11 of these modes are allowed by the selection rules for the conventional spectroscopic techniques: A_{2u} and $3E_{1u}$ in infrared (IR) absorption, and $2A_{1g} + E_{1g} + 4E_{2g}$ in linear Raman scattering. As may be seen from Table I (remembering that $D_{6h} = D_6 \times C_i$), the remaining modes are all active in either three- or four-photon Raman scattering, and one of them, the $\nu_7 = B_{1g}$ mode has been observed[5,6] in an inverse Raman experiment. As yet, no attempt appears to have been made to measure the three-photon Raman spectrum of

benzene. However, the important point remains that most of the transitions which cannot be measured in ordinary spectroscopy are active in nonlinear Raman scattering. We note also that as predicted, IR-active modes are all β-active, and that all modes active in two-photon Raman scattering are also γ-active.

The theory presented in this work predicts that the complete scattering tensors are not fully symmetric, and thus that the selection rules and polarization properties of nonlinear Raman scattering are different from those given in previous work. In particular, there are a number of active modes which are forbidden if fully symmetric scattering tensors are assumed, and the A_{2g} and A_{1u} modes of D_{6h} are examples of these: the function $\bar{\beta}_{16} = \bar{\beta}_{xyz} - \bar{\beta}_{yzx}$ transforms according to the A_{1u} representation, and no component of β does; and similarly $\bar{\gamma}_{19}$ and $\bar{\gamma}_{29}$ are the only fourth-order functions belonging to A_{2g}. In general, the effect of significant nonsymmetric tensors is to further relax the selection rules for high-order transitions.

A mention should be made here of the work of Long and Stanton[23]. These authors obtain an expression for $\beta_{\rho\sigma\tau}^{if}(\omega_0,\omega_1,\omega_1)$ which is consistent with, though less general than the expression (2.4), but their conclusion that the tensor becomes fully symmetric with respect to permutations of its indices in the Placzek approximation is erroneous, being based upon an incorrect expression for the second harmonic scattering tensor.

In the case of light scattering by single crystals, the polarization properties of the scattered light are completely

specified by the selection rule table. The method for evaluating these properties is briefly described later in this chapter. For liquids, gases and multicrystals, Table I provides only limited information, and further calculations are required, to determine the depolarization ratios, if the maximum information is to be obtained. Cyvin et al.[1] and Chu[16] have performed calculations of depolarization ratios for the β tensor, and there is some disagreement between them. In addition, Stanton[24] discusses the polarization of scattered light in three-photon Raman scattering when the incident light is elliptically polarized. As we have mentioned, however, and as is recognised in reference 16, these results are valid only in cases in which the complete scattering tensor is fully symmetric (that is, $\bar{\beta}$ is negligible), and this will not generally be the case. No attempt has been made to extend this work on depolarization ratios.

4.2 THIRD-ORDER LIGHT SCATTERING

The scattering frequencies for inelastic third-order interactions in which the system undergoes a transition from state i to state f are $\omega_1 \pm \omega_2 + \omega_{if}$ $(\omega_1 > \omega_2)$, where ω_1 and ω_2 are the frequencies of the absorbed photons. Reference 3 contains an example of three-photon Raman scattering in which $\omega_1 \neq \omega_2$. In many cases, however, it would be impractical to attempt an experiment in which $\omega_1 \neq \omega_2$, because spectra centred at $\omega_1 \pm \omega_1$, $\omega_2 \pm \omega_2$ and $\omega_1 \pm \omega_2$ would occur, and would overlap unless ω_1 and ω_2 differed considerably.

The selection rules and polarization characteristics of third-order interactions whose scattering frequencies $\omega_0 = \omega_1 \pm \omega_1 + \omega_{if}$ are determined by the group transformation properties of the tensor $\beta+\bar{\beta}$, which are given in Table I. Equation (2.4) gives an explicit quantum mechanical expression for $\beta+\bar{\beta}$. In three-photon Raman scattering, the spectrum is observed as sidebands of $2\omega_1$, and the light source will, of necessity, be a high-intensity pulsed laser. If a ruby laser is used, the spectrum origin, $2\omega_1$, will be at 28806 cm^{-1} in the near ultraviolet. In this region, photomultipliers have low noise and a high quantum efficiency, and, in general, observation of spectra may be performed in a conventional manner[2]. In particular, it is not necessary to use a double monochromator, as is the case in two-photon Raman scattering, because the relative intensity of the light scattered at $2\omega_1$ (second harmonic generation) is not large. In centrosymmetric samples, second harmonic generation is symmetry-forbidden. However, there are two further important considerations in designing a practical experiment: one is the possibility of absorption by the sample in the region of interest, the other the weakness of the spectrum. Both of these factors demand that a choice of exciting frequencies be available: the first so as to enable the spectrum to be removed from an absorption band, the second so as to enable advantage to be taken of a resonance absorption and thereby increase the intensity of the spectrum. High-intensity laser radiation is available from the ruby laser (14403 cm^{-1}), the neodymium laser (~ 9900 cm^{-1}) and from Raman lasers[25], in which laser frequency conversion at up to 60% efficiency is achieved by means of stimulated two-photon Raman scattering. The lasers which show greatest

potential, though, are the organic dye lasers[26], which promise to provide high-intensity tunable lasers suitable for Raman experiments in the range 10000-25000 cm^{-1}. One point to consider when discussing excitation frequencies is that the scattered intensity has a fourth-power dependency on the laser frequencies (see equation (2.1)); when the frequency is reduced by one half, for example, the scattering intensity is reduced by a factor of 16.

Inspection of equation (2.4) shows that the tensor $\beta+\overline{\beta}$ has resonances at ω_1 and at $2\omega_1$, the spectral origin, where these frequencies are taken relative to the initial state i. The second resonance differs from the first in one important respect: such a resonance does not reduce the intensity of the laser radiation. This means that $2\omega_1$ can be chosen to coincide exactly with an absorption frequency, provided of course that such an absorption does not overlap the Raman emission spectrum. Under resonance conditions, equation (2.4) is modified by inclusion of damping constants as described in section 2.2 and it will be seen that the degree to which the resonance contributes to the scattering intensity is dependent on the width of the absorption, the narrower states giving the higher intensities. It should also be noted that resonance conditions are precisely those conditions in which the scattering tensor $\overline{\beta}$ is significant. Reference 3 contains an example of a double resonance in three-photon Raman scattering, and it is also an example in which the resonance states have lower energies than the initial state.

The most important experimental work has been by Maker et al.[2], and recently Savage and Maker have constructed a multi-channel photon counting spectrometer which may be used in low

light level spectroscopy, including nonlinear Raman scattering[27]. The most important feature of the spectrometer is that instead of an exit slit and photomultiplier detector, it employs an image intensifier tube and an isocon camera tube. Using this arrangement, the whole of the spectrum can be observed simultaneously, and the recording time thereby considerably reduced. The instrument represents a considerable advance in experimental technique.

Three-photon Raman scattering in which the scattered light has a frequency $\omega_0 = \omega_{if}$ will generally not constitute a practical experiment, because in most cases ω_{if} will be in the infrared where photodetectors are not very sensitive, and in addition some mechanism must be employed to populate state i (which must have a higher energy than state f). An exception might be the case of an optical transition from an excited state to the ground state which is forbidden in the first-order. A simpler experiment would be an absorption experiment in which an intense laser beam is accompanied by a continuum which covers the region of interest. The laser frequency may be chosen to be close to a narrow resonance frequency, and thereby perhaps compensate for the detection difficulties. We observe that the width of the third-order absorption lines is dependent on the width of the laser beam, so that they could not be observed in a conventional absorption experiment.

4.3 FOURTH-ORDER LIGHT SCATTERING

Two spectra result from four-photon Raman scattering: one is centred at the frequency ω_1, as is the linear Raman effect, and the other at $3\omega_1$. In general, it will be very difficult to observe spectra in the latter case: the transition

probability is very low, the maximum value of ω_1 is limited by electronic absorption bands, and the ω_1^4 factor will thus be much less than is possible in lower-order scattering. It follows that the creation of resonance denominators in the scattering tensor becomes very important. Broadly speaking, the scattering intensity will increase by an order of magnitude for each resonant denominator. That is to say, the intensity of three-photon Raman scattering will approximate that of two-photon Raman scattering if it has one resonance; four-photon scattering will do so if it has two, and so on. Experiments have shown that non-resonant three-photon Raman scattering is observable[2,28], and we can thus expect that it will be possible to record four-photon Raman spectra which involve one or more resonances.

The tensor $\gamma+\bar{\gamma}$ has resonances at the frequencies ω_1, $2\omega_1$ and $2\omega_1 \pm \omega_1$ (for the case in which the resonant states are above the initial state). The $2\omega_1$ and $3\omega_1$ resonances both possess the property of the $2\omega_1$ resonance in three-photon scattering, namely that they do not reduce the effective intensity of the exciting radiation. The $2\omega_1$ resonance in this case has, in addition, the very useful property of being well removed from the Raman spectra, and there is no possibility of the absorption band overlapping the Raman spectrum.

Let us briefly examine the one example of four-photon Raman scattering which has been observed in experiment[5,6]. Before doing so, we should note that $\gamma_{\rho\sigma\tau\nu}^{if}$ has, for the spectrum centred at ω_1, denominators ω_{ki} and ω_{kf}, and thus resonances at 0 and at ω_{if} in addition to those already mentioned. Benzene does not possess any absorption bands near

14403 cm^{-1}, the ruby laser frequency, and inspection of equation (2.5) shows that we cannot, therefore, achieve any double resonances. We thus expect any fourth-order line to be considerably weaker than the normal Raman lines. The line observed in reference 5 is the ν_7 (B_{2g}) = 703 cm^{-1} line of benzene. In order to determine which intermediate states can contribute to the transition, the matrix element theorem (2.14) is used to construct Figure 4.1, which shows the allowed paths whereby any first-, second-, third- or fourth-order electric dipole transition from the ground state can take place. The allowed paths for the fourth-order B_{2g} transition are marked in red. From equation (2.5), giving the quantum mechanical formula for the scattering tensor, we see that the states k are the only intermediate states which can contribute a resonant term to the scattering tensor for benzene (we have noted above that there can be no ω_1 resonances). Figure 4.1 shows that such states must in this case have E_{1g} or E_{2g} symmetry. Although benzene possesses an electronic level close to 28806 cm^{-1}, the doubled laser frequency, transitions to this state are spin-forbidden and only appear weakly in absorption. Therefore, the major contributing intermediate states are likely to be the E_{1g} and E_{2g} vibrational levels of the ground state, two of which have frequencies less than 150 cm^{-1} from the final B_{2g} level[29].

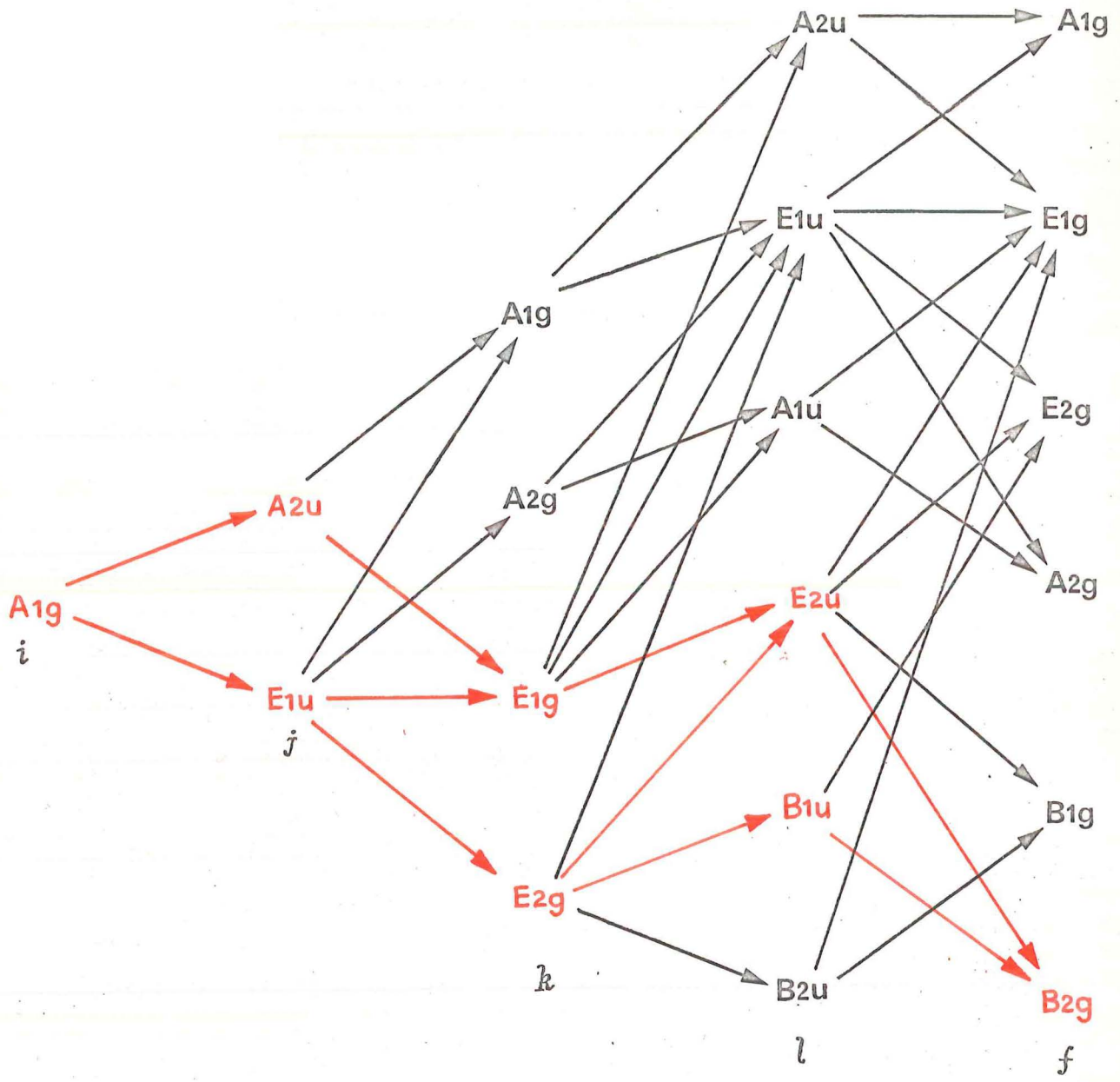

Fig. 4.1. Symmetry allowed electric dipole transition paths up to the fourth order.

4.4 THE FORMS OF THE SCATTERING TENSOR

As has been mentioned, the polarization properties of light inelastically scattered by a single crystal are given directly by Table I (in conjunction with Table II). For example, if a transition of frequency ω_{if} is allowed in three-photon Raman scattering, and if the product of the irreducible representations to which the transition states belong is Γ, then it will be possible to observe a Raman line at $2\omega_l+\omega_{if}$ of polarization ρ due to incident polarizations σ and τ if the tensor component $\beta_{\rho\sigma\tau}$ belongs to a linear combination of components transforming according to Γ. This rule in its generalized form will apply for all orders of interaction.

Tables I and II give, in addition, some information about the forms of the Raman tensors, and thus about the angular dependence of the intensity of the scattered light. Loudon[30] has discussed the case of two-photon Raman scattering. To obtain the form of an irreducible tensor, we project from each component of the reducible tensor the part which transforms according to the particular irreducible representation in which we are interested. If two reducible components project out the same linear combination then the corresponding irreducible components will be equal.

Consider, for example, the fourth-rank totally symmetric tensor which transforms according to the one-dimensional A_1 representation of D_6. The terms $\gamma_3 = \gamma_{zzzz}$, $\gamma_{20} = \gamma_{xxxx} + 2\gamma_{xxyy} + \gamma_{yyyy}$ and $\gamma_{22} = \gamma_{yyzz} + \gamma_{zzxx}$ belong to this representation, and we see that the required tensor has only three independent components. Now γ_{xxxx} and γ_{yyyy} will both reduce to γ_{20}; let $\gamma_{20} = \alpha$. "γ_{xxyy}", however, represents the

sum of six equal components ($\gamma_{xyxy}, \gamma_{xyyx}$, etc.), and each of these will thus appear in γ_{20} with a prefix of one-third. Thus the $xxyy, xyxy, \cdots$ components of the A_1 irreducible tensor will each have the value $3a$. Application of the procedure to the other components yields the following result for this tensor: $xxxx = yyyy = a$; $xxyy = 3a$; $yyzz = zzxx = b$; $zzzz = c$; all other independent components are zero.

Using this technique, the forms of the Raman tensors may be obtained for all one-dimensional or pseudo one-dimensional representations of the point groups. Similar results may be calculated for two- and three-dimensional representations which are obviously "symmetrical": that is, none of the partners of the basis possess in their correct mathematical form a multiplicative factor other than one. In such cases, the magnitudes of the partners in the basis are the same. In the remainder, however, the relative magnitudes depend on the ratio of the multiplicative factors, and these are not available from the selection rule tables.

4.5 CONCLUSION

An investigation of nonlinear Raman scattering has been made, with special attention being focussed on symmetry properties. In Chapter 2, the explicit quantum mechanical expressions for tensors describing three- and four-photon scattering processes, including both elastic and inelastic phenomena, were derived. Using these expressions, we have seen that the scattering tensors are totally symmetric with respect to permutation of their indices only in the case of vibrational Raman scattering when the incident and scattered

radiation frequencies are negligible in comparison with the electronic absorption frequencies of the excited system. Accordingly, selection rules for nonlinear Raman scattering have been derived, and presented in Tables I and II in the form of the transformation properties of the β, $\bar{\beta}$, γ and $\bar{\gamma}$ tensors. The spectra are known from experiment[2,27,28] and theory[6] to be very weak, and thus most experiments will to some extent require resonance conditions in order that the spectra be observable. Even in non-resonant cases, the physical requirements of the experiment, such as sensitive light detection and a value of the laser frequency, ω_1, which is not too low, will effectively rule out cases in which ω_1 and ω_0 are very much less than the absorption frequencies. Therefore, the scattering tensors in practice will not be totally symmetric tensors, contrary to the assumptions made in previous work[1,6,7].

As is indicated by the selection rules, nonlinear Raman scattering can provide a vast amount of information which cannot be obtained by conventional measurement. With the improvements currently being made in spectroscopic tools, particular in the field of tunable lasers, the prospects for obtaining this information are becoming increasingly good.

PART II

RAMAN LIGHT SCATTERING IN COBALTOUS COMPOUNDS

CHAPTER 5

THEORY

5.1 INTRODUCTION

The majority of Raman spectroscopic studies have been concerned with the measurement of vibrational and rotational transitions in solids, liquids and gases. In recent years, and particularly since the advent of the laser, there has been an increasing amount of work in the field of electronic Raman scattering. In particular, there is a growing literature on the subject of Raman scattering by ions in solids[31-38], and on the subject of Raman scattering from magnetic excitations in solids[31,39-42].

Raman spectroscopy is an important complement to infrared absorption (IR) and fluorescence spectroscopy as a means of studying far infrared electronic transitions in solids; in fact it is often the most powerful technique, the relative weakness of the spectra being compensated for by the inherent advantages. Firstly, IR and fluorescence spectra are generally much more complicated than the equivalent Raman spectrum, making assignments of observed transitions more difficult, and making greater the possibility of overlap of spectral lines. Of course, coincidence between Raman allowed vibrational fundamentals and electronic lines can occur, but, in contrast to the IR-active phonons, the Raman-active phonons are usually relatively narrow, and are thus less troublesome (IR-active phonons naturally have a short lifetime and so have a large linewidth). Secondly, polarization studies in Raman spectroscopy provide more information than can be obtained using the

other techniques. Polarization is particularly important because it allows, in principle, a spectroscopic measurement of the symmetries, in addition to the energies, of electronic states, and thus a close comparison between experimental results and those of crystal field theory; the crystal field theory can thus be thoroughly tested. A third advantage arises from the fact that low-lying electronic states commonly arise from a single free ion configuration and are thus of the same parity. The Raman operator has even parity, and Raman transitions between states in this situation are thus parity allowed. In contrast, direct transitions are parity forbidden and the IR electronic lines will thus be weak and easily confused with or buried by vibrational or impurity lines.

In this work a Raman study is made of the low-lying energy levels of the cobaltous ion (Co^{2+}) in $CoCl_2$ and as a substitutional impurity in $CdCl_2$, $CdBr_2$ and $MnCl_2$. The crystal structures are isomorphic, which allows the doping concentrations to be chosen at will and thus ready measurement of the concentration dependence of the spectra. The site symmetry of the Co^{2+} ions is trigonal. Previously, attempts have been made to measure by IR absorption the spin-orbit levels of the Co^{2+} ground state, with only moderate success[43-45]. In contrast to the case for the IR, transitions among the levels are Raman allowed; additionally the phonon spectra are much simpler. Thus it is expected that much better results will be obtained from a Raman experiment, enabling comparisons with crystal field theory to be made.

Crystal field theory has been applied to the case of Co^{2+} in octahedral[46,47] and in trigonal crystal fields[45,48], and Lines[49] has considered in detail the case of $CoCl_2$ and $CdCl_2$(Co).

This theory and the experimental results of previous workers will be reviewed in the next sections. A more exact theory which has some important consequences will then be described, and to conclude the chapter, the selection rules which apply to Raman scattering by Co^{2+} ions in $CdCl_2$-type crystals are derived.

The Raman spectrometer is described in Chapter 6, and, in Chapter 7, the experimental results are presented and analysed. Included in this chapter are preliminary results of an investigation of antiferromagnetic $CoCl_2$.

5.2 CRYSTAL FIELD THEORY: PREVIOUS WORK

Crystal field theory is concerned with the interpretation and prediction of the spectra of ions in a crystal environment which may be approximated by a static electric field, and as such is particularly applicable to the cases of transition metal or rare earth ions in crystals. In these cases, charge transfer bands are generally of a high energy (> 20,000 cm^{-1}), and the lower energy transitions are between crystal field split states of an unfilled electron shell.

The Co^{2+} ion has an unfilled 3d shell containing seven electrons. The ion environment in $CdCl_2$-type crystals is illustrated in Figure 5.1: the structure belongs to the D_{3d}^5 space group[50], and the cation site symmetry is D_{3d}. The Co^{2+} ion in these crystals is surrounded by a nearly octahedral configuration of anions, the octahedron being slightly expanded along one of its trigonal axes. The crystal field is thus predominantly cubic, the trigonal component inducing relatively small splittings in the cubic electronic states.

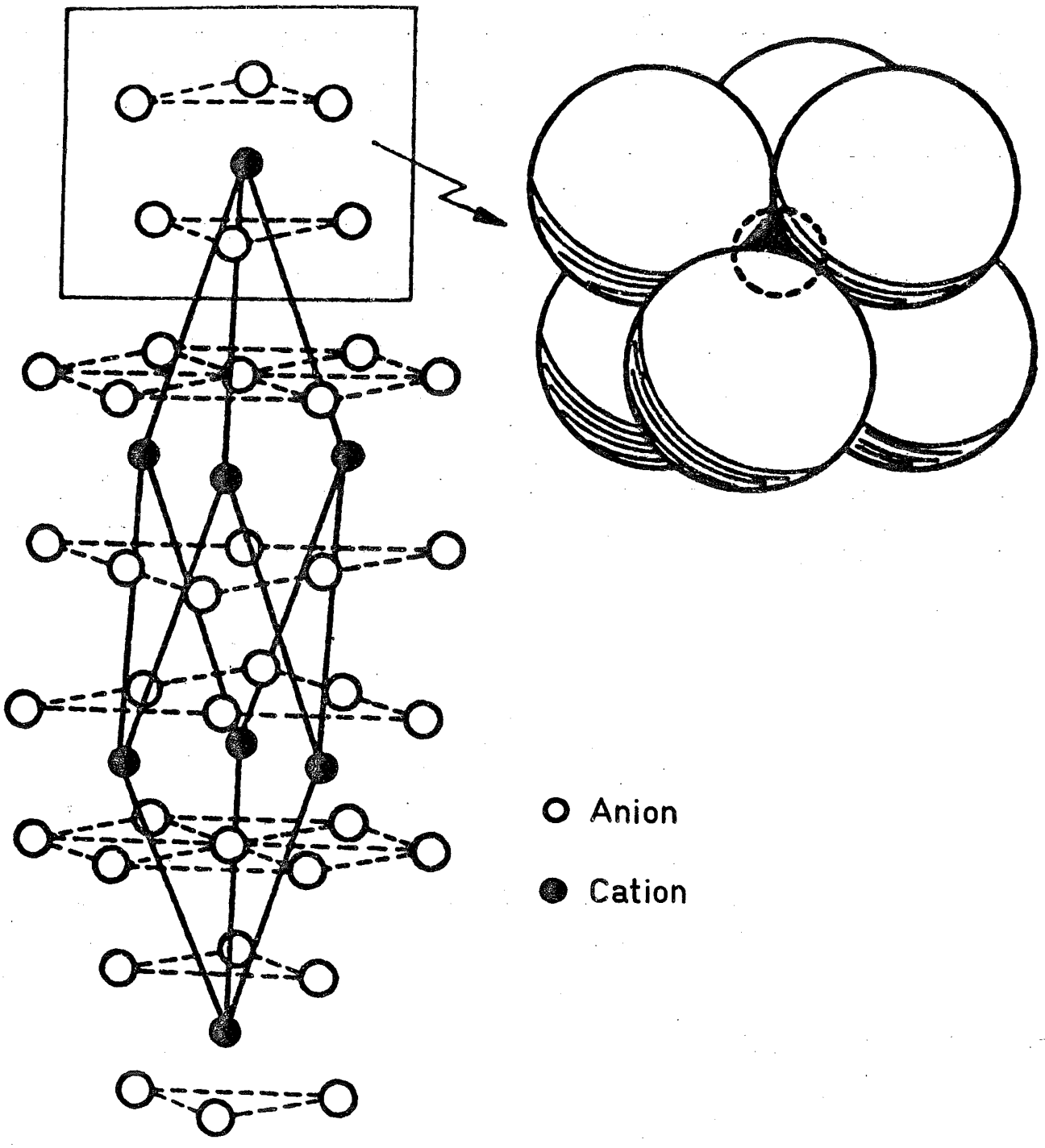

Fig. 5.1 Structure of $CdCl_2$-type crystals.

The Hamiltonian of the ion in a zero magnetic field may therefore be written[48]

$$H = H_F + V_C + V_T + H_{LS} \tag{5.1}$$

where we have neglected interactions whose energies are low ($\sim 1\ cm^{-1}$). H_F is the non-relativistic Hamiltonian of the free ion, and can be expanded as

$$H_F = \sum_k \left(\frac{P_k^2}{2m} - \frac{Ze^2}{r_k} \right) + \sum_{j<k} \frac{e^2}{r_{jk}} \tag{5.2}$$

where the summations are over the electrons, and the other symbols have their usual meanings. The eigenstates of the first summation in (5.2) are called <u>configurations</u>, and it is found in practice that most ionic spectra can be well understood when attention is restricted to the ground or lowest energy configuration. The second summation in (5.2) gives rise to splittings in the ground configuration, the new eigenstates being called <u>terms</u>.

A configuration can be written as a product of single electron wavefunctions, which can be grouped together in electronic shells. A closed shell constitutes the maximum number of single-electron wavefunctions possible in that group, and it can be shown (reference 47, p.68) that the contribution of the closed shells to the energies of all the free ion terms is the same, so that we may neglect such contributions. The effective Hamiltonian for the free ion can therefore be simplified to the single term $\sum_{j<k} \frac{e^2}{r_{jk}}$, where the summation extends over the electrons of the unfilled shells (there is one in the case of Co^{2+}, namely the 3d shell).

This operator, the electrostatic term of the Hamiltonian, commutes with the total angular momentum operators, $\underline{L}$ and $\underline{S}$, and their eigenvalues can thus be used to label the free ion states. These are, for Co^{2+}: ^4P, ^4F, ^2P, $2 \times {}^2D$, ^2F, ^2G and ^2H, in the usual notation. The ^4F and ^4P states lie lowest, in that order.

The term V_c in (5.1) represents the cubic (and therefore the most significant) portion of the electrostatic interaction between the Co^{2+} ion and the neighbouring anions. It causes splitting and mixing of the free ion states, though in the first-order it cannot mix states of different spin multiplicity. The ^4F and ^4P states are reduced to $^4T_{1g} + {}^4T_{2g} + {}^4A_{2g}$ and $^4T_{1g}$ respectively, with the $^4T_{1g}(^4F)$ lying lowest, and noting the above restriction, we expect mixing into the cubic field ground state from the $^4T_{1g}(^4P)$ only.

The trigonal field term V_T is small for the case of ions in $CdCl_2$-type crystals, causing splittings of the order of 10^2 cm^{-1} (compared with 10^4 cm^{-1} for H_F and V_C), and is not expected to cause significant mixing of higher cubic field states into the $^4T_{1g}$ ground manifold. The same assumption is usually made for the case of the spin-orbit coupling interaction, since for transition metal ions of the first series, it is small also. This term, H_{LS} in (5.1), represents a relativistic correction to the Hamiltonian. It couples together the spin and orbital angular momenta, and further splits the cubic field states. The combined effect of $V_T + H_{LS}$ is to split the $^4T_{1g}$ cubic ground state into a manifold of six Kramers doublets (see Figure 5.2), with an energy width of about 1000 cm^{-1}.

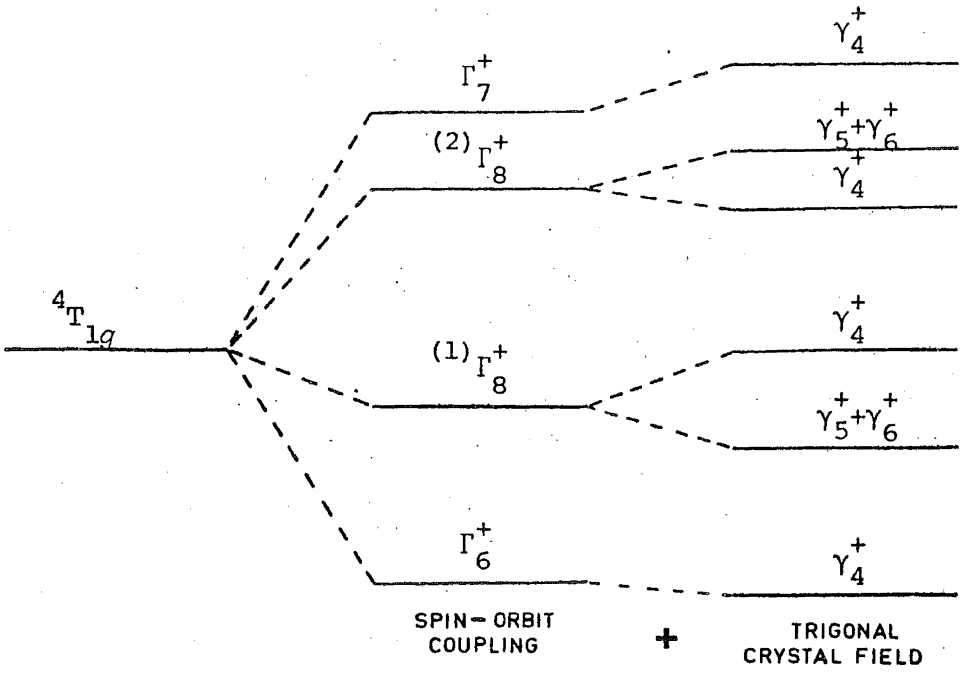

Fig. 5.2 Splitting of the cubic field ground state energy-level by spin-orbit coupling and the trigonal crystal field.

We note finally that the errors induced by the assumption that the crystal field is static can be removed by consideration of the Jahn-Teller effect.

The energies of the spin-orbit and trigonal field split $^4T_{1g}$ states have been calculated by Lines for Co^{2+} in $CdCl_2$ and $CoCl_2$ [49], and by Robson for Co^{2+} in $CdCl_2$ and in $CdBr_2$ [45]. In the former case, the calculation is performed on the isolated $^4T_{1g}$ ground cubic state. Any mixing of the cubic eigenfunctions by V_T or H_{LS} is neglected, and the admixture of $^4T_{1g}(^4P)$ state into the ground state is assumed to be isotropic; under these assumptions the spin orbit coupling can be represented by the expression $H_{LS} = \lambda' \underline{L}.\underline{S}$, where L and S remain good quantum numbers, and an energy level scheme derived which depends on λ' and a trigonal field parameter only.

Using experimental g values, which are a measure of the degree to which the lowest-lying Kramers doublet splits in a magnetic field, and the results of magnetic susceptibility measurements, Lines deduces values for these parameters. In Table III, we list energies of the low-lying states of Co^{2+} in these crystals which have been deduced from the results of Lines. The states are labelled by their symmetries in the trigonal crystal field, and, in brackets, the cubic field level from which they originate.

TABLE III

Energies of the low-lying levels of Co^{2+} in $CoCl_2$, $CdCl_2$ and $CdBr_2$

	$CoCl_2$*	$CdCl_2$*	$CdCl_2$†	$CdBr_2$†
$\gamma_4^+(\Gamma_6^+)$	0	0	0	0
$\gamma_5^+ + \gamma_6^+(^{(1)}\Gamma_8^+)$	278	310	-	-
$\gamma_4^+(^{(1)}\Gamma_8^+)$	446	536	-	-
$\gamma_4^+(^{(2)}\Gamma_8^+)$	918	949	928	825
$\gamma_5^+ + \gamma_6^+(^{(2)}\Gamma_8^+)$	976	1037	988	890
$\gamma_4^+(\Gamma_7^+)$	1057	1134	1063	968

* Calculation based on theory of Lines[49]

† Calculated by Robson[45]

All units are wavenumbers.

Table III also contains the results of Robson[45], who used the theory of Abragam and Pryce to interpret observed IR

absorption spectra of Co^{2+} in $CdCl_2$ and $CdBr_2$. In a more precise approach than that of Lines, the crystal field interaction $V_C + V_T$ is calculated within the $^4P + {}^4F$ free ion manifold, and the spin-orbit interaction within the trigonal field split $^4T_{1g}(^4F)$ term. The parameters of the cubic field and electrostatic interactions are obtained using the optical absorption spectra of Co^{2+} in $CdCl_2$ and $CdBr_2$, as is the admixture of the $^4T_{1g}(^4P)$ state into the $^4T_{1g}(^4F)$ ground state. The energies of the low-lying states are expressed in terms of one trigonal field and three spin-orbit parameters. The calculated g-values are also a function of these parameters, and a fitting to experimental g-values is used to supplement the IR data.

5.3 CRYSTAL FIELD THEORY: THE CALCULATION

The experimental results obtained in this work could not be adequately understood in terms of the theory described in the previous section, and consequently resort has been made to a theory embodying fewer approximations.

The approach to the problem is that of Tanabe and Sugano[51]. As previously, closed shells are ignored, and configuration mixing is neglected. The single electron energy levels are considered to be split by the cubic crystal field into t_{2g} and e_g energy levels only, the splitting having the value 10Dq. In this scheme, the $3d^7$ electrons are accommodated in states of the form $t_{2g}^{\ m}\ e_g^{\ n}$, where m+n = 7 (we note at this stage that the $3d^7$ configuration can be considered to be equivalent to the $3d^3$ configuration, provided that appropriate changes of sign are made to the parameters of the interactions [reference 47, p.245]). The electrostatic, spin-orbit and

trigonal crystal field interactions are now calculated within the entire set of $3d^7$ states, and we expect more accurate results than those achieved in previous calculations, as in those cases the latter two interactions were calculated within severely restricted sets of states.

The energy matrices of the $3d^3$ configuration for the electrostatic interaction, $\frac{e^2}{r_{jk}}$, have been calculated by Tanabe and Sugano[51], and for the spin-orbit interaction by Schroeder[52] using the strong-field coupling scheme described above. The energy matrices for the trigonal field interaction have been calculated by Zdansky and Johnstone[53]. The configuration has a total dimension of 120, but, for purposes of diagonalization, this can be reduced to a 42-dimension set of Υ_4^+ states and a 39-dimension set of Υ_5^+ states, noting that the Υ_5^+ and Υ_6^+ states are degenerate in a zero magnetic field. Diagonalization can be performed by computer using a program described by Robson[45].

If we limit ourselves to simply the approximations that closed shells are ignored and that the $3d^7$ state gives us t_{2g} and e_g cubic field wavefunctions only, the calculation will involve a total of 15 parameters: 10 electrostatic parameters, 1 cubic field, 2 trigonal field and 2 spin-orbit coupling parameters.[52] As the manifold we wish to measure contains at the most five observable transitions, it is obvious that the number of parameters used in the calculation will have to be reduced. This can be done in two steps.

First, we observe that the splittings we wish to measure are caused by the spin-orbit and trigonal field interactions only. The calculation can, therefore, be performed in two stages - firstly a fitting of optical spectra of Robson by

variation of the cubic field and electrostatic parameters, and secondly a fitting of the Raman spectra by variation of the spin-orbit and trigonal field parameters. In each step, the parameters not being varied assume the values calculated in the previous parallel calculation. We can thus refine all parameters, and the fit, by an iterative process.

A second method for simplifying the calculation is to reduce the electrostatic parameters to a set of three parameters, A, B and C, equivalent to the three Racah parameters which are appropriate when the t_{2g} and e_g wavefunctions are derived from pure d orbitals. This procedure will allow an approximate fit to the optical spectrum, and as it does not directly affect the ground state splitting, it should not greatly detract from the generality of the calculation of that splitting. As we are neglecting interconfiguration mixing, the parameter A becomes redundant, and we are left with a three parameter calculation for the optical spectrum.

In Figure 5.3, we show the dependence of the Co^{2+} low-lying electronic energy levels on the spin-orbit and trigonal field interactions, according to the theory developed by Robson and according to the theory outlined in this section. Robson found by analysis of the experimental g-values for $CdCl_2(Co)$ and $CdBr_2(Co)$ that the variable δ/ζ was negative. We should expect, therefore, that the parameter v will be positive.

Note that the primary difference between the diagrams occurs in the upper three energy curves. In the more accurate calculation, the "accidental" degeneracy which had occurred under the spin-orbit coupling has been lifted, and the relative splitting of the lower two curves by the trigonal field is much less. These characteristics are, as we shall

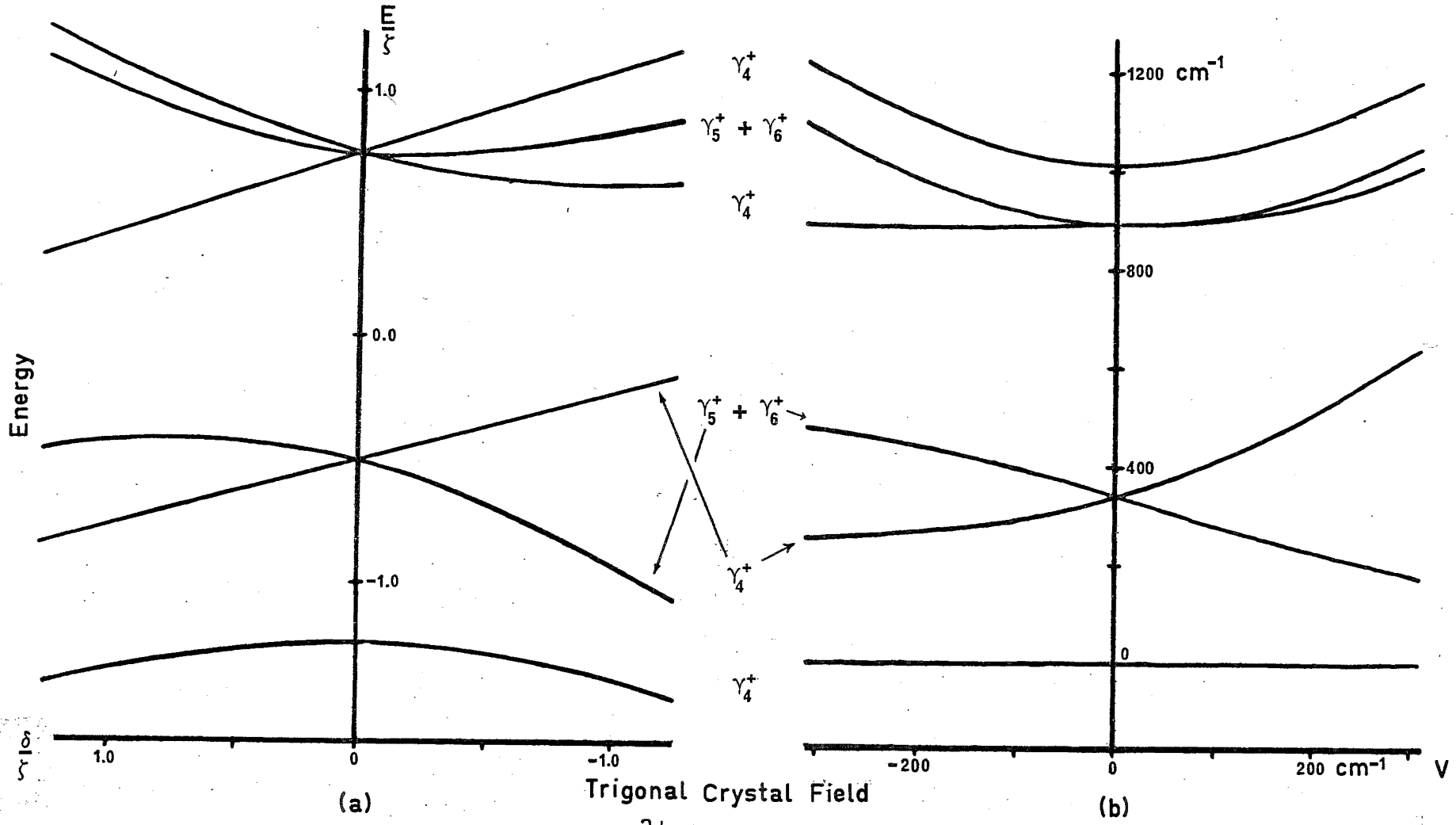

Fig. 5.3 Energy level calculations for Co^{2+} in a trigonal crystal field: (a) Robson's calculation[45] (δ and ζ are the trigonal and spin-orbit parameters respectively); (b) the full $3d^3$ calculation for Dq = -690, B = 780, C = 3430; spin-orbit parameters: ζ = -510, ζ' = -540 (all cm^{-1}); trigonal parameters: v/v' = 0.323.

see, completely in accord with the experimental situation.

5.4 PREVIOUS EXPERIMENTAL RESULTS

Experimental studies of low-lying energy levels of the Co^{2+} ion in a trigonal crystal field have been made by Newman and Chrenko[43] (who studied $CoCl_2$ and $CoBr_2$), Zvyagin et al.[44] ($CoCl_2$ and $CoCO_3$), and Robson[45] [$CdCl_2$(Co), $CdBr_2$(Co) and $MnCl_2$(Co)], using the technique of IR absorption.

In the cobaltous compounds studied by Newman and Chrenko, absorption lines were observed in the 700-1200 cm^{-1} region for all compounds possessing a predominantly cubic crystal field in which the lowest cubic state is $^4T_{1g}$, but not in tetragonal Cs_3CoCl_5, which has a singlet $^4A_{2g}$ lowest level. The absorptions in the cubic crystal are thus attributed to transitions among the spin-orbit and trigonal field split $^4T_{1g}$ levels. In $CoCl_2$, four lines are observed at 1193 cm^{-1}, 985 cm^{-1}, 905 cm^{-1} and 735 cm^{-1}, although the theory predicts only three lines in this region. These authors were prevented from investigating the lower frequency region by absorptions of the crystal lattice, as indeed were the later workers.

Zvyagin et al. were not able to observe transitions associated with the Co^{2+} ions in $CoCO_3$ because of the presence in the 600-1800 cm^{-1} region of the spectra of strong absorption due to the CO_3 group. However, a detailed and fruitful study of $CoCl_2$ was made, using $MnCl_2$, in which one does not expect low-lying electronic energy levels, for a comparison. In particular, a study was made of the effect of impurities on the observed spectra, and it is clearly shown that the 905 and 735 cm^{-1} lines seen by Newman and Chrenko are impurity lines. In pure crystals, three lines at 1188, 1120 and 980 cm^{-1} are observed, and are fitted to the theory of Lines using the

values $\lambda' = -174\ cm^{-1}$ and $\delta/\lambda' = 2.2$, δ being the trigonal field parameter. Using these parameters, the transition energies 261, 501, 985, 1075 and 1188 cm^{-1} are obtained. In spectra measured at temperatures below the Neél temperature, a fourth line appears at 1015 cm^{-1}.

Robson studied the spectra of the Co^{2+} ion in $CdCl_2$, $CdBr_2$ and $MnCl_2$, and the results obtained are particularly relevant to those obtained in the previous work. Firstly, the impurity origin of the 735 cm^{-1} line of Newman and Chrenko is confirmed, although it is attributed to a different impurity. Secondly, we take note of two points: electric dipole transitions among the low-lying Co^{2+} electronic energy levels are parity forbidden, and we should thus expect associated absorption intensities to be weak; and as direct relaxation of an isolated, excited Co^{2+} ion to a lower energy state is parity forbidden, we should expect also that the electronic lines would be narrow. The consequence of these observations is that the observed spectra in the 1000 cm^{-1} region should consist of weak, narrow "no-phonon" lines, followed on the high energy side by vibronic bands of greater intensity, which correspond to transitions between pure electronic states and states coupled to an odd lattice vibration. The peaks in the vibronic "envelopes" should have energies of the form $E = E_{electronic} + E_{phonon}$, E_{phonon} being the energy (frequency) of an odd parity lattice vibration. Broadly speaking, this picture corresponds to the observed spectra, although a number of impurity lines prevent the analysis from being conclusive, and the energies of the vibronic peaks do not agree particularly well with the measured lattice frequencies[54]. Table IV presents the results obtained by Robson for low concentrations of Co^{2+} in various host crystals.

TABLE IV

Experimental results of Robson[45]

	$CdCl_2$(Co)	$MnCl_2$(Co)	$CdBr_2$(Co)
$\gamma_4^+(^{(2)}\Gamma_8^+)$	950	880†	833
$\gamma_5^+ + \gamma_6^+(^{(2)}\Gamma_8^+)$	994	970†	898
$\gamma_4^+(\Gamma_7^+)$	1025	1020†	950

† All units are wavenumbers value is ± 5 cm^{-1}.

The theoretical values obtained by this author are presented in Table III.

The IR absorption experiments will be further discussed in Chapter 8, after the presentation of the Raman results.

5.5 SELECTION RULES

The $^4T_{1g}$ label denotes a state whose wave function is a product of an orbital function transforming according to the T_{1g} representation of the point group O_h, and a spin function belonging to the representation $D_{3/2}^+$ of the full rotation group. The spin-orbit interaction mixes the two functions, producing four wavefunctions having $^4T_{1g} \times \Gamma_8^+(D_{3/2}^+)$ $= \Gamma_6^+ + \Gamma_7^+ + 2\Gamma_8^+$ symmetries. Under trigonal crystal fields, further splitting occurs, the Γ_6^+ and Γ_7^+ states reducing to γ_4^+ states of the group D_{3d}, and the Γ_8^+ states to $\gamma_4^+ + \gamma_5^+ + \gamma_6^+$ (and we note that the γ_5^+ and γ_6^+ states are degenerate in a zero magnetic field).

The relevant portion of the representation multiplication table of the point group D_{3d} is as follows:

$$\gamma_4^+ \times \gamma_4^+ = \gamma_1^+ + \gamma_2^+ + \gamma_3^+$$

$$\gamma_4^+ \times (\gamma_5^+ + \gamma_6^+) = 2\gamma_3^+$$

$$(\gamma_5^+ + \gamma_6^+)\times(\gamma_5^+ + \gamma_6^+) = 2\gamma_1^+ + 2\gamma_2^+,$$

and in Table V, the transformation properties of the Raman tensor components are given.

TABLE V

Selection rules for Raman transitions among the low-lying energy levels of the Co^{2+} ion in a trigonal crystal field.

Symmetry	Raman Tensor	Allowed Transitions
γ_1^+	$\alpha_{xx} = \alpha_{yy} = a;\ \alpha_{zz} = b$	$\gamma_4^+ \to \gamma_4^+; (\gamma_5^+ + \gamma_6^+) \to (\gamma_5^+ + \gamma_6^+)$
γ_2^+	$\alpha_{xy} = -\alpha_{yx} = c$	$\gamma_4^+ \to \gamma_4^+; (\gamma_5^+ + \gamma_6^+) \to (\gamma_5^+ + \gamma_6^+)$
γ_3^+	$-\alpha_{xx} = \alpha_{yy} = \alpha_{xy} = \alpha_{yx} = d$	$\gamma_4^+ \to \gamma_4^+;\ \gamma_4^+ \to (\gamma_5^+ + \gamma_6^+)$
	$\alpha_{yz} = -\alpha_{xz} = e$	
	$\alpha_{zx} = -\alpha_{zy} = f$	

The selection rules are obtained with the help of the matrix element theorem, (2.15), and we remember that for electronic transitions the Raman tensor is a general second-rank tensor possessing no inherent symmetry. It will be seen from Table V that all possible transitions are Raman-allowed.

If the initial state is $\gamma_5^+ + \gamma_6^+$, the final state for a transition can be readily characterized as γ_4^+ or $\gamma_5^+ + \gamma_6^+$ by measuring the off-diagonal z-components, which will be zero if the final state is $\gamma_5^+ + \gamma_6^+$. The Raman scattering efficiencies for the two transitions $\gamma_4^+ \rightarrow \gamma_5^+ + \gamma_6^+$ and $\gamma_4^+ \rightarrow \gamma_4^+$, which are obtained by squaring and adding the irreducible Raman tensors[30], may be written:

$$\gamma_4^+ \rightarrow \gamma_4^+ \begin{pmatrix} a'^2 & c'^2 & f'^2 \\ c'^2 & a'^2 & f'^2 \\ e'^2 & e'^2 & b'^2 \end{pmatrix} \quad ; \quad \gamma_4^+ \rightarrow \gamma_5^+ + \gamma_6^+ \begin{pmatrix} a''^2 & a''^2 & c''^2 \\ a''^2 & a''^2 & c''^2 \\ b''^2 & b''^2 & 0 \end{pmatrix}$$

The two possible final states can thus be distinguished either by measuring the zz component of the tensor, or by comparing the xx and xy components, which should vary for γ_4^+ final states, but not for $\gamma_5^+ + \gamma_6^+$.

CHAPTER 6

THE RAMAN SPECTROMETER

6.1 THE LIGHT SOURCE

The characteristic of Raman spectroscopy which has primary influence on the design of a Raman spectrometer is the extreme weakness of the Raman signal. This weakness is of course expected, as the Raman effect is a second order interaction; typically, the Raman intensity is of the order of 10^{-6} weaker than that of the elastically (Rayleigh) scattered light, the intensities of both spectra being proportional to the intensity of the light source. Thus the ideal Raman spectrometer firstly combines an intense light source with very sensitive signal detection, and second, efficiently discriminates between the elastically and the inelastically scattered light. Figure 6.1 illustrates the arrangement used in this laboratory, which we will now go on to describe in detail.

The laser is the ideal light source, as it provides not only very intense light, but also unidirectional, polarized and highly monochromatic light. The latter property is important because the width of the Raman lines can never be less than that of the exciting radiation, so that the laser linewidth is the ultimate resolution-limiting factor. The other two properties mentioned are also very valuable because they allow polarization properties to be simply measured.

Our system uses a Spacerays Inc. model 5600 argon ion laser. The output power, of which about 80% is shared between the 4880Å and 5145Å lines, is nominally one watt, though this

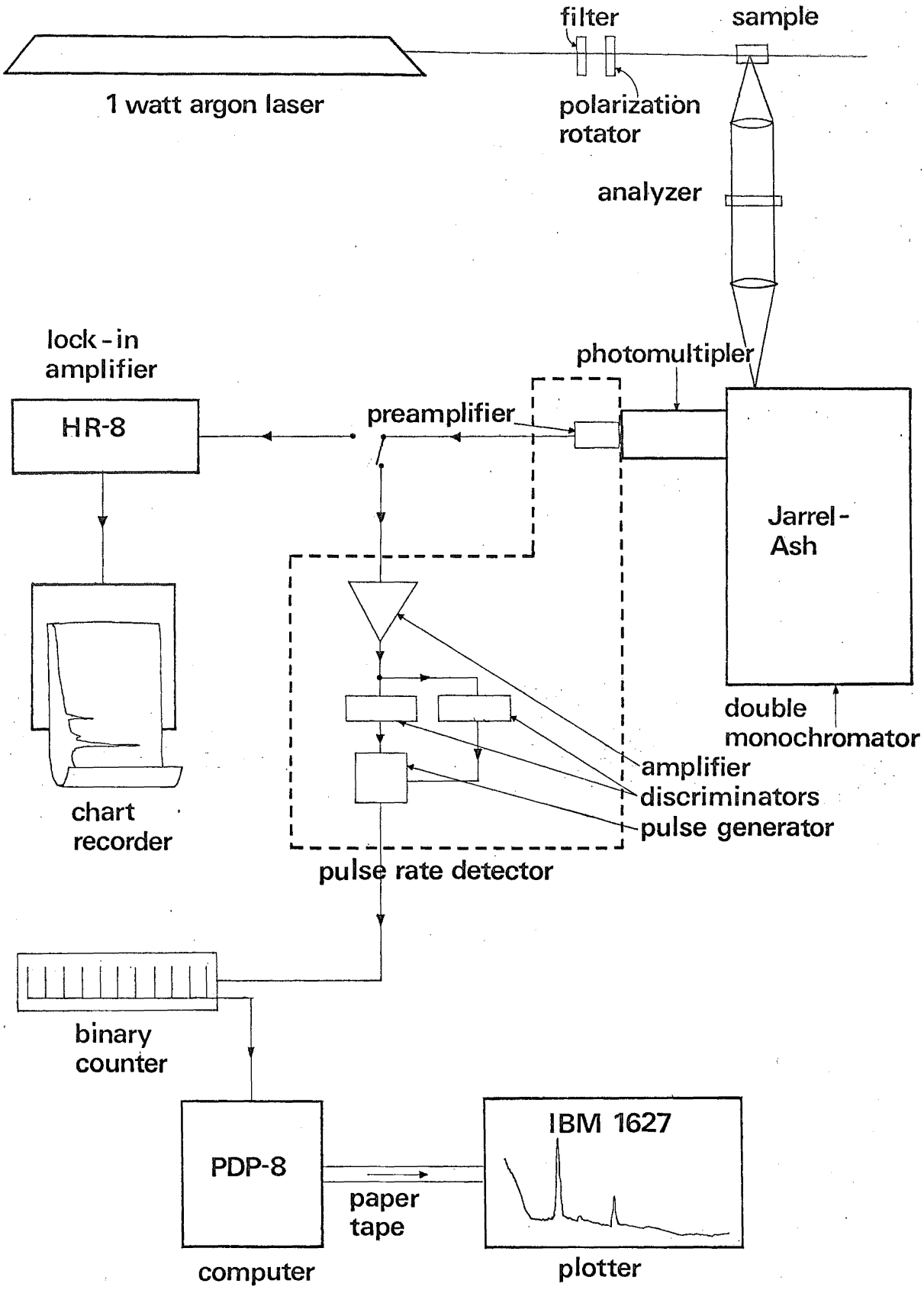

Fig. 6.1. Schematic diagram of the Raman spectrometer.

can be increased considerably by using high quality and very expensive quartz flats as Brewster windows.

The laser operates on a continuous flow principle, in which gas is simultaneously being valved into the laser tube and removed from it by a vacuum pump: this system allows cheap and readily available industrial grade gas to be used, and, in principle, allows an argon laser to be converted to krypton by simply switching gas cylinders. In practice, however, where optimum performance is generally required from the laser, the dump (or output) mirror would also require to be switched, and in our case, the power capacity would have to be increased from the present 10 Kw.

When using a mirror at the reflecting end of the resonant cavity, the laser will operate simultaneously at five wavelengths: 5145, 4965, 4880, 4765 and 4579Å. Selection of a single wavelength is achieved by replacing the mirror with a reflecting prism which can be rotated, and the laser is normally operated with this arrangement.

6.2 THE SAMPLE

The laser beam incident on the sample is filtered by three different techniques, which may all be used simultaneously. The main problem solved by the filters is confusion between Raman signal and non-laser light emitted by the argon plasma and scattered elastically into the spectrometer. The first method is the use of the prism already mentioned, which removes all lasing radiation except that selected; the second depends on the use of a phase sensitive detector, and will be described in the next section. The most effective filter,

however, is a simple interference filter, which may be rotated to match the frequency of the laser line.

Polarization of the incident beam is determined by a half-wavelength plate coupled to a Glan-Thompson prism, and that of the Raman signal by a piece of polaroid or a large calcite crystal analyzer.

6.3 THE SPECTROMETER

The basis of a Raman spectrometer is a monochromator meeting the requirements mentioned previously. The instrument used in this laboratory is a Jarrel-Ash model 25-103 1.0 metre double Czerny-Turner scanning spectrometer. It consists essentially of two 1.0 metre spectrometers placed one on top of the other, with a pivot and drive screw common to both gratings. The gratings contain 1180 grooves/mm, are blazed for 5000Å and are cast from the same master so as to ensure that the groove spacing for each grating is identical. This latter property is essential if the two monochromators are to track perfectly over their full optical range (11000-25000 cm^{-1}). The instrument has a cosecant drive which enables the counter to be read directly in wavenumbers, and includes a difference counter which enables direct reading of Raman frequencies for any exciting frequency. Curved slits ensure that resolution is independent of slit length and equal to the maximum that can be achieved with straight slits.

The specified resolution of each monochromator for 10μ slit widths is 0.12Å using the definition

$$R = \frac{0.28\text{Å} \times \Gamma}{d},$$

where Γ is the half-width of the 3131.83Å emission line of mercury, and d is the separation between the two lines of the 3131Å doublet. We were able to achieve resolutions of 0.027 and 0.031Å for the top and bottom monochromators, and 0.024Å for the combination. This latter resolution gain is characteristic of double monochromators, and arises from the reduction in the scattered light intensity in the second monochromator: it is, of course, for precisely this property that a double monochromator is used in Raman spectroscopy, where the very intense Rayleigh scattered light has to be eliminated.

Although the stray light rejection was sufficient for most of the samples that were investigated, it was not for some. Preliminary measurements have shown that it is possible to attach the 1/3 metre Jarrell-Ash spectrometer in our possession to the double 1.0 metre instrument as a premonochromator, and thereby improve spectra in the more difficult experiments. An alternative procedure for reducing scattered laser radiation inside the spectrometer is to place a narrow-band absorption filter in front of the spectrometer to absorb the laser frequency[55].

6.4 DETECTION AND SIGNAL PROCESSING

The light signal from the spectrometer is converted to electrical signal by a thermoelectrically cooled EMI 6255SA photomultiplier. The cooler is a Jarrell-Ash model 83-056, which provides electrostatic and magnetic shielding for the photomultiplier, and an operating temperature of -25°C. In our case, cooling was found to have little effect on signals

amplified by phase sensitive detection: this undoubtedly occurs because such a technique is strongly discriminatory against photomultiplier noise. However, use of the cooler is critical when the pulse rate detector is being used. Cooling reduces the dark count by a factor of 15 from about 200 counts/second, and in our experiments, a typical Raman line might peak at 100 counts/second.

As has been indicated, we have a choice of two signal processing systems. The phase sensitive detector is a Princeton Applied Research model HR-8 Precision Lock-In amplifier. The instrument "locks in" to signal modulated at a particular frequency, and amplifies only that portion of the input signal, which is then displayed on a chart recorder. A mechanical chopper, placed inside the laser cavity at the prism or reflecting end, modulates the lasing light (and hence the Raman signal), and provides a reference signal for the amplifier. The argon plasma emission is not modulated by the chopper in this arrangement, and is thus, in the main, eliminated. The small portion which originates from a reflection at the prism can be removed with the interference filter if necessary.

The HR-8 amplifier is useful for making rapid preliminary surveys of Raman spectra, and in the rare cases where the spectrum is very strong. For general work, however, the more sensitive pulse rate detector is used.

A pulse rate detector, as its name implies, treats the photomultiplier signal as a digital, rather that an analogue signal as does the Lock-In amplifier. That is, instead of amplifying a current signal, the system counts the number of

photon-induced pulses produced by the photomultiplier within a given time interval. Such systems, often called "photon counting" systems, have three main advantages over conventional analogue techniques: (a) the effects of gain instabilities in the photomultiplier can be virtually eliminated; (b) fluctuation in the signal due to variations in the charge contained in the pulses is eliminated; (c) signal-to-noise ratio can be improved by discriminating against noise pulses. For our photomultiplier, points (b) and (c) are probably the most significant[56].

Since, to a very good approximation, the photons incident on the photomultiplier obey Boltzman statistics, as do the major sources of photomultiplier dark count (thermionic emission and background radiation), the r.m.s. deviation from a pulse count N is $\sqrt{N}$ [57]. The signal-to-noise ratio, R, is therefore

$$R = \frac{N_s}{(N_s + N_d)^{\frac{1}{2}}} \tag{6.1}$$

where N_s is the number of signal pulses and N_d the number of dark pulses counted in a particular time. N_s and N_d are functions of the pulse "height", measured in volts, and the optimum settings, h_1 and h_2 for the pulse height discriminators can therefore be determined by putting $\frac{dR}{dh} = 0$. The result is

$$\frac{dN_d}{dh} = \left(\frac{2N_d}{N_s} + 1\right) \frac{dN_s}{dh} , \tag{6.2}$$

from which three conditions can be derived:

$$\frac{d}{dh}(\log N_d) = 2\frac{d}{dh}(\log N_s) \text{ for } N_d >> N_s \tag{6.3}$$

$$\frac{dN_d}{dh} = 3\frac{dN_s}{dh} \text{ for } N_d = N_s \tag{6.4}$$

and $$\frac{dN_d}{dh} = \frac{dN_s}{dh} \text{ for } N_d << N_s \tag{6.5}$$

For the first case, $N_d >> N_s$, the levels h_1 and h_2 will be near to those values at which the integrated dark pulse distribution curve diverges above that for the signal pulses. As the ratio N_d/N_s decreases, the levels will move towards the extremes of very small and very large pulses. However, in these latter cases R will be large already, so that best overall performance will be obtained by setting the discriminator voltages according to the condition (6.3).

The electronic circuitry is essentially that described by Lockwood[54], with some modifications which have improved the performance. The photomultiplier pulses are first amplified by a charge amplifier which is placed on the photomultiplier socket so as to keep the input capacitance to a minimum: previously, this factor seriously limited the maximum pulse rate which the amplifier could accept. A further amplifier stage follows, and the pulse then enters the logic circuitry, which generates a standard output pulse if the input pulse is between the preset voltage levels. The generated pulses are fed into a remote, unidirectional, 11 bit binary counter, which is controlled by a DEC PDP-8 computer. The counter has an overflow interrupt and is read by the computer at constant time intervals; a twelfth bit is used to provide frequency calibration. The data thus collected is stored in the computer and punched onto paper tape on command. The computer

also provides an oscilloscope display of the stored spectrum. Although the computer operates on a timeshare system which enables it to control two experiments in addition to the Raman experiment, the use of the external counter ensures that the error contributed to the measurements by the system is small: 0.3% for a one second counting period, and proportionally lower for longer counting periods. The PDP-8 program is described in more detail in Appendix III.

The tape output from the PDP-8 is processed by the IBM 360/44 computer, and plotted by an IBM 1627 plotter. The form of the output from the digital detection system is much more convenient than that from the HR-8. Amplification and dimensions of the spectra can be varied readily, and the data can be used directly by analysis and curve fitting programs.

The PDP-8 is also used to obtain the pulse height distribution curves necessary for calibration of the discriminators. Rather than obtaining these by scanning through the full voltage range with a narrow "window", a sample and hold circuit which will enable the curves to be obtained in a few minutes is being built.

The circuit picks up the peak voltages of the pulses entering the discriminators and holds these long enough for an analogue-to-digital converter coupled to the PDP-8 to record their values, which are then stored. This arrangement will enable us to switch photomultipliers, to alter their supply voltages and to effect repairs on the pulse rate detector with much greater ease.

6.5 FURTHER DEVELOPMENTS

While the present system constitutes a powerful Raman spectrometer, there is room for further development work which would improve the performance and capabilities. Two of these have been mentioned already: conversion of the argon laser to a krypton/argon laser, which would give us greater facility to work with coloured samples; and construction of a triple monochromator, using presently available instruments. As a first step, the 1/3 metre spectrometer will not be coupled to the double 1 metre drive mechanism, but will be used as a fixed-frequency premonochromator, the double spectrometer scanning through the frequency "window". This will enable more detailed experiments to be performed on samples such as $CdCl_2(Co)$, where at present the stray light level can be several times greater than that of the Raman signal.

The present digital detection system is to be augmented with a direct chart recorder output, which will operate simultaneously with the computer recording system. The alteration has the advantage of giving immediate visual data, whilst retaining the analytical flexibility of the digital system.

Finally, the accuracy of the data can be improved with the addition of a laser power monitoring system to enable correction to be made for variations in the laser intensity. We have available at present only a relatively insensitive monitoring system.

CHAPTER 7

EXPERIMENT AND RESULTS

7.1 INTRODUCTION

Crystals of $CoCl_2$ and of $CdCl_2$, $MnCl_2$ and $CdBr_2$ containing Co^{2+} have been investigated. As a necessary preliminary to the measurement of the Raman spectra of the Co^{2+} ion in these crystals, the phonon spectra were measured by Lockwood[54,58]. The phonon spectra of $CdCl_2$ and $CdBr_2$ have also been measured by Nakashima et al.[59]. In each case, the spectrum consists of two strong, low frequency lines (of A_{1g} and E_g symmetries) which become very narrow at low temperatures.

The phonon spectra of mixed crystals in this system exhibit "one-mode" behaviour[60]; that is the intensities and frequencies of the Raman lines vary continuously between those of pure crystals of the two components of the mixed crystal. In "two-mode" behaviour, the mixed crystal spectra exhibit four Raman-active vibrational modes, of which two can be associated with each pure crystal, and have intensities proportional to the concentration of each compound in the mixture. In crystals containing an admixture of $CoCl_2$ or $CoBr_2$, as appropriate, the phonons retain their very narrow width, and this coupled with the one-mode behaviour indicates that the Co^{2+} ions in the crystals are distributed in a random fashion. We will thus assume for the present that isolated Co^{2+} ions doped into $CdCl_2$, $CdBr_2$ and $MnCl_2$ crystals experience a crystal field which is essentially that of the unperturbed host crystal. This point is further discussed in section 7.4.

Raman lines associated with electronic transitions of Co^{2+} ions can be identified in three ways: firstly, from the frequencies of the lines; secondly, from their polarization properties; and thirdly, from the dependence of their intensity on the concentration of Co^{2+} ions. The host crystals used in these experiments show no first-order Raman features above about 300 cm^{-1}, and investigation of the Co^{2+} spectra above this frequency is expected to be quite straightforward. In particular, the use of low temperatures, usually $4.2^{o}K$, to minimise relaxation rates and thereby increase peak intensities, will be a standard procedure. However, the theory indicates that one electronic transition is likely to have a low energy, and this is in fact found in experiment. To overcome the problem of observing an electronic line obscured by a strong phonon line, spectra were also recorded at room temperature, where we may expect an electronic level less than 300 cm^{-1} above the ground state to have a significant population, and thus give rise to hot bands in the higher frequency spectrum.

7.2 EXPERIMENTAL

All the crystals are highly hygroscopic and special care must be taken in their preparation and mounting in order to prevent contamination by moisture. The crystals were grown from the melt by the Stockbarger technique. Analar grade powders of the hydrated salts were first dehydrated by heating under vacuum for several days, and then further purified by forcing dry HCl or HBr through the molten material. The liquid then passes through a sintered-quartz sieve, and the crystals are grown by slowly lowering sealed quartz ampoules

through a sharp temperature gradient. Results of far IR absorption experiments show that the crystals contain essentially no water impurity[61].

The $CdCl_2$ crystal has a structure which contains layers of identical ions, with weak bonding between adjacent chlorine ion layers. The crystals cleave readily in planes parallel to the layers, which are perpendicular to the trigonal symmetry axis, but not in any other direction. In order to protect the samples from the atmospheric moisture, the crystals are removed from the quartz ampoules in a dry atmosphere and mounted on the cold finger of a low temperature dewar. The dewar is then evacuated and all spectra are recorded with the sample under vacuum. The geometry was usually such that the laser beam was perpendicular to the trigonal axis, and the viewing direction parallel to it.

7.3 EXPERIMENTAL RESULTS

7.3.1 $CdCl_2(Co)$[62,†]

Pure $CdCl_2$ is optically clear, and the introduction of Co^{2+} into the crystals results in a blue colouring which becomes progressively more dense as the Co^{2+} concentration increases. Crystals containing 0% or 100% were usually of poor structural quality, but some of the lightly doped samples were excellent.

Raman spectra of crystals containing 0%, 3%, 5%, 10%, 50% and 100% by weight of $CoCl_2$ were measured, usually at low temperatures. Figure 7.1 depicts the main features of the observed spectra. Two intense and narrow phonon lines are

† See Appendix IV.

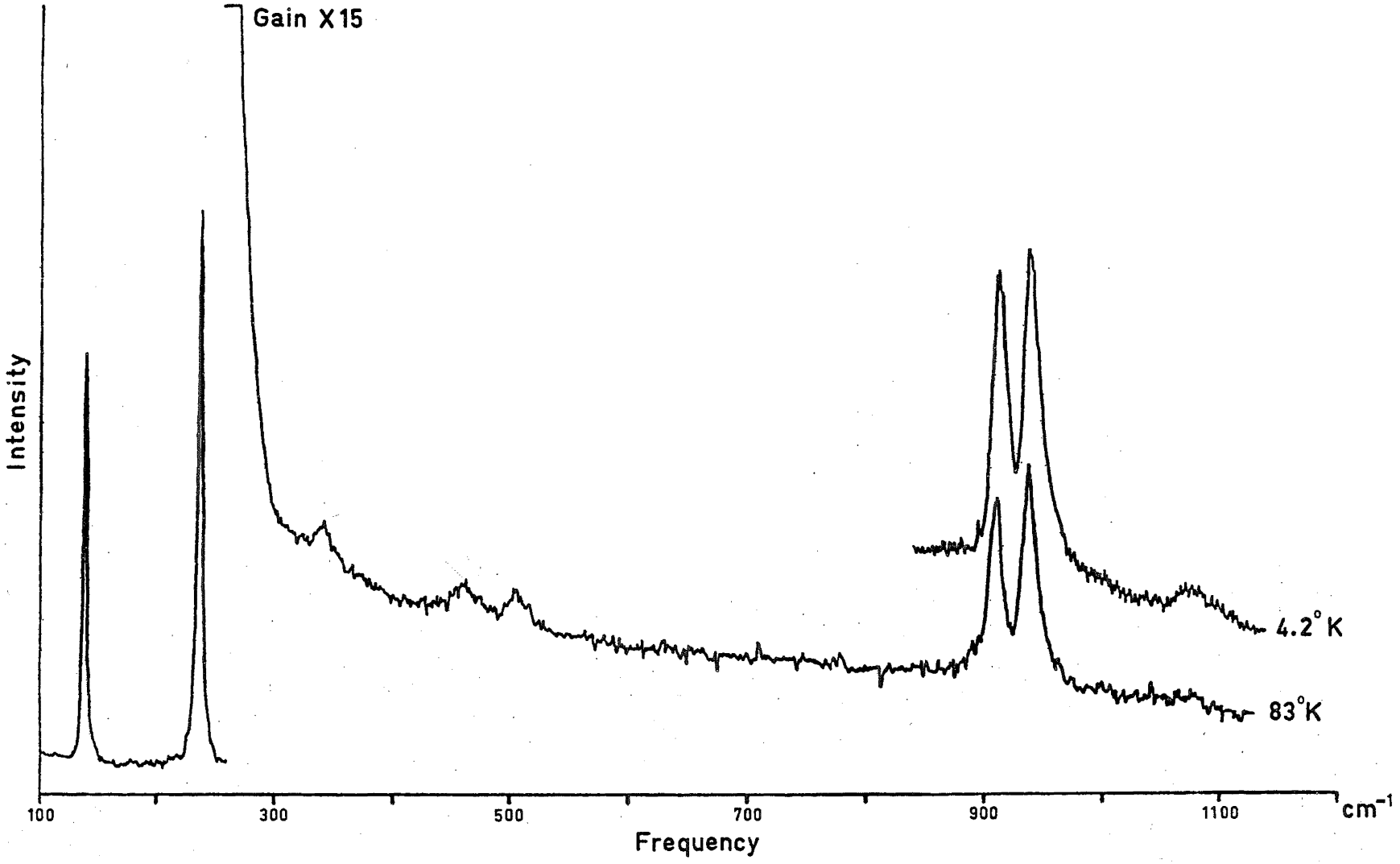

Fig. 7.1 Raman scattering spectrum of $CdCl_2$(Co): 5%. The phonons are measured at a spectral slit width of 1.5 cm^{-1}, and the higher frequency portion at 6 cm^{-1}.

observed in the low frequency (< 300 cm^{-1}) region, and in the high frequency portion of the spectrum, lines are observed at 337, 459, 501, 925, 954 and 1090 cm^{-1}.

Figure 7.2 shows the spectra of crystals containing from 0% to 100% of $CoCl_2$, all except the latter being measured at 4.2°K. As the concentration effects are to be examined in detail in a later section, we will at this stage merely note the main trends in the spectra. Firstly, we observe that as concentration increases, the gross features show increasing intensity, and slight shifts towards higher frequencies, indicating a common nature for the spectral lines of $CdCl_2$(Co) and $CoCl_2$. Secondly, in the 0% spectrum, two weak lines at 338 cm^{-1} and 460 cm^{-1} are evident. These lines appear consistently in spectra of pure $CdCl_2$, and would seem to rule out the possibility of the 337 or 459 cm^{-1} lines being associated with Co^{2+} electronic transitions.

Figure 7.3 shows a comparison between the spectra of crystals of 5% concentration at room and liquid air temperatures. A broad line appears in the spectrum of the hot crystal at 715 cm^{-1}, about 235 cm^{-1} below the broadened and overlapping doublet, but is not evident in the low temperature spectrum.

Polarization measurements were attempted, but yielded no information, even in the case of the phonons for which the polarization properties were already known. The problems preventing the success of these experiments are common to all the crystals measured, and will be discussed in section 7.6.

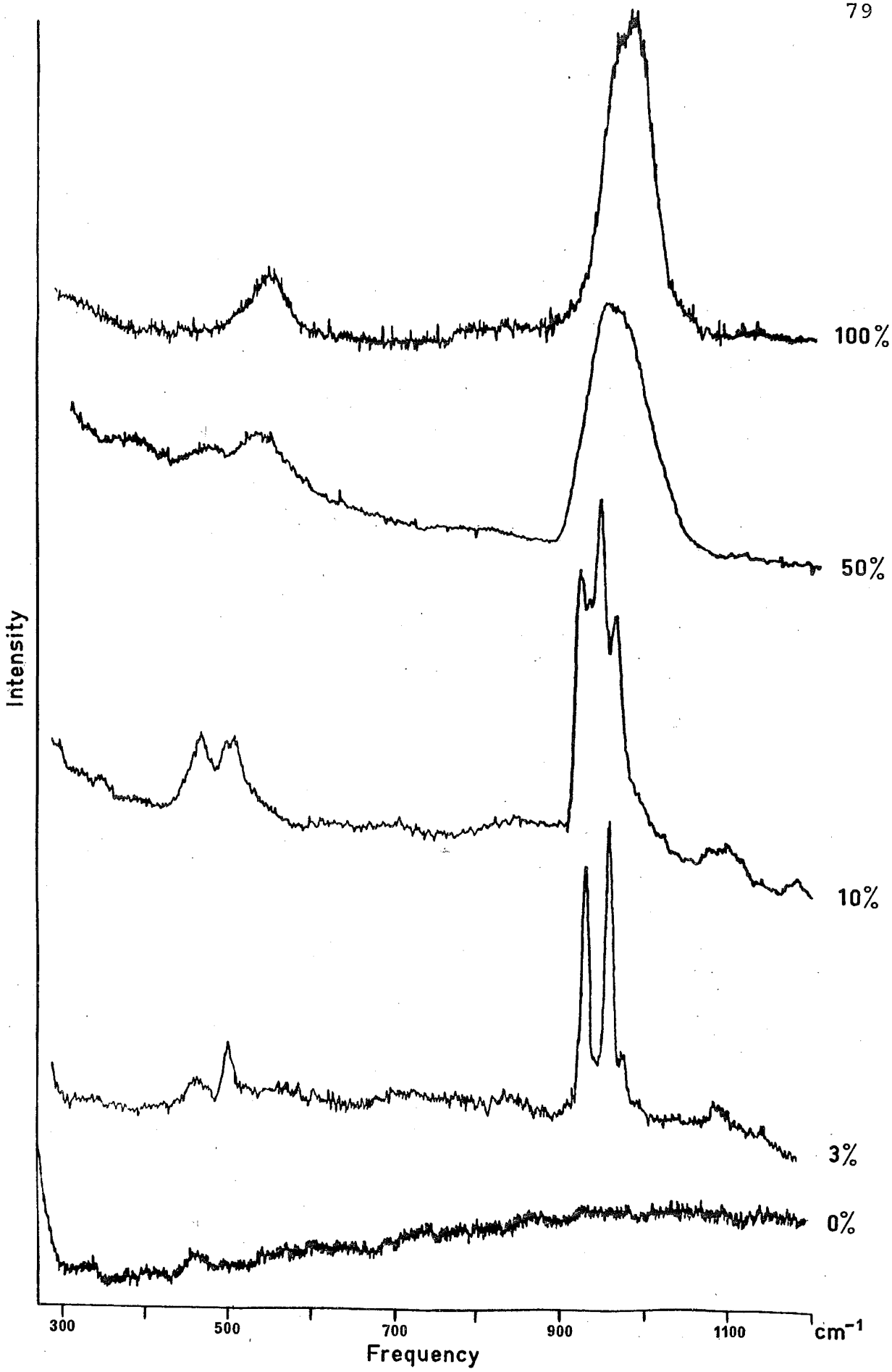

Fig. 7.2 Raman scattering spectra of $CdCl_2$(Co) at different concentrations. The spectral slit widths are all 6 cm^{-1}; all spectra were recorded with the 4880Å, and all except the 100% at 4.2°K.

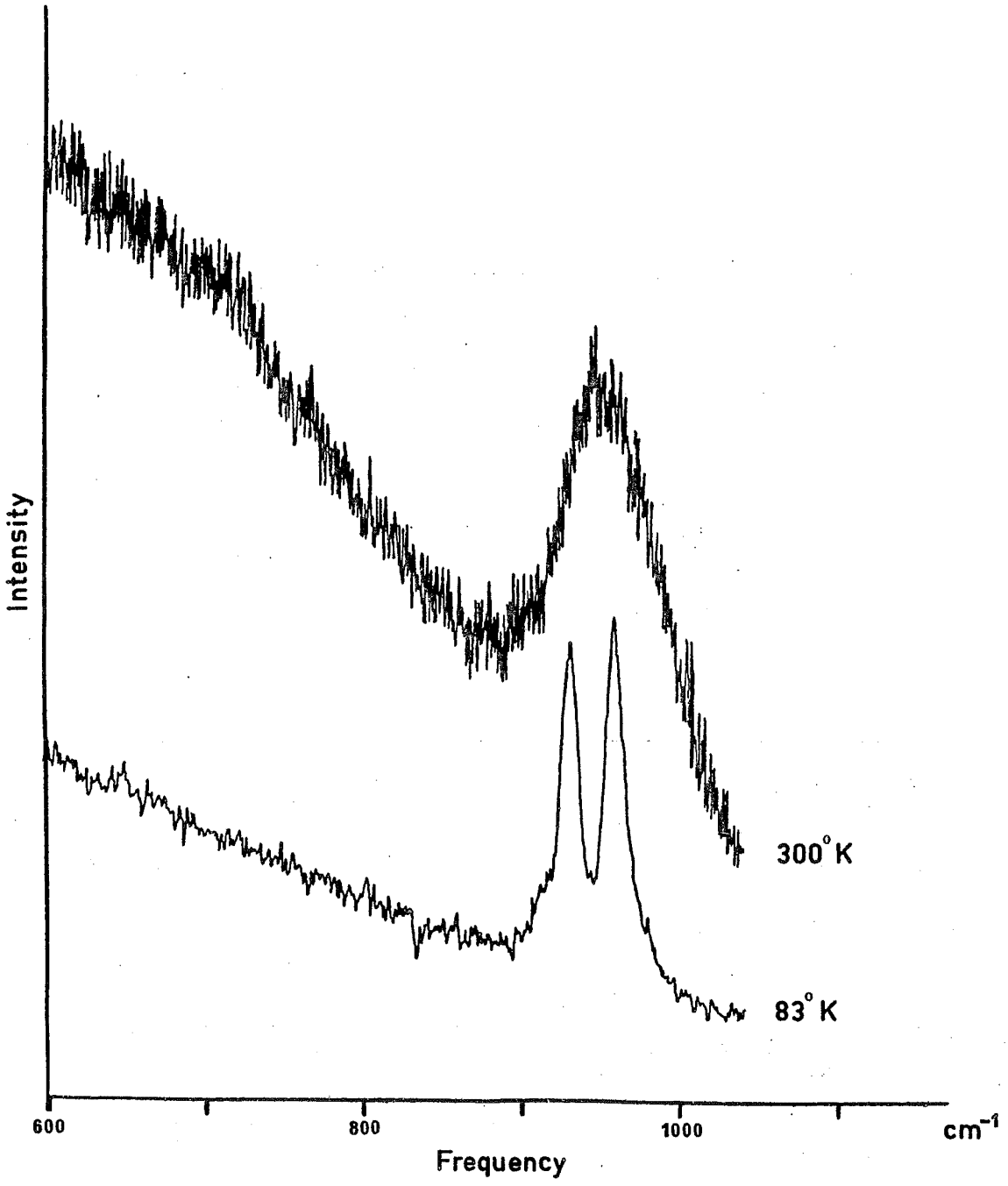

Fig. 7.3 Raman scattering spectra of $CdCl_2$(Co): 5% at 83°K and 300°K. The spectral slit widths are 6 cm^{-1} and 10 cm^{-1} respectively; the spectra were excited by the 4880Å laser line.

7.3.2 $MnCl_2$(Co)

The spectrum of $MnCl_2$(Co), shown in Figure 7.4, is very similar to those of $CdCl_2$(Co): in addition to the strong phonon doublet, pairs of lines are observed in the 500 and 950 cm^{-1} regions, and again the 460 cm^{-1} line appears weakly in the 0% spectrum. Differences observable are the relative weakness of the spectra, probably due to absorption of the laser light by the host crystal (pure $MnCl_2$ is red in colour), the the slightly larger widths of the high frequency lines.

In Figure 7.5, the results of a high gain, low temperature experiment, and of a room temperature experiment are shown. As in the case of $CdCl_2$(Co), a hot band appears at about 230 cm^{-1} below the 975 cm^{-1} doublet, and, at low temperatures, a weak line is found, at 1108 cm^{-1}.

The dependence of the spectra on the Co^{2+} concentration was not measured in such detail as was done for $CdCl_2$(Co), but up to 10% concentration by weight of $CoCl_2$, very similar behaviour was observed.

7.3.3 $CoCl_2$[63,64,†]

The dark blue $CoCl_2$ samples absorbed the laser light of all frequencies to a considerable extent, and only surface scattering experiments were found to give satisfactory results.

Figure 7.6 shows the room and liquid air temperature spectra of $CoCl_2$, the comparison clearly demonstrating the presence of hot bands in the higher temperature spectrum. In each case, these features are approximately 220 cm^{-1} below the next highest low temperature bands, and as can be seen, a line

† See Appendix IV.

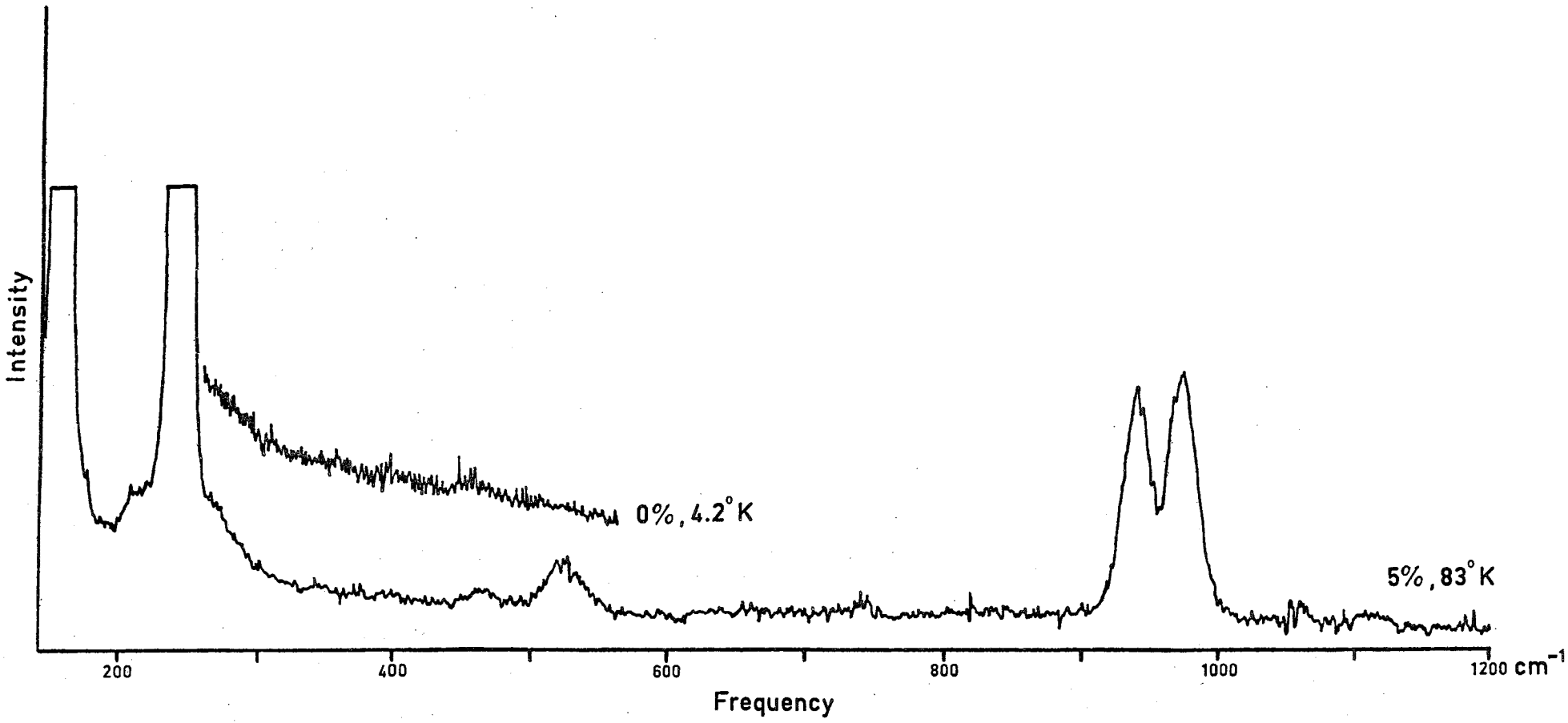

Fig. 7.4 Raman scattering spectra of $MnCl_2$(Co): 5% and of $MnCl_2$. The spectra were recorded with a spectral slit width of 6 cm^{-1}, using the 4880Å laser line.

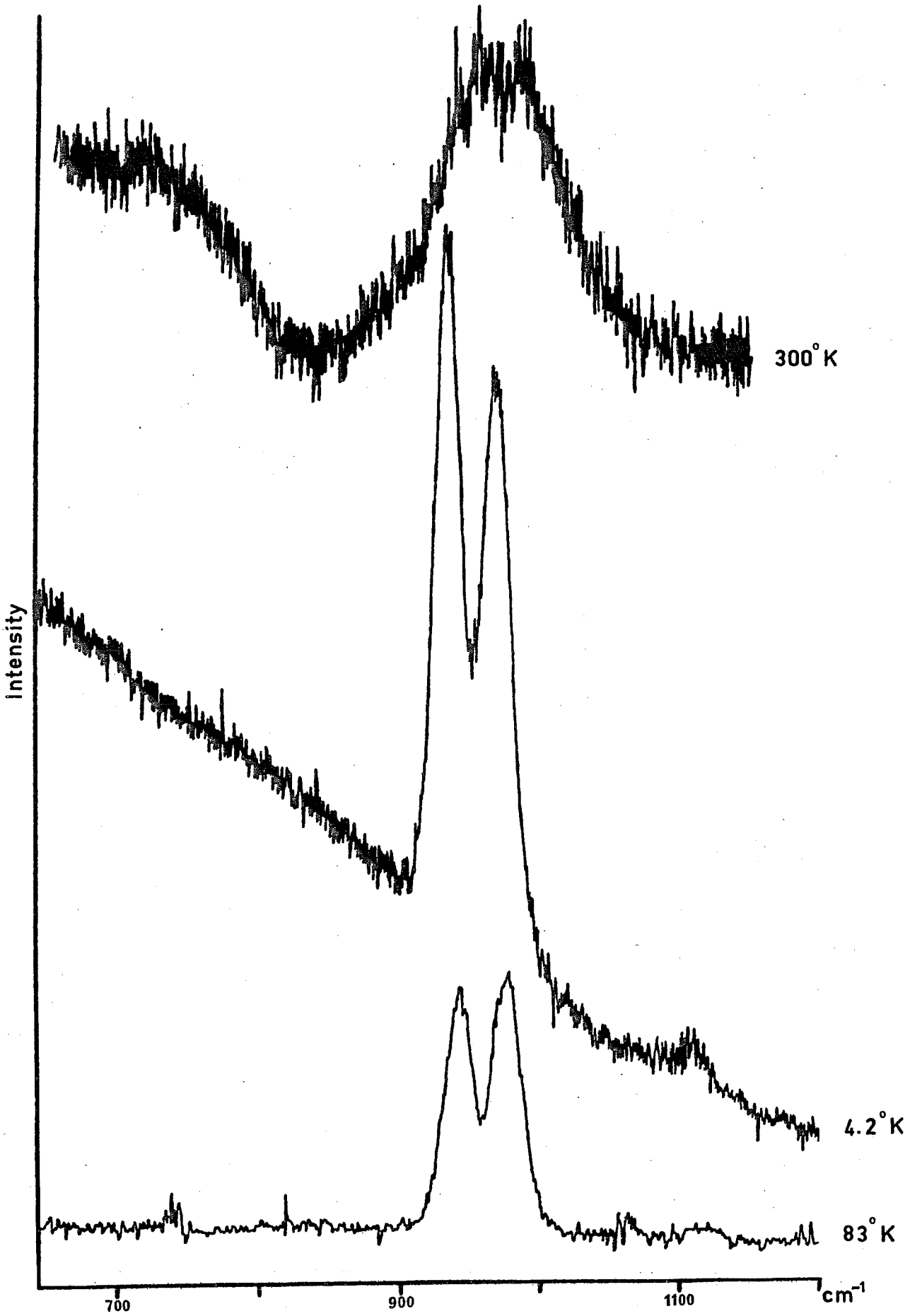

Fig. 7.5 Spectra of $MnCl_2$(Co):5% at 4.2°K, 83°K and 300°K. The slit widths are 9, 6 and 11 cm^{-1} respectively.

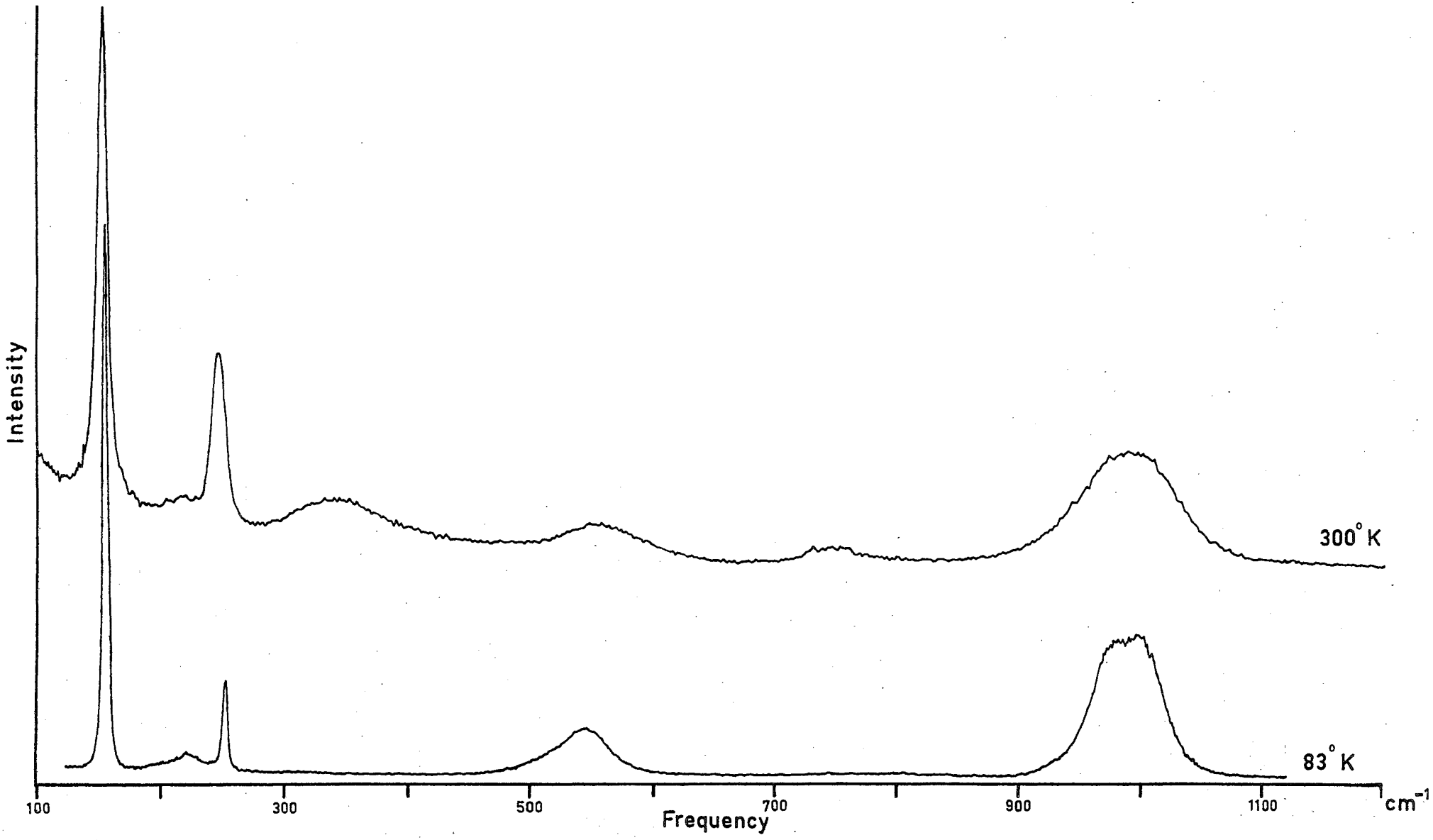

Fig. 7.6 Raman scattering spectra of $CoCl_2$ at 83°K and 300°K. The spectral slit widths were 3 cm^{-1} and 6 cm^{-1} respectively and the spectra were excited by the 4880Å laser line.

exists at this frequency in both spectra.

The 545 cm^{-1} line in the liquid air temperature spectrum exhibits a definite asymmetry, as can be seen from Figure 7.7 which shows a comparison between the normalised 550 and 1000 cm^{-1} bands. If the 1000 cm^{-1} line is reflected about its peak, the leading edge fit is equally as good.

As in the cases of $MnCl_2$(Co) and $CdCl_2$(Co), a search in the 1100 cm^{-1} region met with success, as is shown in Figure 7.8. These spectra were recorded using liquid helium as a coolant, but it was known from observed features (see section 7.7) that the crystal was still in the paramagnetic phase.

7.3.4 $CdBr_2$(Co)

The phonon spectra of $CdCl_2$, $MnCl_2$ and $CoCl_2$ are all very similar (see Table VII), but the $CdBr_2$ phonon frequencies are only about one half of those of the other crystals. It was not altogether surprising, therefore, to find that the high frequency Raman spectra of $CdBr_2$(Co) did not closely resemble those of the other three systems. Figure 7.9 shows the Raman spectra of $CdBr_2$ containing 0%, 3%, 5% and 10% by weight of $CoBr_2$, all measured at liquid helium temperatures and using the 4880Å laser line. In the spectrum of $CdBr_2$(Co) 3%, a large number of lines are observed, most of them weak; of the strong lines, all but three, at 282, 893 and 995 cm^{-1}, are matched by features in the spectrum of pure $CdBr_2$. When the $CoBr_2$ concentration is increased to 5%, these three lines increase in intensity, and three other lines at 351, 394 and 443 cm^{-1} come into prominence. These new lines remain in the 10% spectrum, and yet another line is now evident on the low frequency side of the 282 cm^{-1} line.

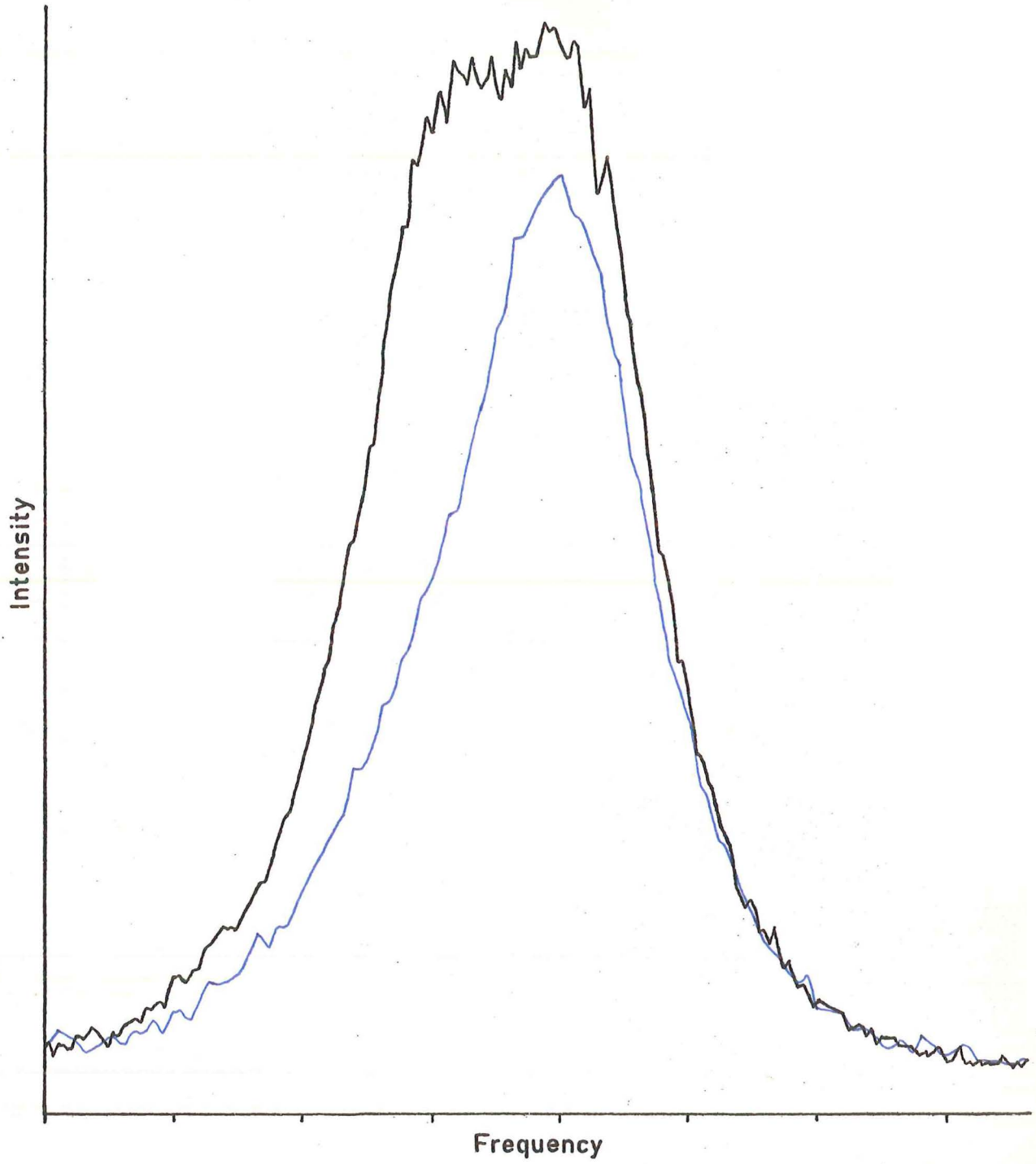

Fig. 7.7 Comparison of the normalised 545 cm^{-1} (in blue) and 1000 cm^{-1} bands of $CoCl_2$. The spectra were recorded at 83°K, using the 4880Å laser line with spectral slit widths of 6 cm^{-1} and 3 cm^{-1} respectively; the scale is in units of 25 cm^{-1}.

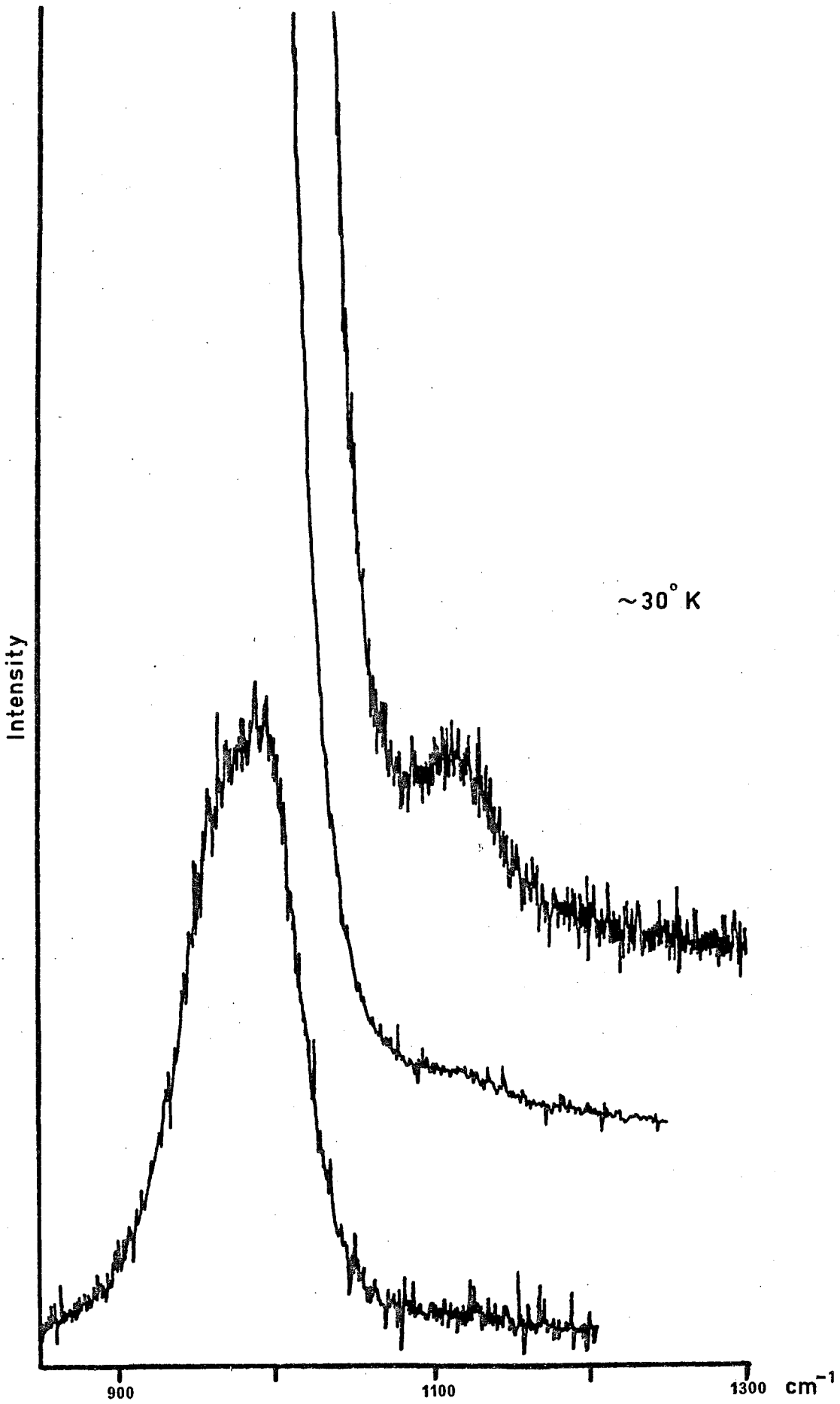

Fig. 7.8 Spectra of $CoCl_2$ recorded at high gain. The spectral slit width is 10.5 cm^{-1}, and the laser line 4880Å.

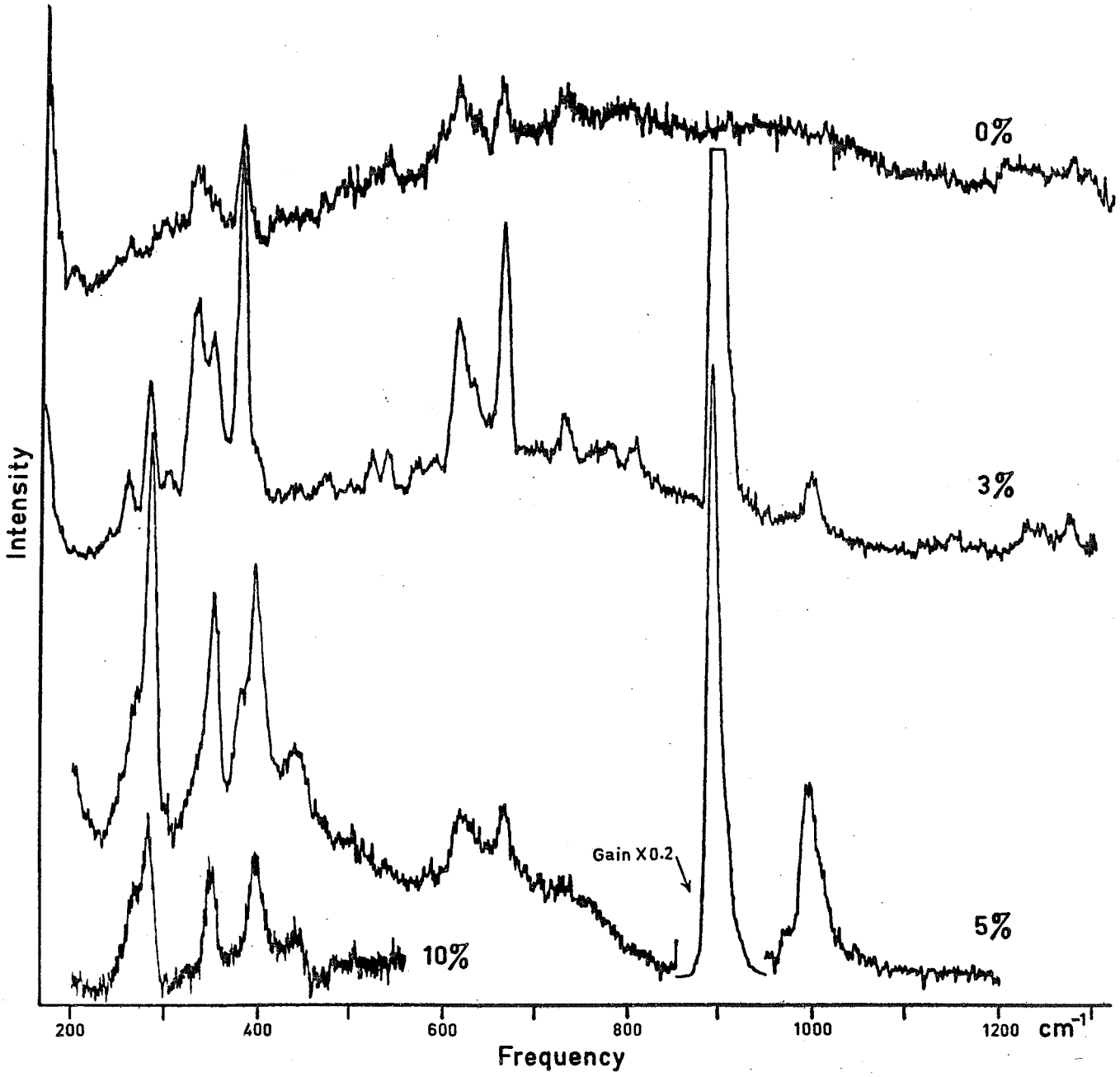

Fig. 7.9 Raman scattering spectra of $CdBr_2$(Co) at different concentrations. The spectral slit widths are all 6 cm^{-1}, and each spectrum was recorded at 4.2°K, using the 4880Å laser line.

In Figure 7.10, the results of Raman experiments using different laser lines are shown. In the high frequency region, the lines at 893 cm^{-1} and 995 cm^{-1} are shown to be Raman lines, and a high resolution scan through the former reveals it to be in fact a narrowly split doublet: the form of the spectrum in this region thus conforms to that discovered in the other three crystals.

The spectrum recorded with the 5145Å laser line indicates that most of the lines observed in the 4880Å spectrum are fluorescence lines, and this assignment is confirmed by the 4765Å spectrum. Table VI contains the frequencies of some of the lines appearing in the 4880Å and 4765Å spectra.

TABLE VI

Fluorescence lines in $CdBr_2$(Co): 3%

4880Å spectrum			4765Å spectrum	
Relative Frequency†	Frequency	Difference	Frequency	Relative Frequency†
260±1 cm^{-1}	20233 cm^{-1}	-4 cm^{-1}	20237 cm^{-1}	~750 cm^{-1}
304±2	20189	2	20187	800±5
333±1	20160	-2	20162	825±5
382±1	20111	3	20108	879±5
618±1	19875	-1	19876	1111±3
632±2	19861	4	19857	1130±3
666±1	19827	0	19827	1160±3

† Energy difference between the laser light and the observed emission.

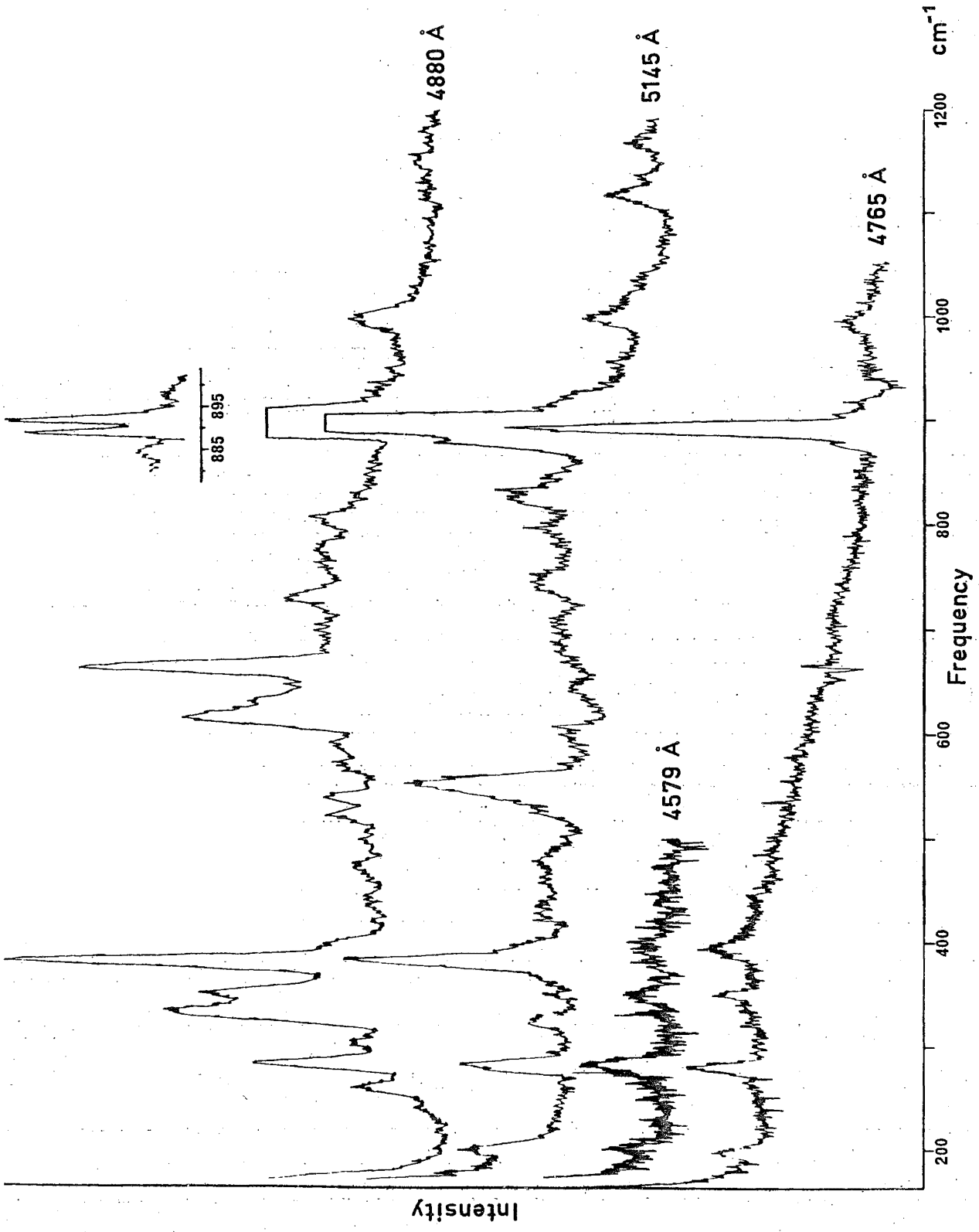

Fig. 7.10 Raman scattering spectra of $CdBr_2$(Co):3% using different laser lines. All spectra were recorded at 4.2°K, and with a spectral slit width of 6 cm^{-1}, except for the inset which is at 3 cm^{-1}.

The lines appearing in Table VI include all the strong lines observed in the 4880Å spectrum other than those that have been determined to be Raman lines.

The four lines in the 200-400 cm^{-1} region of the 5145Å spectrum at 200 cm^{-1}, 282 cm^{-1}, 351 cm^{-1} and 394 cm^{-1} appear with reasonable consistency in all the other spectra of $CdBr_2$(Co): 3%. The 200 line, which is quite evident in all except the 4880Å spectrum, also appears in the pure $CdBr_2$ spectram, and so cannot be associated with the Co^{2+} ion. The position is not as clear for the 351 cm^{-1} and 394 cm^{-1} lines, however, as in the spectrum of pure $CdBr_2$ and in the 4880Å and 4765Å spectra of $CdBr_2$(Co): 3%, one or both lines are partially obscured. The nature of these two lines will be further discussed in the next section.

The fluorescence structure in the 350 cm^{-1} and 630 cm^{-1} regions of the 4880Å spectrum has some interesting properties. Firstly, the shape of each structure is the same, both have frequency widths of 48±2 cm^{-1}, and in each of the different crystals in which they appear, they have similar intensity ratios. The frequency difference between corresponding lines in each structure is 281±2 cm^{-1}, suggesting an association with the 282 cm^{-1} Raman line in the doped crystals. However, the appearance of this line is strongly correlated with the presence of the Co^{2+} ion, whereas the fluorescence appears in the spectra of crystals which do not contain any cobalt. A further point of interest is that the frequencies of the fluorescence lines are independent of the Co^{2+} concentration; as the cubic crystal field is dependent on the Co^{2+} concentration, it should be expected that any fluorescence

characteristic of $CdBr_2$ will vary markedly between the different crystals.

The evidence available is incomplete; however, it can be reasonably concluded that the strong fluorescence lines appearing in the spectrum of $CdBr_2$(Co): 3% originate outside the bulk of the crystal sample, and undoubtedly are caused by an impurity. The same conclusion seems likely to hold for the weak lines in the same spectrum. The possibility that they could be second-order phonon Raman lines, too weak to be seen in any other spectrum, would seem to be ruled out by the behaviour of the 200 cm^{-1} Raman line. This line is virtually invisible in the spectrum of $CdBr_2$(Co): 3% using the 4880Å line, but it appears for other laser lines, and in pure $CdBr_2$: these are properties expected of a second-order phonon line. The weak lines in question are, however, strongest in the 4880Å spectrum in which it seems the second-order phonon lines are weak.

The experimental results discussed in this section are enumerated in Table VII, with the exception of the concentration effects, which will be presented in the next section.

TABLE VII

Summary of the results of Raman experiments on cobalt-doped crystals of $CdCl_2$, $MnCl_2$ and $CdBr_2$, and on paramagnetic $CoCl_2$[a].

Phonon characteristics (at 4.2°K) [b]				
	E_g phonon		A_{1g} phonon	
Crystal	Frequency	Width	Frequency	Width
$CoCl_2$	156.6±0.3	<1.2	253 ± 0.5	<3.5
$MnCl_2$	150 ± 1	<2	242 ± 1	<2
$CdCl_2$	135 ± 1	<2	236 ± 1	<4
$CdBr_2$	81 ± 1	<2	151 ± 1	<2

$CdCl_2$(Co) spectra 300-1200 cm^{-1}					
0%, 4.2°K		5%, 4.2°K		5%, 300°K	
Frequency	Width	Frequency	Width	Frequency	Width
338 ± 5	~30	337 ± 2	20±5	-	-
460 ± 5	<30	459 ± 5	20±5	-	-
-	-	501 ± 2	<15	-	-
-	-	-	-	715 ± 5	broad
-	-	925.0±0.5	<9	950 ± 5	65±5
-	-	954 ± 1	<10	-	-
-	-	1090 ± 5	<30	-	-

a All measurements are in wavenumbers.

b The phonon frequencies in doped crystals vary according to the cobalt concentration.

$MnCl_2$(Co) Spectra 300-1200 cm^{-1}

0%, 4.2°K		5%, 4.2°K		5%, 300°K	
Frequency	Width	Frequency	Width	Frequency	Width
460 ± 10	-	461 ± 5	<20	-	-
-	-	524 ± 2	25 ± 5	-	-
-	-	-	-	745 ± 10	broad
-	-	938 ± 1	<20	975 ± 3	100±10
-	-	972 ± 1	<20	-	-
-	-	1108 ± 2	<30	-	-

$CoCl_2$ spectra 200-1200 cm^{-1} (except A_{1g} phonon)

83°K		300°K	
Frequency	Width	Frequency	Width
221 ± 2	20±3	220 ± 3	-
-	-	344 ± 5	75±5
545 ± 1	51±2	559 ± 3	70±5
-	-	755 ± 5	65±15
978 ± 5	65±5	986 ± 3	90±5
1115 ± 5	40±10	-	-

$CdBr_2$(Co) spectra 200-1200 cm^{-1} (except fluorescence) [c]

0%,4880	3%,5145	3%,4880	3%,4765	3%,4579	Width
200 ± 1	200 ± 1	-	200 ± 2	201 ± 3	<10
-	281 ± 1	283 ± 1	282 ± 1	283 ± 2	<10
-	349 ± 2	352 ± 1	351 ± 2	350 ± 5	<10
-	394 ± 1	~400	-	398 ± 5	<15
-	445 ± 5	439 ± 2	-	-	-
-	892 ± 1	889 ± 1	894 ± 1	-	<3
-	(unsplit)	894 ± 1	(unsplit)	-	<4
-	994 ± 2	995 ± 1	994 ± 2	-	<12

c All measured at 4.2°K.

Fluorescence lines in $CdBr_2(Co)$ [c]

absolute frequency	4880 spectrum	4765 spectrum	Width
20659 ± 3	-	328 ± 3	<13
20606 ± 1	-	381 ± 1	<13
20444 ± 2	-	545 ± 2	35 ± 4
20251 ± 2	242 ± 2	-	-
20233 ± 1	260 ± 1	~750	<9
20189 ± 2	304 ± 2	800 ± 5	-
20160 ± 1	333 ± 1	825 ± 5	<15
20111 ± 1	382 ± 1	879 ± 5	<11
20020 ± 5	473 ± 5	-	-
19969 ± 3	524 ± 3	-	<10
19951 ± 1	542 ± 1	-	<10
~19923	~570	-	-
~19903	~590	-	-
19875 ± 1	618 ± 1	1111 ± 3	<15
19861 ± 2	632 ± 2	1130 ± 3	-
19827 ± 1	666 ± 1	1160 ± 3	<12
19761 ± 1	732 ± 1	-	<12
~19713	~780	-	broad
19687 ± 2	806 ± 2	-	<15
19343 ± 2	1150 ± 2	-	<15
19262 ± 5	1231 ± 5	-	-
19216 ± 3	1277 ± 3	-	<15

c All measured at 4.2°K.

7.4 ANALYSIS OF RESULTS

With the absence at this stage of useful polarization data, the identification of Co^{2+} electronic transitions relies on a comparison between observed concentration dependence and frequency of experimental lines and the expected behaviour for such transitions. In addition, since all the measured crystals are isomorphic, we can expect the electronic Raman spectra to have similar forms in each crystal.

7.4.1 Theory of Concentration Effects

The simplest expected concentration effect is that Co^{2+} electronic Raman lines may be observed in crystals containing cobalt, but not in crystals which do not contain cobalt. However, more detailed knowledge of the expected dependence of the spectra on Co^{2+} concentration is both necessary in order to interpret observed spectra, and useful as a means of giving a more positive identification of the Co^{2+} transition lines.

In the crystals investigated, Co^{2+} ions reside in "boxes" of anions, and since none of these samples contained mixtures of anions, all the Co^{2+} ions in a crystal experience similar nearest-neighbour environments. The nearest-neighbour cations for each Co^{2+} ion can differ, however, and we might expect that different sets of nearest-neighbour cations would, through their effect on the anion boxes, produce changes in Co^{2+} energy levels. Obviously the more distant environment, such as the next-nearest-neighbour cations will also have some effect, and so on, the circumstances of each case determining to what degree such influences can be detected in the observed spectra. We will at present consider only the variations in the nearest-neighbour cations.

Within the cation layer, each ion has four nearest-neighbours (see Figure 5.1); inter-layer effects can be ignored, as each cation layer is separated by two layers of the much larger anions. We have, therefore, five different situations to consider for a Co^{2+} ion in a $CdCl_2$-type lattice: of the nearest-neighbour cations, 0, 1, 2, 3 or 4 may be Co^{2+} ions. In Figure 7.11, the relative probabilities for each situation in crystals such as $Cd_{1-x}Co_xCl_2$ are shown for $0 \leqslant x \leqslant 1$, calculated under the assumption that the Co^{2+} ions are randomly distributed. Evidence in support of this assumption was discussed in section 7.1, and is further supported by the observed Co^{2+} Raman spectra, as will be shown shortly.

7.4.2 Preliminary Interpretation of Results

By comparing the spectra of $CdCl_2(Co)$ with that of $CdCl_2$ itself, it would appear that the lines at 501, 925 and 954 cm^{-1} are associated with the Co^{2+} ions. The lines at 337 cm^{-1} and 459 cm^{-1} appear in both spectra, and are assigned to the second-order phonon spectrum of the crystals. Further supportive evidence for this assignment comes from the large widths of these lines even at liquid helium temperatures, an expected behaviour for second-order phonon transitions, and from the frequencies of the lines: for pure $CdCl_2$, an $A_{1g} + E_g$ phonon transition has an energy of 371 cm^{-1} for k = 0 phonons, and a $2 \times A_{1g}$ transition, 472 cm^{-1} at k = 0. These figures are of the correct order of magnitude, but a more precise correlation would require a knowledge of the dispersion relations and phonon density of states for $CdCl_2$.

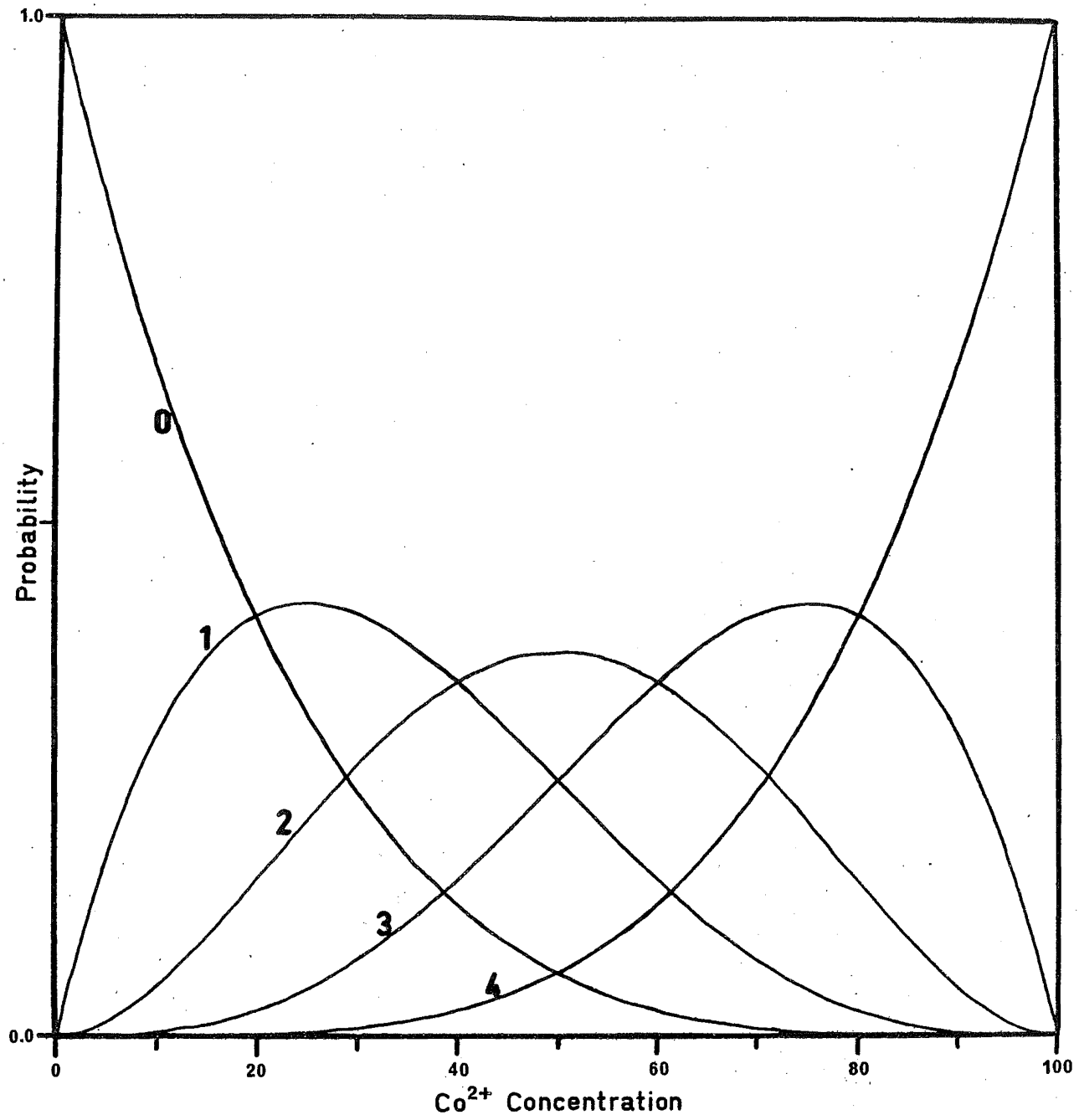

Fig. 7.11 Probability distribution for the nearest-neighbour (n.n.) cation situations in crystals of the type $Cd_{1-x}Co_xCl_2$ as a function of the Co^{2+} concentration. The labels 0-4 on the curves correspond to the number of n.n. Co^{2+} cations for each Co^{2+} ion.

The 715 cm^{-1} line in the $CdCl_2$(Co) room temperature spectrum, and the weak line at 1090 cm^{-1} in the low temperature spectrum are both too weak to enable a meaningful comparison with the pure $CdCl_2$ spectra. However, as hotband scattering is not a characteristic of crystal lattices, the 715 cm^{-1} line can also be assigned to Co^{2+} with reasonable assurance. A consequence of this assignment is a value of 235 ± 10 cm^{-1} for another Co^{2+} electronic energy level. The case for the assignment of the 1090 cm^{-1} line to Co^{2+} is: (a) that it is in the region predicted by the theory, in particular as shown in Figure 5.3; (b) that no lattice mode is expected at this frequency, and that the crystal is known to be free from obvious impurities[61] and (c) that it has parallels in all other crystals containing Co^{2+}. Points (a) and (c) apply qualitatively to the other lines in $CdCl_2$(Co) assigned to Co^{2+}.

Every line in the spectrum of $CdCl_2$(Co) is paralleled in $MnCl_2$(Co), with the sole exception of the weak 337 cm^{-1} line, and consequently identical assignments are made. Although this consistency is gratifying, we should be aware that on account of the great similarity of chemical and physical make-up of the two crystals, any difference between the spectra would be the more unexpected.

However, in the case of $CoCl_2$ and $CdBr_2$(Co), the conditions are less similar, yet the consistency of assignment remains. The hotbands of $CoCl_2$ are quite distinct, and point clearly to the electronic nature of the 221 cm^{-1}, 545 cm^{-1} and 978 cm^{-1} bands in the Raman spectrum. The assymmetry of the 545 cm^{-1} band has been noted previously, and Figure 7.7 suggests that there is more than one line in the 978 cm^{-1} band. We will hypothesise on the basis of the observed nature

of these bands, and on their parallels in $CdCl_2$(Co) and $MnCl_2$(Co), that each band consists of two broad overlapping lines. That the Co^{2+} electronic lines in $CoCl_2$ should be broad can be easily understood by consideration of decay mechanisms for a Co^{2+} ion in an excited state: direct radiative decay to the ground state is parity-forbidden, but for a Co^{2+} ion surrounded by other Co^{2+} ions, the possibility exists for non-radiative exchange interactions between these ions, leading to much shorter lifetimes for excited ions in such circumstances as compared with the isolated ion.

The 545 cm^{-1} and 978 cm^{-1} bands were each fitted to Lorentzian doublets using a computer program, ORGLS, which achieves the fitting by an iterative least squares method. The parameters from the resulting good fits are shown in Table VIII.

TABLE VIII

Parameters of the lines fitted to the 545 cm^{-1} and 978 cm^{-1} bands of $CoCl_2$

Band	Frequency	Width	Relative Intensity
545 cm^{-1}	522 cm^{-1}	53 cm^{-1}	$0.3x$
	549	43	x
978	963	42	$0.9y$
	992	40	y

The 549 cm^{-1}, 963 cm^{-1} and 992 cm^{-1} lines are assigned to Co^{2+} electronic transitions. Although relative to the second-order phonon lines in $CdCl_2$ and $MnCl_2$, the 522 cm^{-1} line is much stronger, it is assigned to the same origin. It

is not unknown for second-order phonon lines to have intensities comparable with the first-order[65], and the possibility of an interaction with the nearby Co^{2+} line also exists. These assignments are entirely consistent with the behaviour of the two bands in antiferromagnetic $CoCl_2$. In particular, whilst the lines assigned to Co^{2+} transitions narrow considerably, and new lines appear, a broad, weak line at about 510 cm^{-1} remains.

For the same reasons as are outlined in the case of $CdCl_2(Co)$, the high frequency 1115 cm^{-1} line is also assigned to Co^{2+}, giving a complete set of energy levels for Co^{2+} in $CoCl_2$: 221 cm^{-1}, 549 cm^{-1}, 962 cm^{-1}, 992 cm^{-1} and 1115 cm^{-1}.

In the high frequency region of $CdBr_2(Co)$, the transitions at 889 cm^{-1}, 894 cm^{-1} and 995 cm^{-1} appear on the basis of the comparison between the pure $CdBr_2$ spectrum and that of $CdBr_2(Co)$ to be unambiguously associated with the Co^{2+} ion. This part of the Co^{2+} spectrum has the same form from the point of view of both frequencies and relative intensities as do the spectra assigned to Co^{2+} in the three other crystals, and thereby reinforces those assignments. Of particular importance in this regard is that for the first time, the highest frequency line can on the basis of concentration effects be assigned to Co^{2+}.

The lower frequency spectrum of $CdBr_2(Co)$ has already been analysed to some extent, but further discussion will require application of the detailed theory of concentration effects, described earlier.

7.4.3 Interpretation of Observed Concentration Dependence

We will in this section examine the preliminary results of the previous section in the light of the theory of section 7.4.1, with a view to testing the theory, and confirming the tentative assignments.

The qualitative agreement between the experiment and the theory is excellent. The most detailed experimental picture is given in Figure 7.2, showing the concentration effects in $CdCl_2$(Co).

The cobalt concentration label "3%" is a weight measure (3 parts $CoCl_2$: 100 parts $CdCl_2$), and in this case corresponds to 4%, by number, of the cations. From Figure 7.11 we see that the most common situation is an isolated cobalt ion, the probability of pairs occurring being lower by a factor of 6. The $CdCl_2$(Co): 3% spectrum in the 1000 cm^{-1} region can therefore be interpreted as follows: the two strong lines belong to isolated cobalt ions, whilst the weak line at 969 cm^{-1}, just above the doublet, belongs to cobalt ions having another cobalt ion in a nearest-neighbour cation position. The partner to this line, not evident in the 3% spectrum, becomes visible when the concentration is increased to 10% (12.4% by number), in which the probability ratio is now 1/1.8. In both these spectra, the intensity ratios correspond reasonably well with the probability ratios.

In the 10% spectrum, a broad tail is evident on the upper side of the doublets. According to the theory, the intensity ratios for the 0, 1 and 2 cobalt nearest-neighbour situations are 1/0.6/0.1, the other two possible situations still having negligibly small probabilities of occurrence. Remembering at this point the earlier discussion of linewidths and their

dependence on cobalt-cobalt exchange interactions, we should obviously expect that as the number of nearest-neighbour cobalt ions increases, the widths of observed transition lines will increase. The spectrum tail observed in the 10% spectrum has, then, the qualitative properties expected for the spectrum of Co^{2+} ions with two nearest-neighbour Co^{2+} ions, namely low intensity and apparently broad linewidths.

In the 50% (58.5% by number) spectrum, the peak has shifted towards higher frequencies, in conformity with the interpretation presented thus far. That is, the lower frequency isolated ion and ion pair now have much lower probability figures, whilst the figures for the triplets and higher sets have increased markedly: the ratios, starting with the isolated ion, are: 1/5.6/11/11.2/4. Not surprisingly, the spectrum at this point is broad and featureless.

The $CoCl_2$ spectrum results from one situation only, namely from Co^{2+} ions surrounded entirely by other Co^{2+} ions. The spectral peak is at a higher frequency than that of $CdCl_2$(Co): 50%, indicating that it is not the main contributor to the 50% spectrum, and the overall width is narrower, as would be expected if the 50% spectrum is the sum of several Co^{2+} situations.

In conclusion, it can be stated that the qualitative behaviour of the 1000 cm^{-1} doublet in $CdCl_2$(Co) is in good agreement with that predicted. A quantitative analysis of these spectra may be possible, using spectra obtained with the improved Raman spectrometer described in Chapter 6, operating at high resolution and in the digital mode. In addition, it should be possible to perform a close analysis of the 501 cm^{-1}

and 459 cm^{-1} lines, clearly impossible with the spectra thus far available.

The assignments made in this section are summarized in Table IX.

TABLE IX

Classification by nearest-neighbour (n.n.) cation environment of the Co^{2+} electronic lines of $CdCl_2(Co)$, in the 1000 cm^{-1} region.†

Number of n.n. Co^{2+} ions	Co^{2+} concentration 3%	5%	10%	100%
0	923 ± 1	925.0±0.5	917 ± 1	-
	953 ± 1	954 ± 1	943 ± 1	-
1	937 ± 3	-	929 ± 1	-
	969 ± 2	968 ± 2	961 ± 1	-
4	-	-	-	963 ± 1
	-	-	-	992 ± 1

† All frequencies in wavenumbers.

The 925-954 cm^{-1} doublet in $CdCl_2(Co)$ has been examined in most detail because it is the most favourable case: the equivalent lines in $CdBr_2(Co)$ are much closer together, and those of $MnCl_2$, whilst having a slightly larger splitting, are broader. However, both these crystals have been examined at the nominal 10% concentration, and the results are very similar.

The theory of the concentration dependence of observed spectral lines was built on three basic assumptions: that the observed lines belonged to Co^{2+} electronic transitions, that the Co^{2+} ions were randomly distributed in the host crystal, and that only changes in the nearest-neighbour cations would affect the spectra. The qualitative agreement with experiment therefore supports these assumptions. That is, the 900-1000 cm^{-1} doublets are confirmed as Co^{2+} lines, and the relative intensities of various doublets are consistent with a random distribution of Co^{2+} ions. As to the effects of changed cations in other than nearest neighbour sites on the spectra, it could be expected that these would be manifest in the gaussian width of the spectral lines. An accurate quantitative analysis should show increasing line width in each particular nearest neighbour situation, as concentration increases.

Armed with this understanding of concentration effects in Co^{2+} electronic lines, we shall now return to the problem of the low frequency $CdBr_2(Co)$ spectrum.

7.4.4 $CdBr_2(Co)$

In Table X, the spectral lines not assigned to fluorescence are listed for the different concentrations of cobalt that were used.

TABLE X

Spectra of $CdBr_2$(Co) for different concentrations of Co^{2+} (excluding fluorescence)

Concentration:	0%	3%	5%	10%
	200±1 cm^{-1}	200±1 cm^{-1}	~200 cm^{-1}	-
		-	268±2	271±3 cm^{-1}
		282±1	284±1	286±2
		351±1	351±1	352±2
		394±1	397±1	400±2
		440±2	439±1	444±2
		889±1	(893±1)	887±1
		894±1	unsplit	893±1
		905±1	-	903±1
		995±1	993±1	unresolved
		-	1007±2	unresolved

All the lines which have already been associated with the cobalt develop sidebands in a similar manner to the $CdCl_2$(Co) lines, thereby confirming the assignments. In particular, and as can be seen in Figure 7.9, the 282 cm^{-1} line has a sideband at about 270 cm^{-1}, whose relative intensity increases with concentration. The sidebands at 270, 903 and 1007 cm^{-1} are assigned to Co^{2+} ions having one other Co^{2+} ion in a nearest neighbour cation position (presumably another line at about 897 cm^{-1} is buried beneath the strong 893 cm^{-1} line).

At this stage, therefore, we have identified four of the five lines of cobalt in $CdBr_2$(Co): 282, 889, 894 and 995 cm^{-1}. Relative to the situation in the other crystals, the trigonal

field splitting of the strong high-frequency doublet is small (5 cm^{-1} as compared with ~30 cm^{-1}).

Therefore, we should expect that the energy difference between the two lowest transitions should also be relatively small (see Figure 5.2) and, consequently, that the absolute values of the energies of these transitions will be between the 235 and 501 cm^{-1} values of $CdCl_2(Co)$. We have already identified one transition at 282 cm^{-1}, not far above 235 cm^{-1}, and we can reasonably expect therefore, that the missing line will be above the 282 cm^{-1} line. The natural candidates are at 351, 394 and 439 cm^{-1}.

The spectra of the Co^{2+} ions having one Co^{2+} nearest-neighbour cation consistently shows an increased trigonal field: as neighbouring cations are well shielded from each other by the anion "boxes", we should expect that the most significant changes in the energy parameters induced by changes in these cations will be in the trigonal parameters. Referring to Figure 5.2, we can see that the sideband to the missing line should be above it, and by considerably more than the 16 cm^{-1} that the 268 cm^{-1} line is below the 284 cm^{-1} line, if the expectation of v being positive is fulfilled.

The lines at 394 cm^{-1} and 439 cm^{-1} are assigned to electronic transitions in isolated Co^{2+} ions and in Co^{2+} ions having one Co^{2+} nearest-neighbour cation respectively, for the following reasons: if the Co^{2+} pair line is visible, then either the 351 or 394 lines must be the isolated Co^{2+} line; as is indicated in Table XI, the relative intensities of the 282, 351 and 394 lines are independent of concentration, whilst there is a strong overall increase in that of the 439 cm^{-1} line; and whilst the 268, 282, 394 and 439 cm^{-1} lines all

show increasing frequencies as concentration increases, there is no significant change in the frequency of the 351 cm^{-1} line (see Table XI).

TABLE XI

Intensities of low energy Raman lines in $CdBr_2(Co)$

Concentration	laser line	282 cm^{-1}	351 cm^{-1}	394 cm^{-1}	440 cm^{-1}
3%	5145Å	1.0	0.5	0.6	-
	†4880	1.0	0.5	buried	-
	4765	1.0	0.3	buried	-
	4579	1.0	0.6	0.4	-

† a different crystal sample was used.

5%		284 cm^{-1}	351 cm^{-1}	397 cm^{-1}	439 cm^{-1}
	4880Å	1.0	0.55	0.55	0.14
10%		286 cm^{-1}	352 cm^{-1}	400 cm^{-1}	444 cm^{-1}
	4880Å	1.0	0.6	0.6	0.2

The 351 cm^{-1} line does not appear to develop a sideband at higher concentrations, suggesting that it is probably a lattice mode. In $CdCl_2(Co)$ and $MnCl_2(Co)$, lines belonging to the host crystal appear in a similar relative position, and from Table VII we see that for k = 0 phonons, $2 \times A_{1g} = 302$ cm^{-1}. The 352 cm^{-1} line is therefore assigned to the second-order phonon spectrum.

7.4.5 Conclusion

The Raman spectra of four isomorphic crystals, $CdCl_2$(Co), $MnCl_2$(Co), $CoCl_2$ and $CdBr_2$(Co) have been qualitatively analysed, and in each case, five electronic transitions of the Co^{2+} ion have been identified. $CdCl_2$, $MnCl_2$ and $CoCl_2$ are all very similar crystals, and the Co^{2+} spectra from each crystal are consistently similar at both room and low temperatures. The appearance of fluorescence lines, and the much lower phonon frequencies make the $CdBr_2$ spectra stand apart from the others. However, the basic form of the Co^{2+} spectrum is exactly the same as in the other crystals, and provides valuable confirmation for the assignments. The study of the concentration dependence of the spectra provides a very useful method for identifying the Co^{2+} lines.

Table XII summarizes the results of the Raman measurements.

TABLE XII

Low-lying electronic energy levels of the Co^{2+} ion in a trigonal crystal field†.

Assignment	$CdBr_2$(Co):3%	$CdCl_2$(Co):5%	$MnCl_2$(Co):5%	$CoCl_2$
$\gamma_4^+(\Gamma_6^+)$	0	0	0	0
$\gamma_5^+ + \gamma_6^+({}^{(1)}\Gamma_8^+)$	282 ± 1	235 ± 10	230 ± 13	221 ± 2
$\gamma_4^+({}^{(1)}\Gamma_8^+)$	394 ± 1	501 ± 2	524 ± 2	549 ± 1
$\gamma_4^+({}^{(2)}\Gamma_8^+)$	889 ± 1	925.0±0.5	938 ± 1	963 ± 1
$\gamma_5^+ + \gamma_6^+({}^{(2)}\Gamma_8^+)$	894 ± 1	954 ± 1	972 ± 1	992 ± 1
$\gamma_4^+(\Gamma_7^+)$	995 ± 1	1090 ± 5	1108 ± 2	1115 ± 5

† All measurements in wavenumbers.

7.5 THE CALCULATION

The experimental results of Table XII have been fitted to the theory by means of the calculation described in section 5.3, and the results are given in Table XIII.

TABLE XIII

Calculated energies of the low-lying electronic levels of the Co^{2+} ion in $CdCl_2$, $MnCl_2$, $CoCl_2$ and $CdBr_2$

$CdBr_2$	$CdCl_2$	$MnCl_2$	$CoCl_2$
282 cm^{-1}	239 cm^{-1}	225 cm^{-1}	217 cm^{-1}
395	496	517	546
889	924	930	966
895	960	968	991
995	1091	1108	1115
R.M.S. deviations from experimental values			
0.6 cm^{-1}	4.0 cm^{-1}	5.6 cm^{-1}	2.6 cm^{-1}

	Parameters of the energy matrix†			
Dq	-610 cm^{-1}	-670 cm^{-1}	-690 cm^{-1}	-690 cm^{-1}
B	790	790	780	780
C	3090	3320	3432	3432
ζ	-542	-511	-508	-533
ζ'	-436	-527	-552	-503
V	246	223	342	623
V'	-647	-1015	-1239	-1700

† Dq is the cubic field parameter, B and C electrostatic parameters[51]; ζ and ζ' are the spin-orbit parameters[52]; V and V' are the trigonal field parameters[53].

The values of Dq, B and C for Co^{2+} in $CdBr_2$ and $CdCl_2$ are those calculated by Robson[45], and for $CoCl_2$, the values derived by Ferguson et al.[66] are used. For each of these cases, the optical absorption spectra of the crystals were available. However, this is not so for $MnCl_2$(Co), and in this case the values for $CoCl_2$ are used in the expectation that, since Mn^{2+} ion is nearest in "size" to the Co^{2+} ion, and since the anions are the same, the two crystal environments will be quite similar.

The very close fits to the experimental data which are achieved indicate that the crystal field theory is perfectly adequate in the cases examined. In particular, neglect of the Jahn-Teller effect seems to be justified. The spin-orbit parameters do not differ greatly from the free ion value of $-540\ cm^{-1}$, and the trigonal field parameters have a consistency one should expect, bearing in mind the identical crystal structures. However, we observe that the amount of data barely exceeds the number of adjustable parameters, and consequently that too much significance should not be given to the particular parameter values. In Table XIV large variations in the $CdBr_2$(Co) parameters are shown to cause only small changes in the closeness of the fit.

TABLE XIV

R.M.S. deviations as a function of the parameters of $CdBr_2$(Co)

(all units are wavenumbers)

ζ	ζ'	V	V'	R.M.S. deviation
-530	-446	-212	- 86	8.3
-543	-431	162	-542	1.0
-542	-436	246	-647	0.6

A deeper analysis of the theory will be possible with an extension of the experimental data, and this can be achieved by means of g-value measurements - g-values of the Co^{2+} ground states in $CdCl_2$ and $CdBr_2$ are available[67], and Zeeman Raman experiments may provide further data. The g-values can be calculated in terms of the existing set of parameters.

Further refinements may also be possible by re-measuring the optical absorption spectra of each crystal in greater detail and refitting the cubic field and electrostatic parameters. These were not varied in the calculations presented in this section.

7.6 POLARIZATION EXPERIMENTS

The importance of polarization measurements is that they allow separation of measured energy levels into either γ_4^+ or $\gamma_5^+ + \gamma_6^+$ states, and they also allow a direct experimental measure of the symmetry of the states. Additionally, it is in principle possible, by appropriate choice of experimental geometry, to observe directly the lowest energy Co^{2+} line in $MnCl_2$(Co) and in $CdCl_2$(Co), if crystal conditions are suitable for polarization measures.

After early and unsuccessful attempts, no polarization experiments were performed and the direction of the experiments turned towards the areas of temperature dependence, concentration dependence, and mere observation of Raman signal. The nature of the crystals, in particular their hygroscopic nature and the existence of only one cleavage plane, prevented any Raman signal being observed except when the z or optic axis of the crystal was aligned along the light collection axis. When, in a relatively dry atmosphere, cuts were attempted perpendicular to the cleavage planes, the surfaces had the appearance of frosted glass, and gave very poor Raman signal.

Porto et al.[68] show that it is quite impossible, in uniaxial crystals such as $CdCl_2$, to obtain polarization results when the optic axis coincides with the light collection axis, unless the half-angle of the collection cone is very, very small - in reality prohibitively small.

Presently, a dry-box using molecular sieves as drying agents is being developed, in an effort to enable the cutting and polishing of crystals in planes perpendicular to the cleavage planes. Johnstone[36] has shown the necessity for extremely low humidity for such operations, and the sieves are adequate according to manufacturers' specifications. However, their performance to date is not particularly good.

7.7 ANTIFERROMAGNETISM IN $CoCl_2$

It has been shown previously that the considerable width of the $CoCl_2$ electronic Raman lines can be attributed to short-range exchange interactions between the Co^{2+} ions. When the crystal is cooled to below 24.9°K, these reduce to a single interaction encompassing the entire crystal; the

magnetic moments of all the ions within a crystal layer are aligned perpendicular to the z-axis[49], and the magnetic direction of each layer is opposite to that of its neighbours: this situation is termed antiferromagnetism.

Single ion electronic excitations of the paramagnetic phase are transformed into excitations of the magnetic lattice, which are normally termed excitons or magnons - the latter is simply an exciton in which the electronic excitation involves a change in spin parameters only.

The derivation of the exciton energy levels from those of the single ion is described by Loudon[69], and the method has been applied by Lockwood[70] to the case of AFM (antiferromagnetic) $CoCl_2$. According to Lockwood, the factor group of the magnetic lattice is C_{2h}, and the low-lying exciton manifold consists of a Γ_1^+ ground state, and eleven Γ_1^+ and Γ_2^+ excited states, a total of 23 energy levels. At present, the only quantitative description of the manifold is an approximation developed by Lines[49].

On the basis of the expectation that the ferromagnetic intralayer interaction is much stronger than the antiferromagnetic interlayer interaction, the exciton energies are expected to approximate those obtained by subjecting the paramagnetic crystal to an equivalent external matnetic field, aligned perpendicular to the trigonal axis. In Figure 7.12, the effect of such a magnetic field on the Co^{2+} energy levels is shown, using the calculation results of Lines. Figure 7.13 illustrates the experimental Raman spectra of $CoCl_2$ below its Neél temperature of 24.9°K, and Table XV lists the energies of the electronic transitions in both magnetic phases.

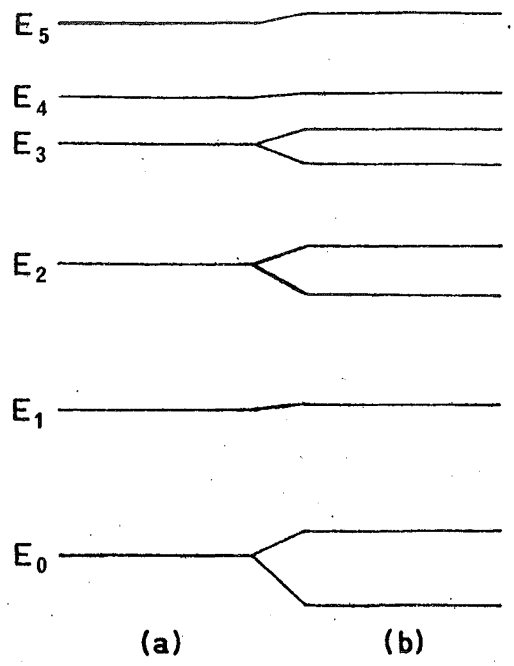

Figure 7.12 Effect of an external magnetic field on the low-lying energy levels of Co^{2+} in a trigonal environment: (a) no magnetic field; (b) magnetic field applied perpendicular to the trigonal axis.

TABLE XV

Frequencies and linewidths of electronic Raman lines of $CoCl_2$ in paramagnetic and antiferromagnetic phases.†

Paramagnetic Assignment	Paramagnetic Frequency	Phase Width	Antiferromagnetic Phase Frequency	Width
$\gamma_5^+ + \gamma_6^+$	221 ± 2	20±3	223.7±0.5	10±1
γ_4^+	549 ± 1	43±1	549 ± 0.5	20±1
			577 ± 2	28±3
γ_4^+	963 ± 1	42±1	961.5±0.5	6±1
$\gamma_5^+ + \gamma_6^+$	992 ± 1	40±1	983.5 ± 1	20±3
			1014.5 ± 1	18±3
γ_4^+	1115 ± 5	-	1150 ± 5	30±5

† All measurements in wavenumbers.

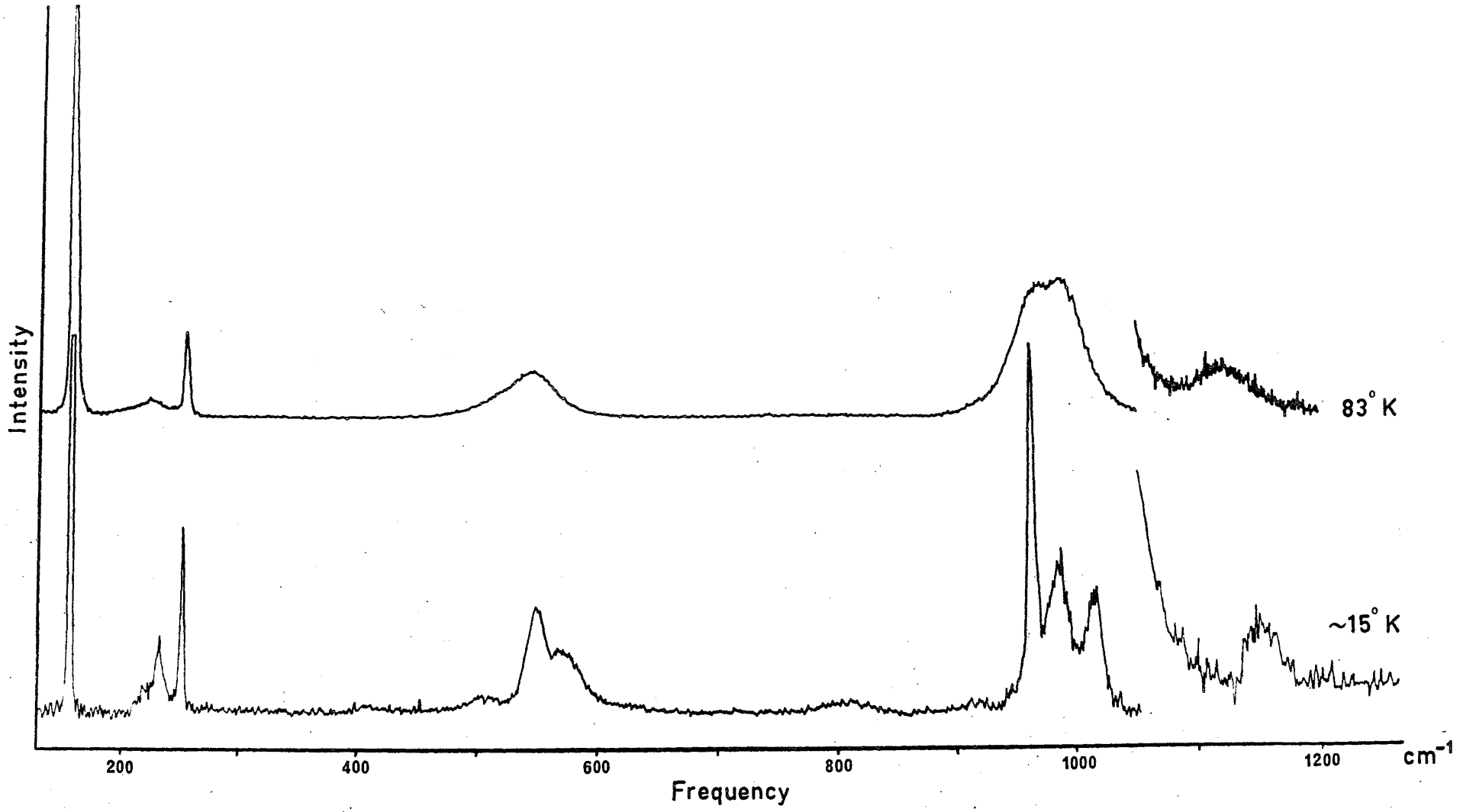

Fig. 7.13 Raman scattering spectra of $CoCl_2$ in its paramagnetic ($T = 83^{\circ}K$) and antiferromagnetic ($T = 15^{\circ}K$) states. The latter spectrum is constructed from several part spectra, as follows: 130-270 cm^{-1} using the 4880Å laser line and a spectra slit width of 1.5 cm^{-1}; 270-460 cm^{-1}, 4579Å and 3 cm^{-1}; 460-650 cm^{-1}, 4579Å and 6 cm^{-1}; 650-900 cm^{-1}, 4765Å and 6 cm^{-1}; 900-1050 cm^{-1}, 4880Å and 1.5 cm^{-1}; 1050-1270, 4880Å and 10.5 cm^{-1}.

The transitions at 233 and 1150 cm^{-1} remain degenerate, and are at higher frequencies than the corresponding paramagnetic transitions, both properties in agreement with the prediction (although we note the relatively large width of the latter, and the suggestion of a weak broad line under the former as indications of small splittings in these lines). Similarly, the 549 cm^{-1} line splits into two at 549 and 575 cm^{-1} in qualitative agreement with Lines' theory. The broad, weak line at 510 cm^{-1} is assigned to the $2 \times A_{1g}$ phonon transition, earlier calculated to be at 520 cm^{-1}. Three lines appear in the 1000 cm^{-1} region, but it appears that the 992 cm^{-1} line, rather than the expected 963 cm^{-1} line has been split by the AFM interaction. A search has been made for the lowest lying exciton level without success; its expected proximity to the laser line entails detection in the presence of intense laser light.

The weak line at about 810 cm^{-1} has appeared at slightly different frequencies for two different laser lines, and so is probably a Raman line. There is no trace of this line in the liquid air spectrum, and it is thus possible the line represents a two-exciton transition; but further work will be necessary to firmly establish its origin.

A few points should be noted. Firstly, the exciton lines are much narrower than Raman lines associated with paramagnetic transitions in $CoCl_2$. This property should be expected, because the electronic excitation is now a lattice excitation with much the same properties as even-parity phonons. Secondly, no splitting of lines by the interlayer interaction is evident, even in the high resolution spectrum. The final point is that the AFM spectra are highly temperature dependent,

the spectra in Figure 7.13 being recorded at the lowest temperatures possible for a cold-finger mounted crystal, about $15^{o}K$ in our case. A more satisfactory, albeit more difficult arrangement is to immerse the sample in liquid helium, which is pumped on to remove bubbles of gas and to effect even lower temperatures. AFM features should be discerned more readily in such experiments[41].

CHAPTER 8

THE PAST AND FUTURE OF Co^{2+}

8.1 PREVIOUS RAMAN EXPERIMENTS

Two instances of published work in the field of Raman spectroscopy are worthy of comment.

Raman spectra of crystals of Co_2GeO_4 have been measured at room and low temperatures by Koningstein et al.[37]. In this crystal, the site symmetry of the Co^{2+} ions is D_{3d}, as in $CoCl_2$, and the Neél temperature is 20^oK, which is again very similar to that of $CoCl_2$. At 83^oK, electronic Raman lines are observed at 229, 900 and 961 cm^{-1}. Not surprisingly, these are quite broad. The polarization of all the lines is given as E_g.

The spectrum is interpreted using the theory of Lines[49], the three lines being assigned respectively to $\gamma_5^+ + \gamma^+{}_6(^{(1)}\Gamma_8^+)$, $\gamma_5^+ + \gamma_6^+(^{(2)}\Gamma_8^+)$ and $\gamma_4^+(\Gamma_7^+)$. It is not possible with the available information to predict with certainty the positions of the missing lines: determination of the relevant polarization data is required. However, if as is indicated by Koningstein et al., the trigonal field parameter V must be positive, a $\gamma_4^+(^{(1)}\Gamma_8^+)$ band should occur in the 500 cm^{-1} region, and another transition should appear either below or in the 900 cm^{-1} band, or well above the 961 cm^{-1} band.

As a technique for measuring the first-order phonon spectrum of MgO, Mon[71] introduced Co^{2+} ions into the crystal and observed its Raman spectra. In crystals containing Co^{2+}, a strong line appears at 934 cm^{-1}, and is assigned by Mon to a

fluorescence transition of 20470 cm^{-1} between the ^4F cubic ground state, and the ^4P "first excited state" of the same symmetry (the site symmetry of the Co^{2+} ions is cubic). Noting, however, the similarity with the strong Raman lines associated with the trigonal field-split $^{(2)}\Gamma_8^+$ level in our crystals, we postulated that the line was in fact a Raman line. In an experiment, using a different laser frequency, this was shown to be the case[72]. There is no trace, in the spectra published by Mon, of the higher frequency Γ_7^+ or of the lower frequency $^{(1)}\Gamma_8^+$ levels, but it may be possible with careful measurement to observe these, and thereby to measure the spin-orbit interaction.

8.2 INFRARED ABSORPTION EXPERIMENTS

As has been described earlier, IR absorption lines associated with low energy Co^{2+} electronic transitions will be weak because they are parity forbidden, and the dominant spectral features will be vibronic peaks arising from simultaneous electronic plus odd-vibrational transitions.

This situation was not recognised by Zvyagin et al.[44] and there can be little doubt that the 1188 cm^{-1} peak observed by these authors is a vibronic sideband to their 980 cm^{-1} line. The difference frequency of 209 ± 11 cm^{-1} is to be compared with Lockwood's[54] values for the A_{2u} and E_u phonons of 157 cm^{-1} and 253 cm^{-1} respectively, and measurements by Kennedy[73] which show a strong absorption in the region 180-220 cm^{-1}. Two lines observed by Zvyagin et al., 980 and 1120 cm^{-1}, coincide well with the Raman frequencies although we note the possibility that the 1120 cm^{-1} peak could be of vibrational origin.

Similarly the line at ~1015 cm^{-1} observed at 10°K is in accordance with equivalent Raman spectra.

Robson's spectra[45] were plagued by impurity lines[61], and by the extreme weakness of most of the Co^{2+} lines. Only the $\gamma_5^+ + \gamma_6^+(^{(2)}\Gamma_8^+)$ line is correctly identified, this line appearing with some strength in each of the three crystals measured - $CdCl_2(Co)$, $CdBr_2(Co)$ and $MnCl_2(Co)$. $CdCl_2(Co)$ and $CdBr_2(Co)$ spectra have also been recorded by Johnstone[74], and it is clear further work is necessary for a full understanding of the IR spectra of all the doped crystals. In $CdCl_2(Co)$, broad peaks occur at 1127, 1160, 1280 and 1320 cm^{-1}, and sharp peaks at 999, 1027, 1166, 1184 and 1196 cm^{-1}.

Note that the 29 cm^{-1} splitting of the 925 and 954 cm^{-1} Co^{2+} lines is reflected in the pairs 1127 and 1160 (average increment 204 cm^{-1}); 999 and 1027 (increment 74 cm^{-1}); 1166 and 1196 (increment 241 cm^{-1}). Assigning the two upper lines to the 1090 cm^{-1} Co^{2+} line, we derive increments of 190 and 230 cm^{-1}. To complete the assembled data Lockwood's A_{2u} and E_u phonon frequencies are 164 and 210 cm^{-1}. Although patterns can be discerned in this, and the data for the other crystals, comprehensive assignments cannot yet be made.

Finally, mention should also be made of the work of Mooney et al.[75], who have in $CdCl_2(Co)$ investigated the $^4T_{1g}(^4P)$ cubic field manifold of the Co^{2+} ion, which is situated at 19000 cm^{-1}. Determination of the Co^{2+} levels in this and other manifolds would add valuable data to that now available for calculation purposes.

8.3 FUTURE WORK

As has been previously mentioned, development of facilities to enable polarization measurements is taking place. When these experiments are completed, and the paramagnetic state of the crystals well understood, three avenues for further work will be open.

The first is a series of IR and optical absorption experiments to enable higher energy electronic levels of the Co^{2+} ion to be determined. As a necessary prerequisite, an exhaustive IR study of the low energy 400-1400 cm^{-1} region must be undertaken, so that the spectra of all crystals are completely understood in cases where the electronic energies are known. This in turn may require further work on the subject of lattice vibrations.

A full investigation of $CoCl_2$ in its antiferromagnetic state is a second and obvious area for further research, and a third is the determination of the g-values of the low-lying paramagnetic states by means of Zeeman Raman experiments. Development work for the latter is currently underway.

8.4 CONCLUSION

The experimental determination of the electronic energy levels of ions in solids is usually attempted by means of either absorption or Raman spectroscopy. The former is the most widely used, but suffers drawbacks which limit the precision of the measurements. We have seen that even when the low-lying Co^{2+} electronic energy levels are known, the IR spectrum of the region still cannot be fully interpreted, at

least without the investment of a large amount of experimental effort.

On the other hand, the Raman technique, whilst generally limited to an energy maximum of a few thousand wavenumbers, does give clear and precise results, as is shown in this and other work in the field of electronic Raman scattering.

The particular value of such results is that they allow a much fuller application of crystal field theory - in this case a measurement of the spin-orbit interaction and the trigonal distortion of the electrostatic field, both too small to be deduced from the optical absorption spectra.

The introduction of Raman spectroscopy into the field of ionic interactions in crystals has, therefore, made a significant contribution to this aspect of physics.

REFERENCES

1. S.J. Cyvin, J.E. Rauch and J.C. Decius, J. Chem. Phys. 43, 4083 (1965).
2. R.W. Terhune, P.D. Maker and C.M. Savage, Phys. Rev. Letters 14, 681 (1965); P.D. Maker in : *Physics of Quantum Electronics*, ed. P.L. Kelley et al. (McGraw-Hill, New York, 1966), p.60; P.D. Maker and C.M. Savage, 24th Symposium on Molecular Structure and Spectroscopy, Ohio State University, Columbus, Ohio, September 1969.
3. S. Yatsiv, M. Rokni and S. Barak, IEEE J. Quantum Electron. QE-4, 900 (1968).
4. N.N. Badalyan, V.A. Iradyan and M.E. Movsesyan, ZhETF Pis. Red. 8, 518 (1968) [JETP Letters 8, 316 (1968)].
5. S. Dumartin, B. Oksengorn and B. Vodar, Compt. Rend. 261, 3767 (1965).
6. L.D. Ievleva and T.Ya. Karagodova, Opt. Spekstrok. 23, 991 (1967) [Opt. Spectrosc. 23, 541 (1967)].
7. Z. Ozgo, Acta Physica Polonica 34, 1087 (1968).
8. J.F. Ward, Rev. Mod. Phys. 37, 1 (1965).
9. R. Wallace, Mol. Phys. 11, 457 (1966).
10. Y.-Y. Li, Acta Physica Sinica 20, 164 (1964).
11. M. Born and K. Huang, *Dynamical Theory of Crystal Lattices* (Clarendon Press, Oxford, 1954), p.200.
12. Op. cit., p.203.
13. S.A. Akhmanov and D.N. Klyshko, ZhETF Pis. Red. 2, 171 (1965) [JETP Letters 2, 108 (1965)].
14. G. Placzek, *Handbuch der Radiologie* (Akademische Verlagsgesellschaft, Leipzig, 1934), 6, Pt. 2, p.209 [English translation: Lawrence Radiation Laboratory, University of California, Translation 526 (L), 1959].

15. Here we follow the treatment of Born and Huang, op. cit., p.204.

16. C.-H. Chu, Acta Physica Sinica 21, 1587 (1965).

17. L.D. Landau and E.M. Lifshitz, *Quantum Mechanics* (Pergamon Press, London, 1958), p.343.

18. D.E. Littlewood, *The Theory of Group Characters and Matrix Representations of Groups* (Oxford U.P., London, 1958), 2nd ed., p.265.

19. Op. cit., p.59.

20. S. Bhagavantam and D. Suryanarayana, Acta Cryst. 2, 21 (1949).

21. J.H. Christie and D.J. Lockwood, J. Chem. Phys. 54, 1141 (1971).

22. E.B. Wilson, J.C. Decius and P.C. Cross, *Molecular Vibrations* (McGraw-Hill, New York, 1955), p.333.

23. D.A. Long and L. Stanton, Proc. Roy. Soc. Lond. A. 318, 441 (1970).

24. L. Stanton, Mol. Phys. 23, 601 (1972).

25. M.L. Bhaumik, Am. J. Phys. 35, 330 (1967).

26. B.B. Snavely, Proc. IEEE 57, 1374 (1969).

27. C.M. Savage and P.D. Maker, Appl. Opt. (USA) 10, 965 (1971).

28. J.F. Verdieck, S.H. Peterson, C.M. Savage and P.D. Maker Chem. Phys. Letters 7, 219 (1970).

29. The ground state frequencies of normal vibration of the benzene molecule are given in G. Herzberg, *Molecular Spectra and Molecular Structure* (Van Nostrand, Princeton, 1966), Vol. 3, p.665.

30. R. Loudon, Adv. Phys. 13, 423 (1964) and 14, 621 (1965).

31. R.J. Elliot and R. Loudon, Phys. Letters 3, 189 (1963).

32. J.T. Hougen and S. Singh, Proc. Roy. Soc. (London) A277, 193 (1964).

33. A. Kiel, T. Damen, S.P.S. Porto, S. Singh and F. Varsanyi, Phys. Rev. 178, 1518 (1969).

34. J.A. Koningstein and O. Sonnich Mortensen, J. Chem. Phys. 46, 2811 (1967); Phys. Rev. Letters 18, 831 (1967).

35. J.A. Koningstein, J. Opt. Soc. Am. 56, 1405 (1966).

36. A. Azima, P. Grunberg, J. Hoff, J.A. Koningstein and J. Preudhomme, Chem. Phys. Letters 7, 565 (1970).

37. J.A. Koningstein, P.A. Grunberg, J.T. Hoff and J. Preudhomme, J. Chem. Phys. 56, 354 (1972).

38. In addition to the work mentioned above, J.A. Koningstein and collaborators have published a large amount of work on the subject of Raman scattering by trivalent lanthanide ions in crystals. References 34-37 and J.A. Koningstein, J. Chem. Phys. 51, 1163 (1969) contain further references to this work.

39. P.A. Fleury, S.P.S. Porto, L.E. Cheesman and H.J. Guggenheim, Phys. Rev. Letters 17, 84 (1966).

40. P.A. Fleury, in: *Light Scattering Spectra of Solids*, ed. G.B. Wright (Springer-Verlag, New York, 1969), p.185.

41. R.M. Macfarlane, Phys. Rev. Letters 25, 1454 (1970).

42. R.M. Macfarlane and H. Morawitz, in: *Proceedings of the Second International Conference on Light Scattering in Solids*, ed. M. Balkanski (Flammarion, Paris, 1971), p.133.

43. R. Newman and R.M. Chrenko, Phys. Rev. 115, 1147 (1959).

44. A.I. Zvyagin, V.V. Eremenko and I.V. Skorobogatova, Ukrayin. Fiz. Zh. 11, 520 (1966).

45. A.B. Robson, M.Sc. Thesis, University of Canterbury, 1969.

46. W. Low, Phys. Rev. 109, 256 (1958).

47. J.S. Griffith, *The Theory of Transition Metal Ions* (Cambridge U.P., London, 1964), p.360.

48. A. Abragam and M.H.L. Price, Proc. Roy. Soc. A 205, 135 (1951); 206, 173 (1951).

49. M.E. Lines, Phys. Rev. 131, 546 (1963).

50. R.W.G. Wyckoff, *Crystal Structures*, 2nd ed., Vol. I (Interscience, New York, 1963), p.270.

51. Y. Tanabe and S. Sugano, J. Phys. Soc. Japan 9, 753 (1954).

52. K.A. Schroeder, Ph.D. Thesis, University of Canterbury, 1963.

53. K. Zdansky and I. Johnstone, to be published.

54. D.J. Lockwood, Ph.D. Thesis, University of Canterbury, 1969.

55. *Ramalogues* (Spex Industries, Metuchen, N.J.), 2, No. 4, 4 (1969).

56. *R.C.A. Photomultiplier Handbook* (R.C.A., Electronics Components, Harrison, N.H., 1970), p.56.

57. G.A. Morten, Appl. Optics 7, 1 (1968).

58. D.J. Lockwood, J. Opt. Soc. Am. 63, 374 (1973).

59. S. Nakashima, H. Yoshida, T. Fukumoto and A. Mitsuishi, J. Phys. Soc. Japan 31, 1847 (1971).

60. I.F. Chang and S.S. Mitra, Phys. Rev. 172, 924 (1968).

61. I. Johnstone, Physics Honours III Project, University of Canterbury, 1972.

62. D.J. Lockwood and J.H. Christie, Chem. Phys. Letters 9, 559 (1971) contains initial results for this and the other doped crystals.

63. J.H. Christie and D.J. Lockwood, Chem. Phys. Letters 8, 120 (1971).

64. J.H. Christie and D.J. Lockwood, in : *Proceedings of the Second International Conference on Light Scattering in Solids*, ed. M. Balkanski (Flammarion, Paris, 1971), p.145.

65. S.P.S. Porto, in: *Light Scattering Spectra of Solids*, ed. G.B. Wright (Springer-Verlag, New York, 1969), p.1.

66. J. Ferguson, D.L. Wood and K. Knox, J. Chem. Phys. 39, 881 (1963).

67. K. Morigaki, J. Phys. Soc. Japan 16, 1639 (1961).

68. S.P.S. Porto, J.A. Giordmaine and T.C. Damen, Phys. Rev. 147, 608 (1966).

69. R. Loudon, Adv. Phys. 17, 243 (1968).

70. D.J. Lockwood, private communication.

71. J.P. Mon, Phys. Letters 36A, 479 (1971).

72. J. Le Heron, private communication.

73. R. Kennedy, Physics Honours III Project, University of Canterbury, 1972.

74. I. Johnstone, private communication.

75. A. Mooney, R.H. Nuttall and W.E. Smith, Chem. Phys. Letters 16, 534 (1972).

APPENDIX I

THE COMPUTER PROGRAMS

In this appendix, the program which was used to calculate the transformation properties of the $\bar{\beta}$ tensor is described. The other programs are similar, except that the γ and $\bar{\gamma}$ programs had to be split into two parts in order to fit them into the computer.

I.1 Input

The first card carries the group name and a carriage control character, the second the order of the group, G, the number of classes, H, and the orders of the classes, GPCLSS. Next come G-1 cards containing matrices of the form (3.8), which describe the group operations. The condensed character of the first representation is then read, and is converted to a real two-dimensional representation if it is complex. The character is now expanded to its full form (one element of the character corresponding to each group element). For two and three-dimensional representations the (11), (12) and (23) elements of each representation matrix is read in, as appropriate, having been calculated by another program.

I.2 Calculation

A subroutine BASEFN performs projection operations on a third-rank tensor possessing no symmetry in any of its indices. For two- and three-dimensional representations, BASEFN is used first to calculate the terms transforming according to the first row of the representation, and then,

from that term, to calculate its partners. Subroutine ANTISM is then used to obtain the terms belonging to each representation which have $\bar{\beta}$ symmetry (see Chapter 3). An output routine presents the results in a readable form.

I.3 The Program

The program, which is written in Fortran IV, appears on the next two pages.

Computer Program for Calculating the Transformation Properties of the $\bar{\beta}$ tensor

```
FORTRAN IV     MODEL 44  PS        VERSION 3,  LEVEL 1   DATE  69096
0001                 COMPLEX XXX(12)
0002                 REAL XYZ(27,27),XX(48,3),ZXY(27,27),YZX(27,27),ALPHA(27,27),X(27,8
                    *),Y(27,8),Z(27,8)
0003                 INTEGER GROUP(20),GPCLSS(12),G,H,DISC
                C
                C    THE FOLLOWING STATEMENT DEFINES OUTPUT REQUIREMENTS.
                C
0004                 INTEGER U(8),V(8),W(8),P(3)/3*'    '/,Q(3)/3*'    '/,R(3)/3*'    '
                    */,NU(8),NV(8),NW(8),R1(8),R2(8),R3(8),BR/' ('/,KET/' )'/,COMMA/' ,
                    *'/,PLUS/'  + '/
0005                 COMMON /BLANK/ XX,E(3,3,48),G,NN,H,GPCLSS
0006                 EQUIVALENCE            (GROUP(1),XYZ(1),YZX(1)),(ZXY(1),ALPHA(1),XX(
                    *1)),(ZXY(217),Y(1)),(ZXY(433),Z(1))
0007                 DATA BR/'('/
0008                 DISC=1
0009                 DO 99 I=1,3
0010                 DO 99 J=1,3
0011                 E(I,J,1)=0.
0012            99   E(I,I,1)=1.
0013          1000   CALL MAS<1
0014                 READ(5,1) GROUP
0015                 WRITE(6,1) GROUP(1)
0016                 WRITE(6,1) GROUP
0017                 CALL MAS<0
0018                 READ( 5,2) G,H,GPCLSS
0019                 IF(G.EQ.1) GO TO 10
0020                 READ(5,3) (((E(I,J,K),J=1,3),I=1,3),K=2,G)
0021           10    NL=0
0022            1    FORMAT(20A4)
0023            2    FORMAT(2I3,12I1)
0024            3    FORMAT(9F8.4)
0025            4    FORMAT(10F8.4)
0026            5    FORMAT(I2)
0027          100    READ(5,4) (XXX(I   ),I=1,H)
0028                 WRITE(6,7) (XXX(I   ),I=1,H)
0029            7    FORMAT('1'/(10(F8.4,1X,F8.4,5X)))
0030                 NL =NL+1
0031                 MM=XXX(1)
                C
                C    COMPLEX 1-D REPRESENTATIONS ARE NOW CONVERTED TO 2-D REPRESENTATION
                C
0032                 LLL=0
0033                 IF(MM.NE.1) GO TO 6
0034                 DO 8 I=1,H
0035                 IF(ABS(AIMAG(XXX(I))).GT.0.1) LLL=LLL+1
0036                 XX(I,1)=REAL(XXX(I))
0037            8    XX(I,2)=AIMAG(XXX(I))
0038            6    CONTINUE
0039                 IF(MM.GT.1) READ(5,5) NN
                C
                C    DATA INPUT COMPLETED. S/R,S DIMEN PLACE APPROPRIATE REPRESENTATION
                C    ELEMENTS IN XX.
                C
0040                 IF(MM.EQ.1) CALL DIMEN1(LLL)
0041                 IF(MM.GT.1) READ(5,12) ((XX(I,J),J=1,MM),I=1,G)
0042           12    FORMAT(12F8.4)
0043                 DO 101 I=1,27
0044                 DO 101 J=1,27
0045                 ALPHA(I,J)=0.
0046          101    ALPHA(I,I)=1.
                C
                C    PREPARES A GENERAL FUNCTION FOR BASEFN.
                C
0047                 IF(LLL.GT.1) MM=2
                C
                C    BASEFN PROJECTS OUT OF EACH ROW OF ALPHA INTO XYZ.
                C
0048                 CALL BASEFN(ALPHA,XYZ,MM,1,DISC)
0049                 IF(LLL.EQ.0) GO TO 9
0050                 DO 11 I=1,27
0051                 DO 11 J=1,27
0052                 XYZ(I,J)=0.
0053           11    XYZ(I,I)=1.
0054                 MM=2
0055            9    IF(MM.GT.1) CALL BASEFN(XYZ,ZXY,MM,2,DISC)
0056                 IF(MM.EQ.3) CALL BASEFN(ZXY,YZX,MM,3,DISC)
0057                 REWIND DISC
0058                 CALL ANTISM(XYZ,X,DISC,27)
0059                 IF(MM.GT.1) CALL ANTISM(XYZ,Y,DISC,27)
0060                 IF(MM.EQ.3) CALL ANTISM(XYZ,Z,DISC,27)
0061                 REWIND DISC
                C
                C    END OF CALCULATION, BEGINNING OF OUTPUT ROUTINE.
                C
0062                 DO 20 I=1,27
0063                 DO 21 J=1,8
0064                 U(J)=PLUS
0065                 V(J)=Q(1)
0066                 W(J)=U(1)
0067                 P(2)=KET
0068                 Q(2)=Q(1)
0069                 R(2)=Q(1)
0070                 NV(J)=Q(1)
0071                 NW(J)=Q(1)
0072                 IF(MM.EQ.1)GO TO 22
0073                 P(2)=COMMA
0074                 V(J)=PLUS
0075                 Q(2)=KET
0076                 IF(MM.EQ.2) GO TO 22
0077                 Q(2)=P(2)
0078                 R(2)=KET
0079                 W(J)=PLUS
0080           22    R1(J)=0
0081                 R2(J)=0
0082                 R3(J)=0
0083                 IF(X(I,J).GT.0.) R1(J)=X(I,J)+0.5
0084                 IF(Y(I,J).GT.0.) R2(J)=Y(I,J)+0.5
0085                 IF(Z(I,J).GT.0.) R3(J)=Z(I,J)+0.5
0086                 IF(X(I,J).LT.0.) R1(J)=X(I,J)-0.5
0087                 IF(Y(I,J).LT.0.) R2(J)=Y(I,J)-0.5
0088           21    IF(Z(I,J).LT.0.) R3(J)=Z(I,J)-0.5
0089                 II=0
0090                 JJ=0
0091                 KK=0
0092                 CALL PRINT(R1,U,II,NU,R)
0093                 IF(II.EQ.0) GO TO 20
0094                 IF(MM.GT.1) CALL PRINT(R2,V,JJ,NV,R)
0095                 IF(MM.EQ.3) CALL PRINT(R3,W,KK,NW,R)
0096                 WRITE(6,23) BR,(U(J),R1(J),NU(J),J=1,II),P,(V(J),R2(J),NV(J),J=1,
                    *JJ),
                    *Q,(W(J),R3(J),NW(J),J=1,KK),R
0097           23    FORMAT(1H ,A2,2X,12(A4,A2, 1X,A4,1X))
0098           20    CONTINUE
0099                 IF(NL.EQ.4) GO TO 1000
0100                 GO TO 10
0101                 END
```

```
0001              SUBROUTINE DIMEN1(LLL)
0002                 REAL XX(48,3)
0003              INTEGER G,H,GP(12)
0004              COMMON /BLANK/ XX,E(3,3,48),G,NN,H,GP
0005              K=1
0006        10    I=1
0007              M=H+1
0008         1    LL=5
0009              M=M-1
0010         3    XX(G+1-I,K)=XX(M,K)
0011              I=I+1
0012              IF(I.EQ.G+1) GO TO 2
0013              LL=LL+1
0014              IF(LL.EQ.GP(M)) GO TO 1
0015              GO TO 3
0016         2    K=K+1
0017              IF(K.EQ.3) RETURN
0018              IF(LL.GT.1) GO TO  10
0019              RETURN
0020              END


0001              SUBROUTINE BASEFN(ALPHA,XYZ,MM,EUREKA,NN)
0002              REAL STO(27,27),PROJT(27),ALPHA(27,27),XYZ(27,27),XX(48,3)
0003              REAL PQR(27)
0004              INTEGER EUREKA
0005              INTEGER G
0006              COMMON /BLANK/ XX,E(3,3,48),G
0007              DO 18 LL=1,27
0008              DO 9 J=1,27
0009         9    PQR(J)=0.
0010              DO 7 I=1,27
0011         7    PROJT(I)=ALPHA(LL,I)
0012              DO 1 I=1,3
0013              DO 1 J=1,3
0014              DO 1 IJ=1,3
0015              II=9*(I-1)+3*(J-1)+IJ
0016              C=PROJT(II)
0017              DO 5 L=1,27
0018         5    STO(II, L)=0.
0019              IF(C.LT..001) GO TO 1
0020              DO 6 K=1,G
0021              D=XX(K,EUREKA)*C
0022              DO 6 M=1,3
0023              A=E(I,M,K)*D
0024              DO 6 N=1,3
0025              B=A*E(J,N,K)
0026              DO 6 MN=1,3
0027              NN=9*(M-1)+3*(N-1)+MN
0028         6    STO(II,NN)=STO(II,NN)+B*E(IJ,MN,K)
0029         1    CONTINUE
0030              DO 8 I=1,27
0031              DO 8 J=1,27
0032         8    PQR(J)=PQR(J)+STO(I,J)*MM/G
0033              DO 18 J=1,27
0034        18    XYZ(LL,J)=PQR(J)
0035              WRITE(NN) ((XYZ(I,J),J=1,27),I=1,27)
0036              RETURN
0037              END


0001              SUBROUTINE ANTISM(XYZ,X,NN,N)
0002              REAL XYZ(N,N) ,LEVEL ,X(27,8)
0003              LEVEL =0.01
0004              READ(NN) ((XYZ(I,J),J=1,N),I=1,N)
0005              DO 1 I=1,N
0006              X(I,1)=(XYZ(I,2)+XYZ(I,4))*0.5-XYZ(I,10)
0007              X(I,2)=(XYZ(I,3)+XYZ(I,7))*0.5-XYZ(I,19)
0008              X(I,3)=(XYZ(I,13)+XYZ(I,11))*0.5-XYZ(I,5 )
0009              X(I,4)=(XYZ(I,15)+XYZ(I,17))*0.5-XYZ(I,23)
0010              X(I,5)=(XYZ(I,25)+XYZ(I,21))*0.5-XYZ(I,9 )
0011              X(I,6)=(XYZ(I,25)+XYZ(I,24))*0.5-XYZ(I,18)
0012              X(I,7)=(XYZ(I,6)+XYZ(I,8)-0.5*(XYZ(I,16)+XYZ(I,12)  +XYZ(I,20)+XYZ
                 L(I,22)))
0013         1    X(I,8)=XYZ(I,16)+XYZ(I,12)-0.5*(XYZ(I,20)+XYZ(I,22)+XYZ(I,6)+XYZ(I
                 J,8))
0014              DO 12 I=1,N
0015              RMIN=1000
0016              IMIN =1000
0017              DO 13 J=1,8
0018              RR=ABS(X(I,J))
0019        13    IF(RR.LT.RMIN.AND.RR.GT.LEVEL) RMIN=RR
0020              DO 12 J=1,8
0021              YY=X(I,J)/RMIN
0022        12    X(I,J)=YY
0023              RETURN
0024              END


0001              SUBROUTINE PRINT(R1,U,II,NU,M)
0002              INTEGER MINUS/'  -'/,R1(M),U(M),NU(M)
                 W,D(8)/'XXY','XXZ','YYX','YYZ','ZZX','ZZY','*XYZ','*YZX'/
                 *,NUMBER(6)/'  ',' 2',' 3',' 4',' 5',' 6'/
0003              DO 1 J=1,M
0004              IF(R1(J).EQ.0) GO TO 1
0005              II=II+1
0006              NU(II)=D(J)
0007              R1(II)=R1(J)
0008              IF(R1(II).GT.0) GO TO 1
0009              U(II)=MINUS
0010              R1(II)=-R1(II)+0.5
0011         1    CONTINUE
0012              DO 2 J=1,II
0013              IF(R1(J).GT.6) WRITE(6,3)
0014         3    FORMAT('0TROUBLE IN PRINT')
0015         2    R1(J)=NUMBER(R1(J))
0016              RETURN
0017              END
```

APPENDIX II

THE TENSORS $\beta(\omega_0,\omega_1,\omega_2)$, $\gamma(\omega_0,\omega_1,\omega_2,\omega_3)$ AND $\gamma(\omega_0,\omega_1,\omega_2,\omega_2)$

Table XVI describes the distribution of the components of the tensors $\beta(\omega_0,\omega_1,\omega_2)$, $\gamma(\omega_0,\omega_1,\omega_2,\omega_3)$ and $\gamma(\omega_0,\omega_1,\omega_2,\omega_2)$ among the irreducible representations of the important molecular point groups. The tensors are denoted β', γ' and γ'' respectively in the table.

The ranks of the tensors are three, four and four respectively. The first two possess no symmetry, but the third is invariant with respect to permutation of its last two indices. The numbers are obtained by application of the method of Bhagavantum and Suryanarayana[20], which is described in section 3.4. The characters of the transformation matrices are:

$$T^{\beta(\omega_0,\omega_1,\omega_2)}(G) = 8\,\mathrm{Cos}^3\theta \pm 12\,\mathrm{Cos}^2\theta + 6\,\mathrm{Cos}\theta \pm 1$$

$$T^{\gamma(\omega_0,\omega_1,\omega_2,\omega_3)}(G) = 16\,\mathrm{Cos}^4\theta \pm 32\,\mathrm{Cos}^3\theta + 24\,\mathrm{Cos}^2\theta \pm 8\,\mathrm{Cos}\,\theta + 1$$

$$T^{\gamma(\omega_0,\omega_1,\omega_2,\omega_2)}(G) = 16\,\mathrm{Cos}^4\theta \pm 24\,\mathrm{Cos}^3\theta + 12\,\mathrm{Cos}^2\theta \pm 2\,\mathrm{Cos}\,\theta.$$

TABLE XVI The symmetric structure of the tensors $\beta(\omega_0,\omega_1,\omega_2)$, $\gamma(\omega_0,\omega_1,\omega_2,\omega_3)$ and $\gamma(\omega_0,\omega_1,\omega_2,\omega_2)$.

Group	Rep.	Number of tensor components β'	γ'	γ''
C_s	A'	14	41	28
	A''	13	40	26
C_2	A	13	41	28
	B	14	40	26
C_3	A	9	27	18
	E	9	27	18
C_4	A	7	21	14
	B	6	20	14
	E	7	20	13
C_5	A	7	19	12
	E_1	6	17	11
	E_2	4	14	10
C_6	A	7	19	12
	B	2	8	6
	E_1	6	16	10
	E_2	3	11	8
D_2	A	6	21	15
	B_1	7	20	13
	B_2	7	20	13
	B_3	7	20	13
D_3	A_1	4	14	10
	A_2	5	13	8
	E	9	27	18
D_4	A_1	3	11	8
	A_2	4	10	6
	B_1	3	10	7
	B_2	3	10	7
	E	7	20	13
D_5	A_1	3	10	7
	A_2	4	9	5
	E_1	6	17	11
	E_2	4	14	10
D_6	A_1	3	10	7
	A_2	4	9	5
	B_1	1	4	3
	B_2	1	4	3
	E_1	6	16	10
	E_2	3	11	8
C_{2v}	A_1	7	21	15
	A_2	6	20	13
	B_1	7	20	13
	B_2	7	20	13
C_{3v}	A_1	5	14	10
	A_2	4	13	8
	E	9	27	18
C_{4v}	A_1	4	11	8
	A_2	3	10	6
	B_1	3	10	7
	B_2	3	10	7
	E	7	20	13
C_{5v}	A_1	4	10	7
	A_2	3	9	5
	E_1	6	17	11
	E_2	4	14	10
C_{6v}	A_1	4	10	7
	A_2	3	9	5
	B_1	1	4	3
	B_2	1	4	3
	E_1	6	16	10
	E_2	3	11	8
C_{3h}	A'	2	19	12
	E'	6	11	8
	A''	7	8	6
	E''	3	16	10
C_{3h}	A'	0	19	12
	E_1'	6	1	1
	E_2'	1	10	7
	A''	7	0	0
	E_1''	0	16	10
	E_2''	3	4	3
D_{3h}	A_1'	1	10	7
	A_2'	1	9	5
	E'	6	11	8
	A_1''	3	4	3
	A_2''	4	4	3
	E''	3	16	10
D_{3h}	A_1'	0	10	7
	A_2'	0	9	5
	E_1'	6	1	1
	E_2'	1	10	7
	A_1''	3	0	0
	A_2''	4	0	0
	E_1''	0	16	10
	E_2''	3	4	3
D_{2d}	A_1	3	11	8
	A_2	3	10	6
	B_1	3	10	7
	B_2	4	10	7
	E	7	20	13
D_{3d}	A_1	0	10	7
	A_2	0	9	5
	B_1	3	1	1
	B_2	4	1	1
	E_1	6	4	3
	E_2	3	10	7
	E_3	1	16	10
D_{6d}	A_1	0	10	7
	A_2	0	9	5
	B_1	3	0	0
	B_2	4	0	0
	E_1	6	0	0
	E_2	0	10	7
	E_3	1	4	3
	E_4	3	1	1
	E_5	0	16	10
S_6	A	6	21	14
	B	7	20	14
	E	7	20	13
S_8	A	0	19	12
	B	7	2	2
	E_1	6	4	3
	E_2	3	10	7
	E_3	1	16	10
T	A	2	7	5
	E	2	7	5
	F	7	20	13
T_d	A_1	1	4	3
	A_2	1	3	2
	E	2	7	5
	F_1	3	10	6
	F_2	4	10	7
O	A_1	1	4	3
	A_2	1	3	2
	E	2	7	5
	F_1	4	10	6
	F_2	3	10	7
$C_{\infty v}$	A_1	4	10	7
	A_2	3	9	5
	E_1	6	16	10
	E_2	3	10	7
	E_3	1	4	3
	E_4	0	1	1

APPENDIX III

PDP-8 PROGRAM FOR THE PULSE-RATE DETECTOR

III.1 General

The PDP-8 program which forms a part of the pulse rate detector operates within the framework of a timeshare program which allocates one millisecond in every four to the Raman program. The timeshare program also provides standard subroutines for reading, printing or punching data, for program interrupt response and a facility enabling user programs to be controlled by typed command. The basic function of the Raman program is to time counting periods and to record the counts that accumulate in the external counter during each one. At the end of each experimental scan, !RO is typed, the stored spectrum is punched onto paper tape and the program reinitialized. Initialization can also be accomplished with the command !RC. Two memory locations are used per data point, which gives a maximum allowable count of over 16×10^6. Whenever the counter is half-full (2^{10} counts), a program interrupt occurs which allows an interim count to be stored and the counter to be reset.

III.2 The Program

A spectrum can be started by a switch in Raman laboratory (6331 on) provided that DATA has been put to zero (by !RO or !RC). After further initialization, the program goes into a loop, watching for the end of the count period, or for the end of the scan (6331 off). In the former case, the count and any

wavelength marker is stored, in the latter DATA is made non-zero, and the program returns to the waiting loop at the beginning (this also occurs when the storage area is full).

In the listing which follows, references to several routines of the timeshare program appear:

CLOCK2 is a one second clock;

LEXIT is a standard interrupt return;

LOTCH is a teletype output routine;

LOPCH is a punch output routine;

LWAIT is the timeshare waiting loop;

LCMND is the routine which watches for commands.

Three input/output instructions are used:

6331 - off/on switch

6332 - counter overflow flag.

6334 - read and clear counter.

Computer Program for the Raman Pulse-Rate Detector

```
                /TIMESHARE 2  RAMAN SCATTERING EXPERIMENT
                  /AUTOINDEX REGISTERS 0012 AND 0013
                  /PAGE ZERO LOCATIONS 0120 TO 0147
                  /COMMAND TABLE 0750 TO 0757
                  /DATA STORE 3200 TO 5177
                  /PROGRAMS 5200 TO 5577
                  *0012
0012  3177      ADD,   3177          /USE FOR INCREMENTING STORE ADDRESS
                  COUNT=0120
                  CNTSAV=0121
                  *0122
0122  0001      DATA,  0001          /SET TO ZERO BY !RC AND !RO. ONLY
                                     /THEN CAN PROGRAM PROCEED
0123  0000      TALLY, 0000
0124  3177      C3177, 3177
0125  0000      KEEP,  0000
0126  3777      MASK,  3777
0127  5400      PARITY,IPARIT
0130  6000      M2000, -2000
0131  7770      MEIGHT,-10
0132  0100      PAR,   0100
0133  0200      IDENTI,0200
0134  0000      ROTATE,0000          /ENTRY SR ROTATE
0135  7012            RTR
0136  7012            RTR
0137  7012            RTR
0140  5534            JMP I ROTATE
0141  0000      REDEPS,0000          /ENTRY FOR IRS
0142  1121            TAD CNTSAV
0143  3120            DCA COUNT
0144  5541            JMP I REDEPS

                  *5200                /BEGINNING OF MAIN PROGRAM
5200  6331      START, 6331          /SKIPS IF SWITCHED ON
5201  5200            JMP.-1
5202  7300            CLA CLL
5203  1122            TAD DATA     /WAITS UNTIL DATA IS ZERO
5204  7640            SZA CLA
5205  5200            JMP START
5206  3035            DCA CLOCK2   /0035 IS INCREMENTED EVERY SEC
5207  1035            TAD CLOCK2
5210  7550            SPA SNA      /WAITS UNTIL CLOCK AGAIN INCREMENTED
5211  5207            JMP.-2       /NO
5212  6334            6334         /YES - CAN NOW BEGIN 1ST COUNT PERIOD
                                     /AS CLOCK HAS JUST BEGUN A SECOND
5213  7200            CLA
5214  3035            DCA CLOCK2
5215  3253            DCA LESIG    /INTERRUPT MAY HAVE OPERATED TO FILL
5216  3254            DCA MORSIG   /THESE WHILE IN WAIT LOOP
5217  6331      WAIT,  6331         /WAIT FOR COUNTING PERIOD TO EXPIRE
5220  5251            JMP SAVE     /WHEN RUN SWITCHED OFF
5221  1035            TAD CLOCK2
5222  1255            TAD TIME     /TIME IS MINUS COUNTING PERIOD
5223  7710      C0100, SPA CLA      /IS ACCUMULATOR POSITIVE?
5224  5217            JMP WAIT     /NO - CONTINUE WAITING
5225  7100            CLL          /YES - PERIOD HAS EXPIRED
5226  3035            DCA CLOCK2
5227  6334            6334         /STORE ROUTINE - READ AND CLEAR CTR
5230  7510            SPA          /WAVELENGTH MARKER?
5231  2257            ISZ FLAG     /YES - SKIP
5232  7000      GAMMA, NOP
5233  0126            AND MASK     /REMOVE THE WAVELENGTH MARKER
5234  1253            TAD LESIG    /CONTAINS COUNTER OVERFLOW
5235  3412            DCA I ADD    /STORE PART OF COUNT
5236  7004            RAL
5237  1254            TAD MORSIG
5240  2257            ISZ FLAG     /7777 IF NO MARKER
5241  1256            TAD WAVEM    /A MARKER PUT IN BIT ZERO
5242  3412            DCA I ADD    /STORE THE OTHER PART
5243  7040            CMA
5244  3257            DCA FLAG     /RESET TO 7777
5245  3253            DCA LESIG
5246  3254            DCA MORSIG
5247  2120            ISZ COUNT    /SKIP WHEN STORAGE IS FILLED
5250  5217            JMP WAIT
5251  2122      SAVE,  ISZ DATA     /PROTECTS RECORDED SPECTRUM
5252  5200            JMP START
5253  0000      LESIG, 0000
5254  0000      MORSIG,0000
5255  7772      TIME,  7772          /STANDARD COUNTING PERIOD 6 SECS
5256  4000      WAVEM, 4000
5257  7777      FLAG,  7777
                  CLOCK2=0035

                /INTERRUPT ROUTINE - CLEARS COUNTER TO PREVENT OVERFLOW
                /INTERRUPT OCCURS WHEN COUNTER IS HALF FULL
5260  0000      MINT,  0000
5261  6332            6332         /SKIP IF COUNTER INTERRUPT
5262  5660            JMP I MINT   /NO - RETURN TO TEST OTHER DEVICES
5263  6334            6334         /YES - READ AND CLEAR COUNTER
5264  7510            SPA          /WAVELENGTH MARKER?
5265  5273            JMP WAVE     /YES
5266  1253            TAD LESIG    /NO
5267  3253            DCA LESIG
5270  7430            SZL
5271  2254            ISZ MORSIG   /ADD ANY OVERFLOW INTO MORSIG
5272  5405            JMP I LEXIT /JMP TO INTERRUPT EXIT
5273  0126      WAVE,  AND MASK
5274  1253            TAD LESIG
5275  3253            DCA LESIG
5276  7004            RAL
5277  1254            TAD MORSIG
5300  1256            TAD WAVEM
5301  3254            DCA MORSIG
5302  5405            JMP I LEXIT
                  LEXIT=0005
```

```
                /PUNCHOUT PROGRAM FOR RAMAN EXPERIMENT
                /4 CHARACTERS PER DATA POINT
                /CHANNELS 1-6 FOR DATA EXCEPT CHL6 CHA4 FOR WAVELENGTH
                /MARKER. CHANNEL 7 SETS ODD PARITY AND A PUNCH IN
                /CHLF CHA1 TO DENOTE FIRST CHARACTER.
5303  0000      PNCOUT,0000
5304  6331            6331         /PREVENTS READ OUT WHILE A
5305  5311            JMP.+4       /RUN IS STILL IN PROGRESS
5306  1211            TAD START+11 /RINGS BELL
5307  4423            JMS I LOTCH
5310  5425            JMP I LWAIT
5311  1120            TAD COUNT    /=NO OF POINTS - 1000
5312  7041            CIA
5313  1232            TAD GAMMA
5314  7500            SMA
5315  5370            JMP RECET+1  /IF COUNT IS -1000
5316  3367            DCA RECET    /=-NO OF POINTS
5317  1124            TAD C3177
5320  3012            DCA ADD      /RESETS ADD
5321  4353            JMS LEADER
5322  1412      PUNCH, TAD I ADD
5323  3303            DCA PNCOUT   /RETURN ADDRESS NOT NEEDED
5324  1303            TAD PNCOUT
5325  0352            AND MASKA    /=0077 TO OBTAIN LOWER 6 BITS
5326  1133            TAD IDENTI   /1ST-CHARACTER MARKER
5327  4527            JMS I PARITY /ENSURES ODD PARITY
5330  4424            JMS I LOPCH  /PUNCHES CHARACTER
5331  1303            TAD PNCOUT
5332  4134            JMS ROTATE   /TOP 6 BITS TO BOTTOM OF ACC.
5333  4362            JMS MASKPP   /MASKS. SETS PARITY AND PUNCHES
5334  1412            TAD I ADD
5335  3303            DCA PNCOUT
5336  1303            TAD PNCOUT
5337  4362            JMS MASKPP   /PUNCHES CHARACTER 3
5340  1303            TAD PNCOUT
5341  4134            JMS ROTATE
5342  4362            JMS MASKPP   /PUNCHES CHARACTER 4
5343  4403            JMS I LCMND  /CHECKS FOR A COMMAND
5344  2367            ISZ RECET    /OUTPUT FINISHED?
5345  5322            JMP PUNCH
5346  1023            TAD LOTCH    /YES - PUNCH EOF MARKER
5347  4424            JMS I LOPCH
5350  4353            JMS LEADER
5351  5370            JMP RECET+1
5352  0077      MASKA, 0077
5353  0000      LEADER,0000          /GENERATES LEADER TAPE
5354  1223            TAD C0100    /=7710
5355  3303            DCA PNCOUT
5356  4424            JMS I LOPCH  /PUNCHES A ZERO
5357  2303            ISZ PNCOUT
5360  5356            JMP.-2       /56 TIMES
5361  5753            JMP I LEADER /WITH CLA CLL
5362  0000      MASKPP,0000
5363  0352            AND MASKA
5364  4527            JMS I PARITY
5365  4424            JMS I LOPCH
5366  5762            JMP I MASKPP
5367  0000      RECET, 0000          /!RC ENTRY AND !RO EXIT .
5370  1120            TAD COUNT
5371  3121            DCA CNTSAV   /TO RETAIN VALUE OF COUNT
5372  1124            TAD  C3177
5373  3012            DCA ADD
5374  1232            TAD GAMMA
5375  3120            DCA COUNT    /RESET COUNT
5376  3122            DCA DATA
5377  5425            JMP I LWAIT
                  LCMND=0003
                  LOTCH=0023
                  LOPCH=0024
                  LWAIT=0025

                  *5400    /PARITY SUBROUTINE DETERMINES AND SETS PARITY
5400  0000      IPARIT,0000
5401  3141            DCA REDEPS
5402  3125            DCA KEEP
5403  1131            TAD MEIGHT   /= -8
5404  3123            DCA TALLY
5405  1141            TAD REDEPS
5406  7110            CLL RAR
5407  7430            SZL          /IS LINK ZERO?
5410  2125            ISZ KEEP     /NO - INCREMENT KEEP
5411  2123            ISZ TALLY
5412  5206            JMP.-4
5413  1125            TAD KEEP
5414  7010            RAR          /IF EVEN LINK IS NOW ZERO
5415  7220            CLA CML
5416  1141            TAD REDEPS
5417  7430            SZL          /SKIP IF ODD PARITY
5420  1132            TAD PAR      /= 0100
5421  5600            JMP I IPARIT
5422  0000      CLEAN, 0000          /ENTRY FOR !RR
5423  1130            TAD M2000    /ENTERED AFTER CLA CLL
5424  3141            DCA REDEPS
5425  1124            TAD C3177
5426  3012            DCA ADD
5427  3412            DCA I ADD
5430  2141            ISZ REDEPS
5431  5227            JMP.-2
5432  5622            JMP I CLEAN

                /RAMAN COMMAND TABLE
                *0750
0750  2217            2217    /!RO - COMMENCE OUTPUT
0751  5303            PNCOUT
0752  2223            2223    /!RS - RESETS THE SCALAR COUNT
0753  0141            REDEPS
0754  2203            2203    /!RC - INITIALISATION AND RESETTING
0755  5367            RECET
0756  2222            2222    /!RR - CLEAR MEMORY 3200 - 5177
0757  5429            CLEAN
```

APPENDIX IV

PUBLICATIONS

The results presented in Part I have been published in the *Journal of Chemical Physics*, volume 54, page 1141, 1971 in collaboration with D.J. Lockwood.

Similarly, the preliminary results of the investigation described in Part II have been published jointly with D.J. Lockwood. The measurements of $CdCl_2$(Co), $MnCl_2$(Co) and $CdBr_2$(Co) appear in *Chemical Physics Letters*, volume 9, page 559. $CoCl_2$ results appear in *Chemical Physics Letters*, volume 8, page 120, and in *Proceedings of the Second International Conference on Light Scattering in Solids*, edited by M. Balkanski and published by Flammarion Sciences, Paris, in 1971.

The full results presented in Part II are to be published. This appendix reproduces the already published work.